December 1992 THESIS/DISSERTATION

Determination of Momentum Flux Using a Bivane and Cup Anemometer

Thomas L. Schiano, Captain

AFIT Student Attending: Purdue University

AFIT/CI/CIA- 92-119

AFIT/CI
Wright-Patterson AFB OH 45433-6583

DISCLAIMER NOTICE

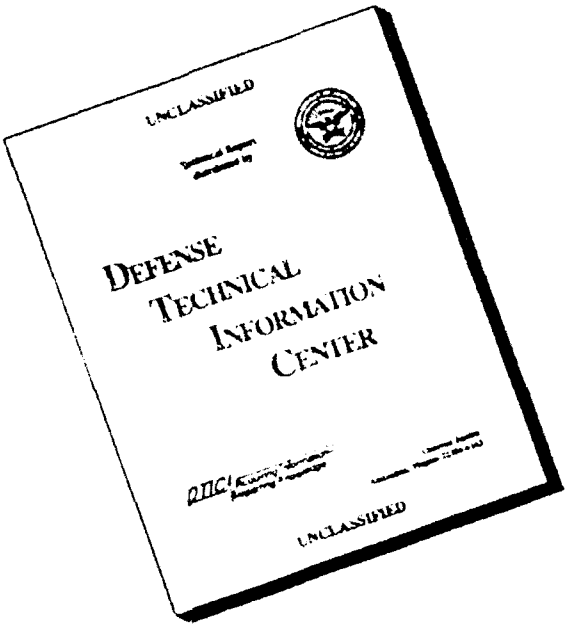

THIS DOCUMENT IS BEST QUALITY AVAILABLE. THE COPY FURNISHED TO DTIC CONTAINED A SIGNIFICANT NUMBER OF PAGES WHICH DO NOT REPRODUCE LEGIBLY.

DETERMINATION OF MOMENTUM FLUX USING A BIVANE AND CUP ANEMOMETER

A Thesis

Submitted to the Faculty

of

Purdue University

by

Thomas L. Schiano

In Partial Fulfillment of the

Requirements for the Degree

of

Master of Science

December 1992

Graduate School Form 9
(Revised 8/89)

PURDUE UNIVERSITY
GRADUATE SCHOOL
Thesis Acceptance

This is to certify that the thesis prepared

By Thomas L. Schiano

Entitled

Determination of Momentum Flux Using a Bivane and Cup Anemometer

Complies with University regulations and meets the standards of the Graduate School for originality and quality

For the degree of Master of Science

Signed by the final examining committee:

John T. Lewis, chair

William L. Woods

Dayton G. Vincent

Approved by:

Ernest M. Agee
Department Head

11 Sept 92
Date

Accession For	
NTIS GRA&I	☑
DTIC TAB	☐
Unannounced	☐
Justification	
By	
Distribution/	
Availability Codes	
Dist	Avail and/or Special
A-1	

☐ is
This thesis ☒ is not to be regarded as confidential

John T. Lewis
Major Professor

ACKNOWLEDGEMENTS

I would like to express my sincere gratitude to all who have participated or assisted in this endeavor. Particular thanks are extended to my advisor, Dr. John Snow, who suggested the study in question and was an invaluable source of guidance and wisdom. During my assignment at Purdue, Dr. Snow spent nearly one year in the Persian Gulf in service to our country. As a fellow military officer, I appreciate his valor and salute his patriotism.

I would also like to express profound appreciation to the other members of my committee, Dr. Dayton Vincent and Dr. William Wood, and to C.J. Fuqua, the department engineer. Dr. Vincent acted as my advisor in Dr. Snow's absence, and providing invaluable guidance and insight. Dr. Wood was also a valuable source of these as well. And without C.J.'s inestimable help and knowledge, I would be not have been able to finish this study.

I would be remiss if I did not expressly thank several of my peers, who always had a good idea and words of encouragement. Foremost amongst these were Tom McClelland, Dan Vietor, and Doug Miller. A special word of thanks is reserved for Tony Lupo, whose help and support cannot be overstated.

I would like to thank the United States Air Force and the American taxpayers for giving me the opportunity to enhance my knowledge, expertise, and self-confidence. Hopefully I can reimburse

them through a distinguished service.

A special thanks goes to my mother, for her unwavering support and love. I credit both my parents for teaching me the value of an honest day's work, without which this accomplishment would never have been realized.

Last, but certainly not least, I would like to thank god, whom I constantly pestered with prayers and pleadings for this day to come. Through all of my successes and failures, he has always been the one constant on which I could depend. He has truly made me a better person for the experience.

TABLE OF CONTENTS

Page

LIST OF TABLES

Table Page

LIST OF FIGURES

Figure Page

Figure Page

Figure Page

Appendix
Figure Page

ABSTRACT

Schiano, Thomas Louis. M.S., Purdue University, December 1992. Determination of Momentum Flux Using a Bivane and Cup Anemometer. Major Professor: John T. Snow.

The ability of a bivane and cup anemometer system to provide data that can be used to determine momentum flux is examined for conditions in the near-surface boundary layer. Use of a bivane for such a purpose was first proposed by Chimonas (1980), who suggested a method for obtaining an approximation of the flux magnitude from time-mean values of angular deflection and horizontal wind speed. Both the approximation proposed by Chimonas and an accepted statistical method (covariance of wind components, $u'w'$) are examined.

A three-axis sonic anemometer was used to obtain the reference values of $u'w'$. The evaluated system consisted of a three-cup anemometer for determination of the horizontal wind vector, and a dual annulus bivane, used to determine the elevation (vertical) angle of the wind vector. In three field tests under various degrees of stability, the instruments were suspended from an instrumented tower on a boom oriented relative to the prevailing horizontal wind flow. Output voltages from the instrumentation were collected and subsequently converted to the desired components through the use of empirically-derived transfer functions.

Examination of data reveals high degrees of correlation between

the patterns and magnitudes of the components derived from the bivane/three-cup anemometer system as compared to those measured with the sonic anemometer. Computations of momentum flux yielded comparable values between the two systems. Based on these results, conclusions are presented concerning the validity of the different methods of estimating momentum flux.

1. INTRODUCTION

Knowledge regarding the kinematic and thermodynamic transfer of atmospheric properties near the surface is critical in understanding the atmosphere and its interactions with the human race. In many situations, these transfers have a direct impact on the state of the atmosphere as well as on plant and animal life. One specific instance where such knowledge is essential is the bulk transfer of airborne contaminants or pollutants.

As instantaneous values for such transfers are not terribly meaningful, temporally and/or spatially averaged values are utilized to provide useful information. Since this transport is turbulent in nature, it is necessary to use statistical methods to reach quantitative solutions. Many such methods have been developed to quantify the net transfer of atmospheric properties such as heat, moisture, and kinematic energy (or momentum) within the Atmospheric Boundary Layer (ABL). Measurement of the momentum flux (also referred to as Reynolds' stress) is key; if one can determine its value, fluxes for the other parameters can be readily estimated.

One statistical method, known commonly as the covariance or cross-correlation method, generally is used for estimating the momentum flux. This method is also known as the eddy-correlation method, as the two statistical quantities required are the horizontal and vertical wind components that characterize a parcel of air moving in an

atmospheric eddy. However, stringent data acquisition requirements regarding equipment capabilities and location must be satisfied if high accuracy and low uncertainty are required. This method requires the use of equipment that can sample the horizontal and vertical wind components at a high rate with a high degree of accuracy. Unfortunately, the equipment needed to satisfy these requirements, usually a sonic anemometer, is often prohibitively expensive, precluding its use when many units are required. In addition, many of these instruments cannot be exposed to a wide range of meteorological conditions--many are temperature sensitive, and some are not able to function while precipitation is occurring.

Chimonas (1980) has proposed another method of estimating momentum flux using two pieces of less complicated instrumentation: a bivane (a wind vane capable of motion in both the horizontal and vertical planes) and a cup anemometer. While these instruments lack the near-instantaneous, linear output of the sonic anemometer, they cost a great deal less. Thus, in applications where numerous sampling locations are required, the instrumentation used in the Chimonas' momentum flux approximation method (herewith referred to as the 'Chimonas Approximation Method' or CAM) is much more cost effective than the bulk use of sonic anemometers.

Chimonas used time-averaged values of u and ϕ in the CAM, since traditional cup anemometers and bivanes were bulky and slow-responding. However, their modern counterparts are much more sensitive. Often they are constructed using light-weight 'space-age' materials, which permit much quicker instrument response. Thus, it is theoretically feasible to estimate momentum flux using the eddy-correlation method with

vertical and horizontal component data from a cup and bivane system.

1.1. Purpose

The purpose of this study is to determine whether two momentum flux estimation methods yield representative values when compared to the measured 'true' flux values. Both of the estimation methods utilize data from a cup anemometer and bivane, while the 'true' flux value is obtained with measurements made by a sonic anemometer. The estimation methods are: (1) A slightly-modified version of the CAM, using time-series mean quantities of horizontal wind speed and vertical deflection (or angle), and (2) a direct application of the eddy-correlation technique to time-series of u and w covariances.

One should keep in mind that the 'true' flux value determined with the sonic anemometer is not the actual momentum flux. Rather, it is the closest estimation of the true flux we can obtain, as ideally-responding (i.e., instruments capable of responding to changes in measured parameters (1) instantaneously, and (2) with complete accuracy) instruments do not yet exist. However, since the sonic anemometer has a near-ideal response, it is acceptable to regard its measurements as 'true'. Conversely, both the cup anemometer and bivane exhibit a less-than ideal response, so it is to be expected that flux estimations made with them will yield less accurate values.

Additionally, to determine the overall usefulness of these estimations, experiments are undertaken in varying atmospheric stability conditions (characterized by the Monin-Obukov (M-O) length scale). Once overall accuracy is assessed under varying conditions, a

determination regarding the validity of the estimation methods is made.

Note: items appended with superscripted numbers are explained in greater detail in the notes located near the end of this publication.

2. METHODS USED TO CALCULATE MOMENTUM FLUX

Although several statistical methods exist to estimate momentum flux, this study utilizes the eddy-correlation method to determine a 'true' value. This method has strict restrictions that govern its use that were considered carefully prior to the experiment. In each case, the constraints were judged to be satisfactorily addressed. The sonic anemometer and test site were determined to be acceptable and appropriate for the use of this method. While the requirements for equipment and experiment site were not as strenuous for the CAM (all instrumentation co-located as best it could be on a macro scale), concerns regarding their selections were also addressed. Specifications for and selection of equipment are covered in detail in chapter three.

2.1. The Wind

The wind is a vector quantity; it has both direction and magnitude. A wind vector is normally thought of as existing in three-dimensional space. If, however, one is able to constantly align the local frame of reference along the horizontal component, the wind can be thought of in a two dimensional framework. Thus, the wind vector can be represented as

$$\mathbf{V} = u\hat{\mathbf{i}} + w\hat{\mathbf{k}} \qquad (1)$$

where u is the horizontal wind speed, w is the vertical wind speed, and $\hat{i}$ and $\hat{k}$ are unit vectors. Note that u is the speed measured by a cup anemometer.

Assuming an ideal bivane (one that responds instantaneously to changes in the azimuth and elevation), the elevation angle is given by:

$$\phi = \tan^{-1}\left[\frac{w}{u}\right] \tag{2}$$

Note that to specify **V**, one may measure u and w as in (1), or measure u and ϕ, with

$$\mathbf{V} = u(\hat{i} + \tan\phi\hat{k}) \tag{3}$$

2.2. The Eddy-Correlation Method

A preferred method for estimating Reynolds stress is through the use of the eddy-correlation method applied to data from a three-axis sonic anemometer. Only one instrument, placed at a specific location, is needed to acquire the necessary time-series of horizontal and vertical wind components. Momentum flux is then easily computed using standard statistical techniques. However, use of this method is restricted by the following conditions: (1) The instrumentation used must faithfully sample the wind with a high degree of accuracy to ensure the indicated data reflect the actual flow; (2) the sampling must take place over an 'ideal' surface (flat, extensive, homogeneous), with the instrumentation properly positioned and leveled to preclude

non-desirable anomalous surface or wake interactions. While the latter restriction is usually not difficult to accommodate, the former requires the use of expensive and complicated equipment to meet response requirements.

If one pictures the geometry of the horizontal and vertical wind components as in Figure 1, at any time t, the following generalizations of the wind flow can be made:

$$u(t) = \bar{U} + u'(t) \tag{4}$$

$$w(t) = \bar{W} + w'(t) \tag{5}$$

where $u(t)$ and $w(t)$ are the horizontal and vertical wind components, $\bar{U}$ and $\bar{W}$ are the time-averaged component means, and $u'(t)$ and $w'(t)$ are the departures from the mean of the respective components.

By statistical definition, the covariance of two parameters, in this case the u- and w- components, is simply the time-average of the product of the two. Thus

$$uw = (\bar{U} + u')(\bar{W} + w') \tag{6}$$

Multiplying and taking the time average of both sides,

$$\overline{uw} = \overline{\bar{U}\bar{W}} + \overline{u'\bar{W}} + \overline{\bar{U}w'} + \overline{u'w'} \tag{7}$$

By definition, the time-averages of the instantaneous departures from

Geometry of the Wind

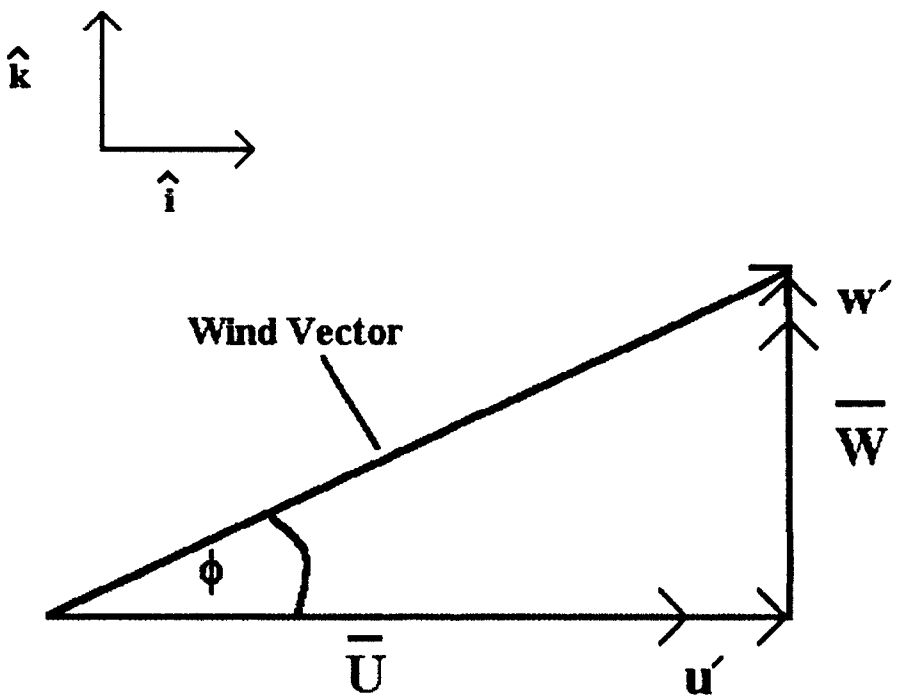

Figure 1. Geometry of decomposed wind vector and relationship between horizontal (u) and vertical (w) components and vertical angle ϕ. Instantaneous departures from the component means are given by u' and w'. Unit vectors $\hat{i}$ and $\hat{k}$ are provided for reference.

the respective component means approach zero with increasing time. Neglecting instrument leveling error, the mean vertical transport of mass in the atmosphere must approach zero as time increases. This implies the. Thus, the first three terms in (7) approach zero with increasing time. This yields the covariance:

$$\overline{uw} = \overline{u'w'} \tag{8}$$

Using the covariance of the components, time averaged as in (8), the eddy-correlation estimation for the vertical flux of horizontal momentum is obtained by multiplying the remaining term by standard atmospheric density.

$$\tau_{EC} = -\rho\overline{u'w'} \tag{9}$$

The purpose of the negative sign is simply for directional convention. It is important to remember that momentum flux is almost always directed towards the surface. This is a consequence of the structure of the vertical wind profile of the ABL, which by definition has a boundary condition of a zero wind speed at the surface and increasing wind speed with height. That (9) is prefaced with a negative sign reflects the fact that momentum flux is usually directed in an opposite manner to the fluxes of heat and moisture. Accordingly, for the purposes of this study, a positive momentum flux will refer to a flux directed towards the surface.

2.3. Chimonas and Modified Chimonas Approximation Methods

The derivation of the Chimonas Approximation Method (CAM) is presented as in Chimonas (1980). However, as his technique does not allow for either leveling errors or non-zero mean vertical velocity contributions, a modified version (the Modified Chimonas' Approximation Method, or MCAM) is subsequently derived. The MCAM is an extension of the CAM, therefore separate derivations are unnecessary.

As in Figure 1, the wind vector field can be represented by:

$$\mathbf{V} = (\bar{U} + u')\hat{i} + (\bar{W} + w')\hat{k} \tag{10}$$

Again, this presumes a frame of reference in which the vector field remains aligned with the horizontal component, thus eliminating the need to consider a transverse component. The elevation angle ϕ of a bivane is given by

$$\phi = \tan^{-1}\left[\frac{\bar{W} + w'}{\bar{U} + u'}\right] \tag{11}$$

For convenience, 'smallness' parameters ϵ_1 and ϵ_2 are given by

$$\epsilon_1 \leq \frac{|u'|}{|\bar{U}|}, \tag{12}$$

$$\epsilon_1 \leq \frac{|w'|}{|\bar{U}|}, \tag{13}$$

$$\epsilon_2 \leq \frac{|\bar{W}|}{|\bar{U}|} \tag{14}$$

Thus, from a Taylor expansion of (11), separating the equation into mean and fluctuating components,

$$\phi = \frac{w'}{\bar{U}} - \frac{(u'w' - \overline{u'w'})}{\bar{U}^2} - \frac{u'\bar{W}}{\bar{U}^2} +$$

$$\left[\frac{\bar{W}}{\bar{U}} - \frac{\overline{u'w'}}{\bar{U}^2}\right] + O((\epsilon_1 + \epsilon_2)^3) \tag{15}$$

Taking the time average of both sides yields:

$$\bar{\phi} = \left[\frac{\bar{W}}{\bar{U}} - \frac{\overline{u'w'}}{\bar{U}^2}\right] + O((\epsilon_1 + \epsilon_2)^3) \tag{16}$$

Under ideal conditions (flat, homogeneous, extensive), and with an increasing time interval ($t \to \infty$), as $\bar{W} \to 0$, so that $\epsilon_2 \to 0$ as well, implying:

$$\epsilon_2 \ll \epsilon_1^3 \tag{17}$$

Then (16) becomes:

$$\bar{\phi} = \frac{\overline{-u'w'}}{\bar{U}^2} + O(\epsilon_1{}^3) \tag{18}$$

Solving for the covariance, we obtain Chimonas' approximation:

$$\tau_{CAM} = \overline{u'w'} = -\bar{U}^2\bar{\phi} + O(\epsilon_1{}^3) \tag{19}$$

However, if it is not feasible to take a continuous data sample for a sufficiently long time (due to software limitations), and since it is often not possible to eliminate all leveling concerns (as the underlying surface is not truly 'flat'), allowances should be made for a small, non-zero factor of $\bar{W}$. Using the same geometry, an offset angle which takes into account these factors is given by

$$\phi_{off} = \tan^{-1}\left[\frac{\bar{W}}{\bar{U}}\right] \tag{20}$$

Thus, (18) is modified as:

$$(\bar{\phi} - \phi_{off}) = \frac{\overline{-u'w'}}{\bar{U}^2} + O(\epsilon_1{}^3) \tag{21}$$

This implies

$$\overline{u'w'} = -\bar{U}^2(\bar{\phi} - \phi_{off}) + O(\epsilon_1{}^3) \tag{22}$$

Multiplying by a factor of $-\rho$ (as in the Eddy-Correlation method), the modified Chimonas approximation of momentum flux is:

$$\tau_{MCAM} = \rho\bar{U}^2(\bar{\phi} - \phi_{off}) + O(\epsilon_1{}^3) \tag{23}$$

Note that often $O(\epsilon_1{}^3)$ will be minute (at least two orders of magnitude smaller than the mean of the horizontal wind component), as the magnitudes of u' and w' are much smaller than $\bar{U}$, and so can be neglected.

The final form of the modified Chimonas approximation is:

$$\tau_{MCAM} = \rho\bar{U}^2(\bar{\phi} - \phi_{off}) \tag{24}$$

3. INSTRUMENTATION

To satisfactorily answer the questions posed in this study, the instruments selected for use had to meet specific performance standards. Each had to obtain highly-accurate data while also satisfying requirements for rapidity of output, durability, ease of operation, and reliability. To be certain the chosen instruments satisfied these requirements, each was tested prior to the experiment. The testing served two primary purposes. It ensured: (1) the personnel conducting the experiment were thoroughly familiar with the operational characteristics of the instruments, and (2) the derivation of the exact transfer functions required for accurate conversions from output instrument voltages to component magnitudes.

This chapter details instrument selection considerations, operational capabilities and characteristics, and testing results for the instruments used in the experiment.

3.1. Sonic Anemometer

The determination of the covariance of u and w in the eddy-correlation method requires an instrument capable of accurately measuring both horizontal and vertical wind components at a near-instantaneous rate (i.e., having ideal-response). A three-axis sonic anemometer was chosen for use because of its high sampling rate, nearly instantaneous response, and linearity of response. The anemometer

chosen[1] is a solid-state ultrasonic instrument capable of measuring wind components along three orthogonal axes (standard u-, v-, and w-components), as well as virtual temperature (Figure 2).

3.1.1. Operation

Each axis has transducers embedded at the ends of aligned posts, which run parallel to the sampled component. These transducers emit and receive sonic pulses at a set frequency. Internal software provides wind velocity calculations based on the time needed for the pulse to traverse the distance from the emitting transducer to its receiving counterpart. These calculations are completed each one-tenth of a second, and are immediately relayed for output in either a digital or analog format. There is only a one-tenth of a second delay between pulse emission and reception, velocity calculation, and data output (Applied Technologies, 1980).

The sonic anemometer, configured for an analog output, has measurement ranges of $\pm$ 20 m s^{-1} for the horizontal component and $\pm$ 5 m s^{-1} for the vertical component. These measurement ranges are scaled over an output voltage of $\pm$ 5 vdc for each axis. The different voltage polarities refer to component direction. System specifications for resolution are $\pm$ 0.01 m s^{-1} with an accuracy of $\pm$ 0.05 m s^{-1}. The anemometer and its accompanying circuitry are powered by a standard 120 vac electrical outlet, and can also be powered with a portable 12 vdc power source. Both are weather-proof, since the probe's transducers are embedded in a waterproof material, and the main circuitry can be isolated from the elements. The circuitry is housed in an aluminum case containing circuit cards mounted in a card cage. The case is

sealable, and thus can be exposed to harsh outdoor conditions as long as the ambient temperature is between -20° C and 50° C (Applied Technologies, 1980).

3.1.2. Determination of Operational Characteristics

Unlike the other wind-sensing instruments, the sonic anemometer was not pre-tested in The Purdue University wind tunnel[2] to determine its exact transfer functions and output linearity. Since it is in essence three instruments in one, it would have required the axis being tested to be aligned perfectly with the tunnel flow (meaning no cross-axis components would exist). Due to tunnel flow irregularities (the flow was not completely laminar) and instrument positioning difficulties, this was not possible. There was no means of positioning the sonic anemometer in as precise a manner as recommended (to within ±0.5° of the flow axis) to ensure test accuracy (Dr. Bruce Baker, private communication). However, the senior engineer for the manufacturer gave assurances that the transfer functions listed in the operations manual were sufficiently accurate for the purposes of this study (Mr. Herb Zimmerman, private communication). These transfer functions were

$$u_d = 2V_u \tag{25}$$

$$v_d = 2V_v \tag{26}$$

$$w_d = 0.5V_w \tag{27}$$

where u_d, v_d, and w_d are the derived u, v, and w wind speeds in m s^{-1}, respectively, and V_u, V_v, and V_w are the respective output voltages in vdc.

An additional consideration required addressing; the computer card which computes flow distortion correction algorithms in conjunction with the unit's data processing software was removed by the unit's owner. Flow distortion occurs when the wind vector is less than $\pm 70^{\circ}$ off the centerline of any axis, and results in anomalously low output wind speeds. The manufacturer subsequently provided the information needed to correct the data for flow distortion[3].

3.2. Three-cup Anemometer

The instrument chosen for the determination of u(t) in the approximation method was a three-cup anemometer. The cup anemometer selected for use in the approximation method displayed the rapid response required for high-frequency oscillations characteristic of turbulent flow near the surface. The chosen unit was manufactured by Weathertronics[4] (Figure 2). It was chosen because of superior responsiveness and dynamic characteristics (Snow et al., 1989). The manufacturer's published specifications (a starting threshold of 0.5 m s^{-1}, a distance constant of 1.2 m, and an accuracy of ± 0.15 m s^{-1}) (Qualimetrics, 1985) made this anemometer ideal for use in the approximation. To ensure the anemometer's suitability and verify its response characteristics (Snow et al., 1989), it was tested in a wind tunnel at Purdue University.

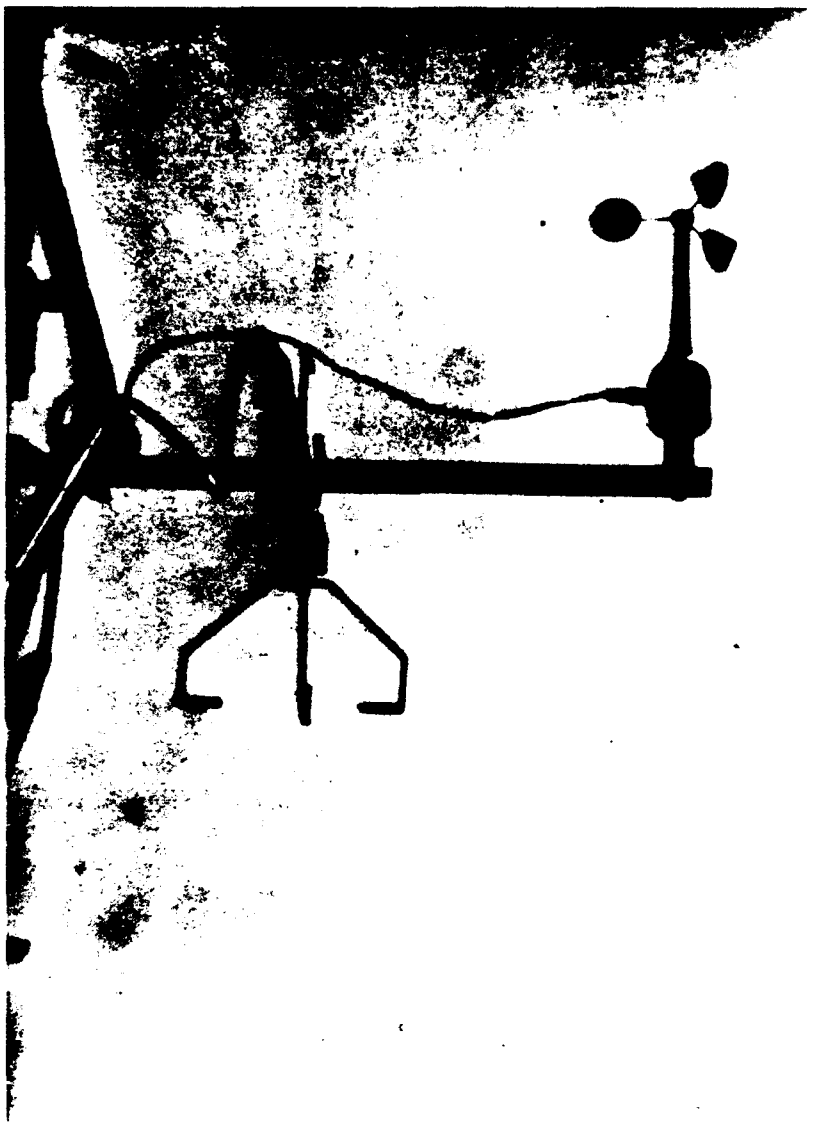

Figure 2. Weathertronics 2030 Micro Response Three-Cup Anemometer (right), adjacent to Applied Technologies model SWS-211/3 three-axis sonic anemometer probe.

3.2.1. Operation

A three-cup anemometer is designed to measure the total horizontal wind component. This particular model is used in conjunction with a wind translator, which acts to condition the output signal[5].

The cup uses a light chopper system. As the wind turns the cup wheel, it also turns a slotted wheel in the main housing. This wheel has 30 slots, and is attached to the main rotational shaft. A light emitting diode and a light sensitive transistor are mounted so that the as the wheel turns, the solid sections of the slotted wheel interrupt a light beam generated by the diode. The result is the formation of a pulse train, with the frequency of the pulses proportional to the rate of rotation of the cup wheel. The pulses are amplified and conditioned by the wind translator to provide an analog or digital output (depending on translator configuration), which is proportional to the frequency of the generated pulse train.

One factor to keep in mind when examining and evaluating output data from cup anemometers is that they overestimate the mean windspeed in turbulent conditions. This phenomena, known as cup overspeeding, occurs because the cup acts like a flywheel; it speeds up faster than it slows down. The cup will speed up proportionally to the increased wind speed during the onset of a gust, but will slow down less rapidly during the lull. The result is, for a finite period of time, the anemometer indicates a higher speed than is truly occurring. This anomalously high speed continues until the increased angular momentum from the gust can be dissipated by frictional forces within the cup

shaft and bearings (Figure 3).

3.2.2. Determination of Operational Characteristics

To determine an appropriate transfer function relating output voltage to applied wind speed, the cup anemometer was placed in the large section of the Purdue University wind tunnel. The anemometer was leveled and thus oriented such that the flow was parallel to its axis of revolution. The translator was set to its low output range, where the manufacturer's output relationship is given by

$$V_{out} = 0.2\ U_{in}, \tag{28}$$

where V_{out} is the anemometer's output voltage in vdc, and U_{in} is the input windspeed in m s^{-1}. The wind tunnel was then set to operate at five wind speeds ranging between 3.5 and 10.0 m s^{-1}. The output data was recorded using commercial software[6]. At each speed, the output voltage of the anemometer was recorded over 10 runs at a frequency of 20 Hz for a duration of 10 seconds. The data were then reduced through the use of a commercial spreadsheet[7] as follows: for each run, an average voltage was computed. The resultant averages from each of the ten runs were then averaged. These final averages were the experimental values for the output voltages recorded for regression analysis. The use of this method, as opposed to a standard regression using all of the averages from each individual run, was deemed acceptable due to the very small amount of variation of the averages from the individual runs. The transfer function for speeds between 3.5 m s^{-1} and 10.0 m s^{-1} was determined to be

Figure 3. An example of cup overspeeding. The cup acts as a flywheel, speeding up rapidly as the gust builds, but slowing down less rapidly as the lull sets in, leading to an erroneously high average wind speed over the time-series.

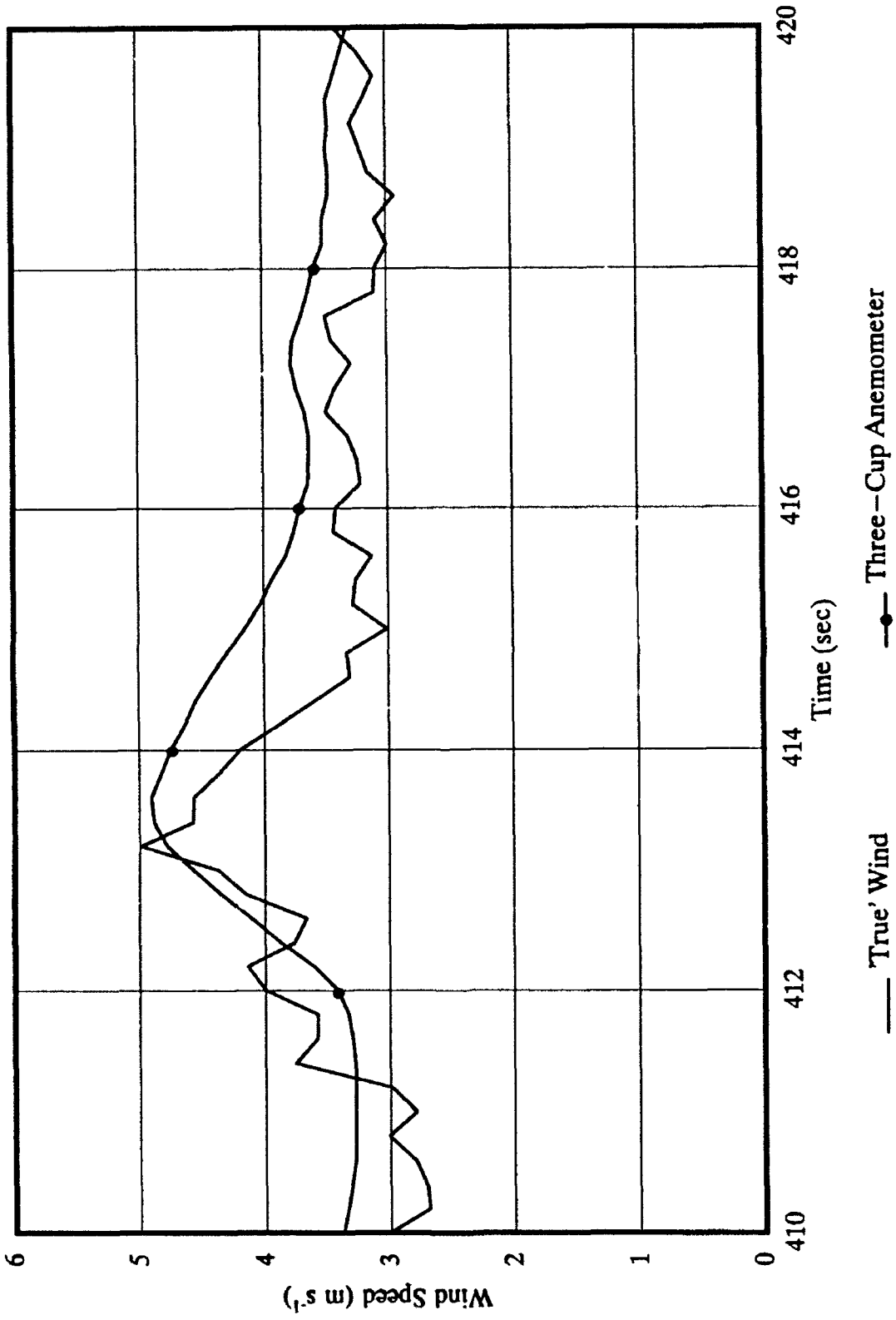
Wind Speed (m s-1)
0
1
2
3
4
5
6
410
412
414
416
418
420
Time (sec)
True' Wind
Three-Cup Anemometer

Figure 3

$$U_d = 4.244598V_a + 0.442731 \quad (29)$$

where U_d is the derived windspeed in m s^{-1}, and V_a is the output voltage from the anemometer in vdc.

However, using a linear transfer function for all possible wind speeds with a cup anemometer is not a valid option. A cup anemometer, due to mechanical resistance, will not rotate if the applied wind is below a certain magnitude. Only when the applied wind speed exceeds that particular starting threshold will the cup wheel rotate. Thus, a more representative transfer function for use at low wind speeds should resemble the curve in Figure 4. To determine the starting threshold, more wind tunnel tests were undertaken.

A sonic anemometer was used to determine tunnel speeds below 2.0 m s^{-1}, the lowest tunnel speed detectable by the tunnel's Pitot system. Data were acquired and processed as in the previous test. The lowest tunnel speed obtained was 0.149 m s^{-1}, which was still above the starting threshold. As the resultant curve for the output data resembled the solution to a first-order overdamped system, an analogous transfer function was derived using all of the test data. The data and shape (or trend) of the function were used to estimate a starting threshold. The best estimate of the starting threshold was determined to be 0.116 m s^{-1}, which is significantly better than the manufacturer's standard of 0.5 m s^{-1} (Qualimetrics, 1985). This method was not perfect; the latter function's speeds varied by as much as 0.40 m s^{-1} on the high end of the scale (above 5.0 m s^{-1}) from (29), which had displayed a very high correlation between 3.5 and 10 m s^{-1}.

Figure 4. Response of first-order overdamped system with ramp forcing function, similar to graph of transfer function adoopted for three-cup anemometer (starting threshold $u_0 = 0.116$).

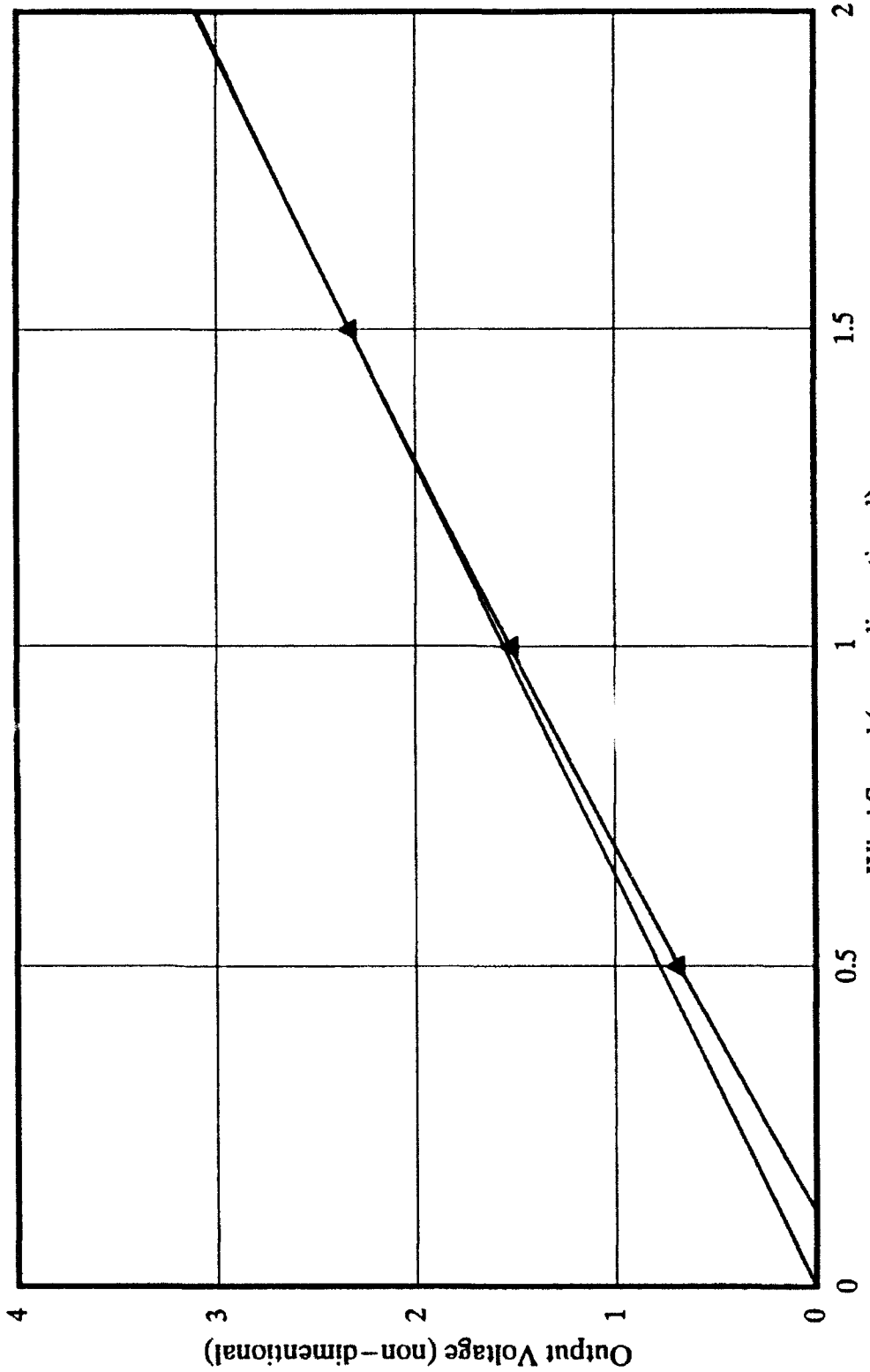
Output Voltage (non-dimentional)
0
1
2
3
4
0
0.5
1
1.5
2
Wind Speed (non-dimentional)
Overdamped Response
Linear Response

Figure 4

But to accommodate all ranges of input wind speeds, the latter solution was determined better suited for use than (29).

The solution chosen for use as the transfer function was

$$U_d = 0.116 + (4.5320(V_{ca} - 0.256)) + 0.116e^{\left[\frac{-V_{ca}}{0.116}\right]} \qquad (30)$$

where U_d is the derived windspeed in m s^{-1}, and V_{ca} is the output voltage from the cup anemometer in vdc.

3.3. Bivane

The other factor required for the approximation method is the time-averaged vertical angle $\bar{\phi}$, which is described by the geometry in Figure 1. Prior to this study, Coats (1991) examined the response characteristics of three different bivanes. He determined that a dual annulus bivane demonstrated the fastest response, least interaction between the two components of motion, and highest sensitivity to high-frequency wind fluctuations. A dual-annulus bivane was selected for use in the experiment[8] (Figure 5). It displayed the rapid response required for high-frequency oscillations characteristic of turbulent flow near the surface (refer to Coats (1991) for specific details regarding quality testing and response characteristics).

During the field experiments, the dual-annulus bivane suffered a system failure that necessitated its replacement. The vane selected for use in its place was a cruciform-tailed gill bivane[9]. This vane had also been tested previously by Coats (1991), thus its dynamic

Figure 5. Climatronics model P/N 101456 Dual Annulus bivane, (left), alongside helicoid propeller anemometer.

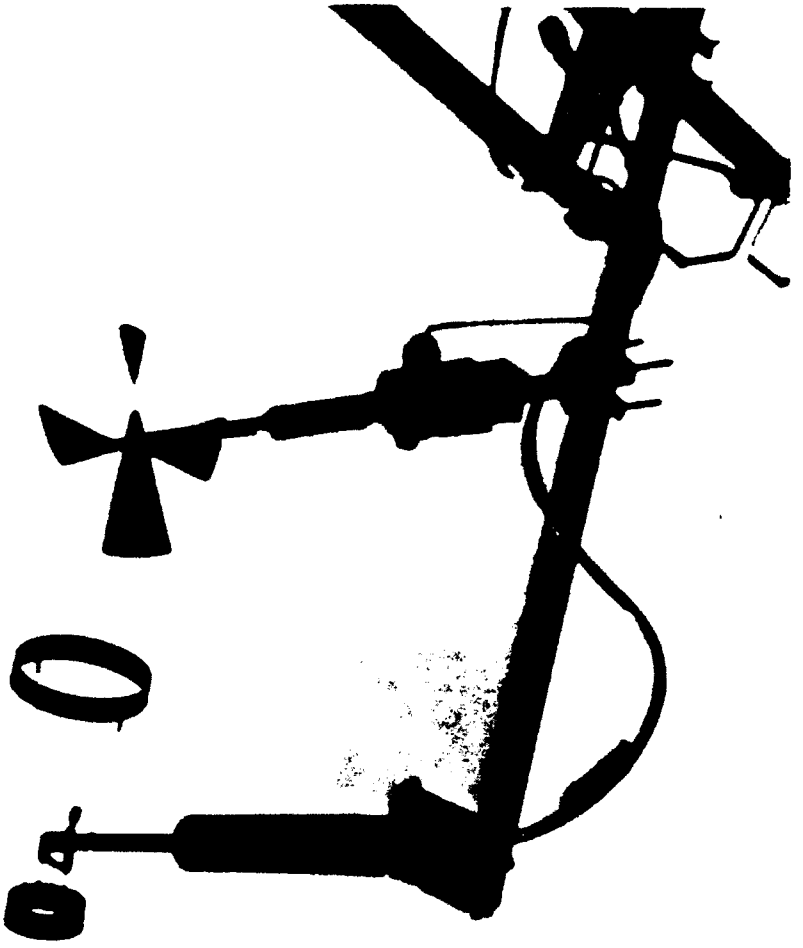

Figure 5

response characteristics were known. This vane does not display the rapidity of response seen in the dual-annulus bivane. The natural wavelength (4.93 meters) is roughly twice the value for the dual-annulus vane, requiring interaction with much larger turbulent eddies in order to respond faithfully to the 'true' wind.

3.3.1. Operation

3.3.1.1 Dual-Annulus Bivane

The dual annulus bivane chosen for use in this experiment is unique in design and construction, resulting in better response characteristics compared with the more common cruciform-tailed vanes. The vane assembly, constructed of carbon fibers, weighs less than 28 grams. The manufacturer's literature states the dual annulus design and very low mass structure were designed specifically for enhanced Reynolds stress detection capability. The published specifications (accuracy to $\pm 3^{\circ}$, damping ratio ζ of 0.45, natural wavelength λ_n of 2.85 meters, and a starting threshold of less than one m s^{-1}) (Climatronics, 1980) are indicative of the sufficient alacrity of response at high frequencies needed to obtain accurate angular displacements.

The bivane requires a 12-volt power source, and produces an output signal between 0-1 vdc for both the horizontal angle θ and the vertical angle ϕ. The vertical component is determined by a Linear Variable Displacement Transducer (LVDT), which consists of a metal slug suspended within a cylindrical, hollow-core transformer in the main shaft. The LVDT scales the output voltage over a range of ϕ equal to

± 45° (Coats, 1991), although output voltages exist for the entire vertical range of the bivane (+50° with tail up, -60° with tail down).

3.3.1.2. Cruciform-Tail Bivane

Similarly, the gill (or cruciform) bivane is powered by an outside power source. However, the vane's use of dual potentiometers allowed for a desired input/output voltage range to be determined by the user. Both azimuth and vertical angles are determined through the use wiper potentiometers, where the contact point of the wiper rotates with the vane for the particular plane of motion. A bead chain moves with the wiper potentiometer measuring the vertical angle, and is attached to a pulley in the base of the vane. A small counterweight prevents the chain from kinking, and eliminates backlash (R.M. Young, 1977).

3.3.2. Determination of Operational Characteristics

As with the three-cup anemometer, the bivane was tested to determine its linearity of response and exact transfer function. The vane was secured in an upright position, with the shaft perpendicular to a leveled surface. The vane was then displaced by known angles, and the resultant output voltages were recorded. Five runs per angle were made, with increments of 5° between zero and ± 50° (Note: a positive value of ϕ corresponds to the tail of the vane being lifted past the horizontal reference point, where ϕ = 0). The five runs were averaged to determine a mean output voltage per angle, which was plotted and analyzed using commercial software[10].

3.3.2.1 Dual-Annulus Bivane

Unlike the other instruments tested, the output voltages for the dual-annulus bivane displayed a pronounced non-linearity (Figure 6). Although output voltages for angles ranging between -10° and -50° were nearly linear, the remaining output voltages were decidedly not. An empirically derived linear regression function was not sufficiently representative of the output voltages for angles between -5° and +50°, and neither were several curve fitting techniques attempted. Separate least-squares, best-fit regressions between each adjacent angle were subsequently chosen to create a piece-wise overall transfer function. This approach, while somewhat unusual, was deemed adequate because the average output voltage per angle over each of the five runs was virtually identical. The voltage output pattern also was nearly identical to the last test conducted on this vane (Coats, 1991). The resultant regression functions between angles is listed in Table 1.

3.3.2.2. Cruciform-Tail Bivane

One distinct advantage of using the gill bivane was the high linearity of output voltages. The vane had a maximum range of motion of ± 57° in the vertical plane. With a 5.0 vdc power source applied to the vane, output voltages ranged from 0.0 vdc with the tail displaced downward to its furthest extent, to 4.93 vdc for a maximum upward tail displacement. Voltages from intermediate angles confirmed the nearly perfect linearity of output voltages.

Figure 6. Average output voltages for Climatronics Dual-Annulus bivane, showing non-linear output (especially between +20° and +50°).

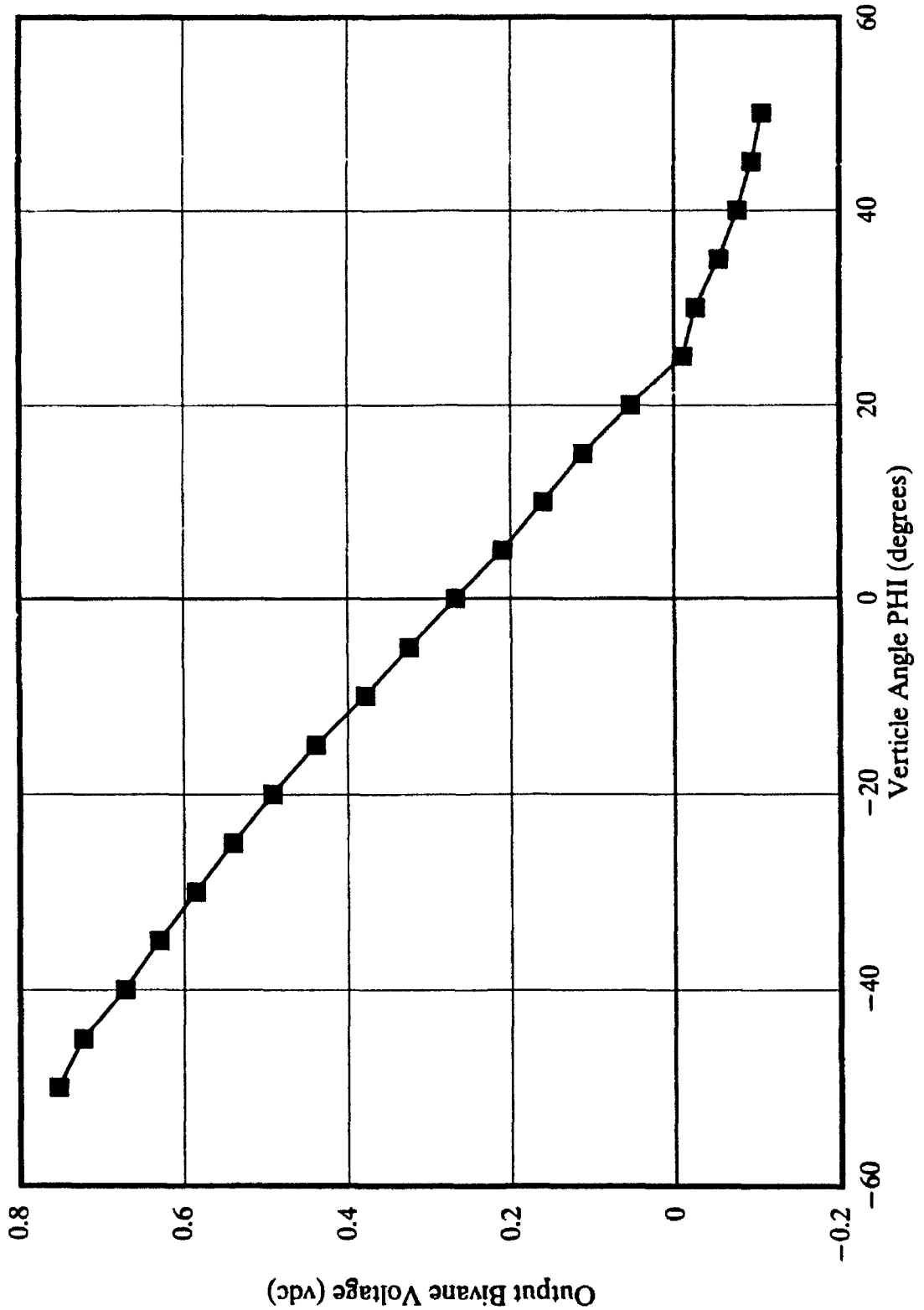
Output Bivane Voltage (vdc)
0.8
0.6
0.4
0.2
0
-0.2
-60
-40
-20
0
20
40
60
Verticle Angle PHI (degrees)

Figure 6

Table 1. Piece-wise Transfer Function Used for Climatronics Dual-Annulus Bivane.

ANGULAR RANGE	TRANSFER FUNCTION
<-45°	ϕ = (volt * -166.6666667) + 75.5
≥-45° to <-40°	ϕ = (input voltage * -98.039216) + 25.882353
≥-40° to <-35°	ϕ = (input voltage * -119.047619) + 40.0
≥-35° to <-30°	ϕ = (input voltage * -113.636364) + 36.5909091
≥-30° to <-25°	ϕ = (input voltage * -108.6956526) + 33.695652
≥-25° to <-20°	ϕ = (input voltage * -104.1666667) + 31.25
≥-20° to <-15°	ϕ = (input voltage * -92.592592) + 25.555556
≥-15° to <-10°	ϕ = (input voltage * -83.333333) + 21.5
≥-10° to <-5°	ϕ = (input voltage * -92.5925926) + 25.0
≥-5° to <0°	ϕ = (input voltage * -87.71929825) + 23.4210526
≥0° to <5°	ϕ = (input voltage * -87.7192983) + 23.4210526
≥5° to <10°	ϕ = (input voltage * -100.0) + 26.0
≥°10 to <15°	ϕ = (input voltage * -102.0408163) + 26.326531
≥15° to <20°	ϕ = (input voltage * -86.206897) + 24.568966
≥20° to <25°	ϕ = (input voltage * -79.3650794) + 24.206349
≥25° to <30°	ϕ = (input voltage * -312.5) + 21.875
≥30° to <35°	ϕ = (input voltage * -178.571429) + 25.357143
≥35° to <40°	ϕ = (input voltage * -217.391304) + 23.2608696
≥40° to <45°	ϕ = (input voltage * -294.1176706) + 17.352912
≥45°	ϕ = (input voltage * -416.6666667) + 5.8333333

The transfer function derived for the vane was:

$$\phi = 23.119 v_{out} - 56.494 \qquad (31)$$

where v_{out} is the bivane output voltage in vdc, and ϕ is the derived vertical angle in degrees.

4. FIELD PROCEDURES

The field experiments were carried out from 30 April through 13 August 1992. The location was the Cherry Lane Meteorological Field Observation Station, about three kilometers northwest of the Purdue University campus. This area satisfied the criteria for the experiment location; the terrain was nominally flat and extensive, consisting of a grassy surface surrounded by farm fields (Figure 7). There were few protruding surface elements, the largest being a row of instrument shelters. The shelters were 1.5 meters high, and were located approximately 17 meters from the test site. There were a few trees, the closest located 60 meters from the test site. The site was nominally flat, with no noticeable sloping (Figures 8 and 9).

The experiment utilized an existing free-standing tower, which allowed for the placement of a boom on which the instruments could be mounted. The tower had a triangular cross-section, with the boom mounted along one face. The boom consisted of two metal beams. The upper-most beam was extended orthogonally from the tower at a height of 3.8 meters from the ground. The lower beam was extended diagonally upwards from the tower to the end of the upper beam. The boom had a cross-bar mounted on its end, upon which the instruments were mounted. The cross-bar was approximately 1.8 meters long, and was situated 2.5 meters from the closest tower face. (Figure 10). The bar was leveled to within one-half degree after instrument installation with the aid of

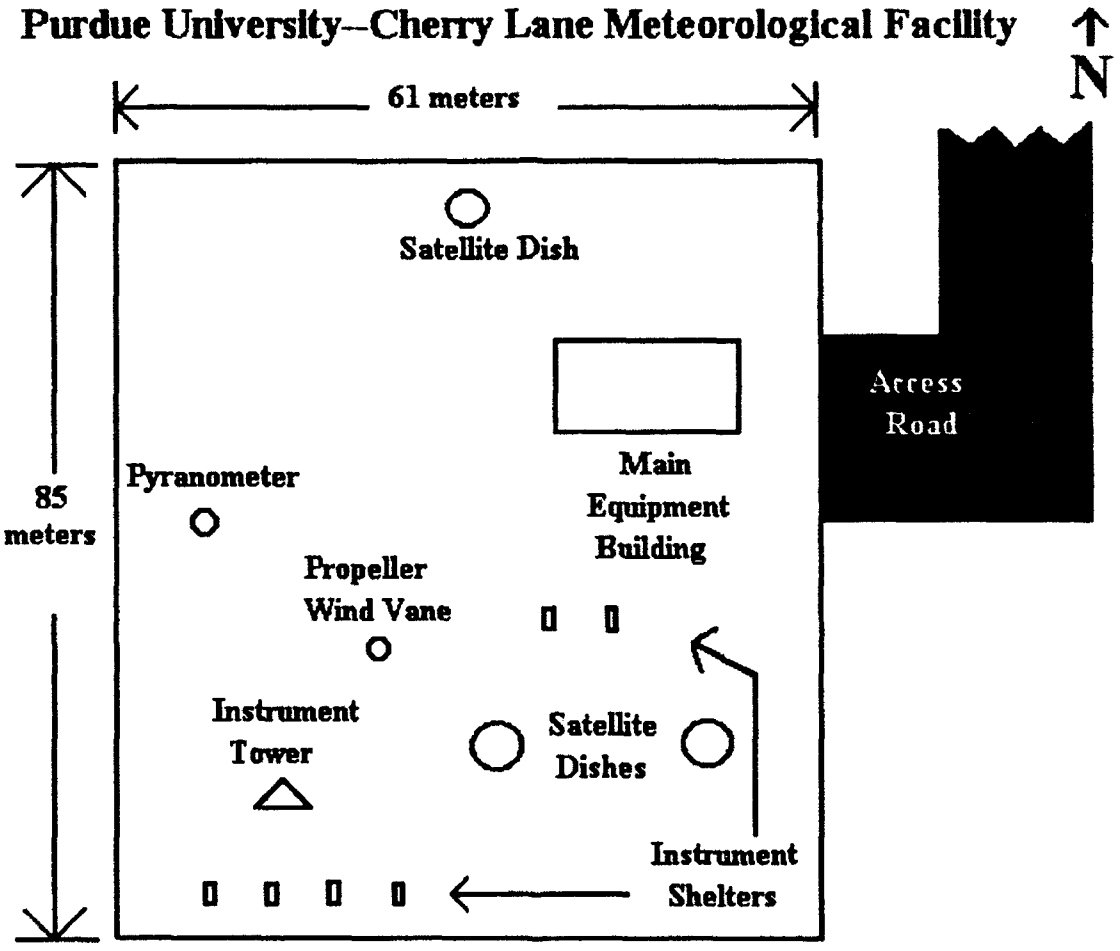

Figure 7. Overhead layout of Cherry Lane Meteorological Facility (Note: drawing is not exactly to scale).

Figure 8. Experiment site at Cherry Lane Meteorological Facility, with instrument shelters adjacent to instrument tower.

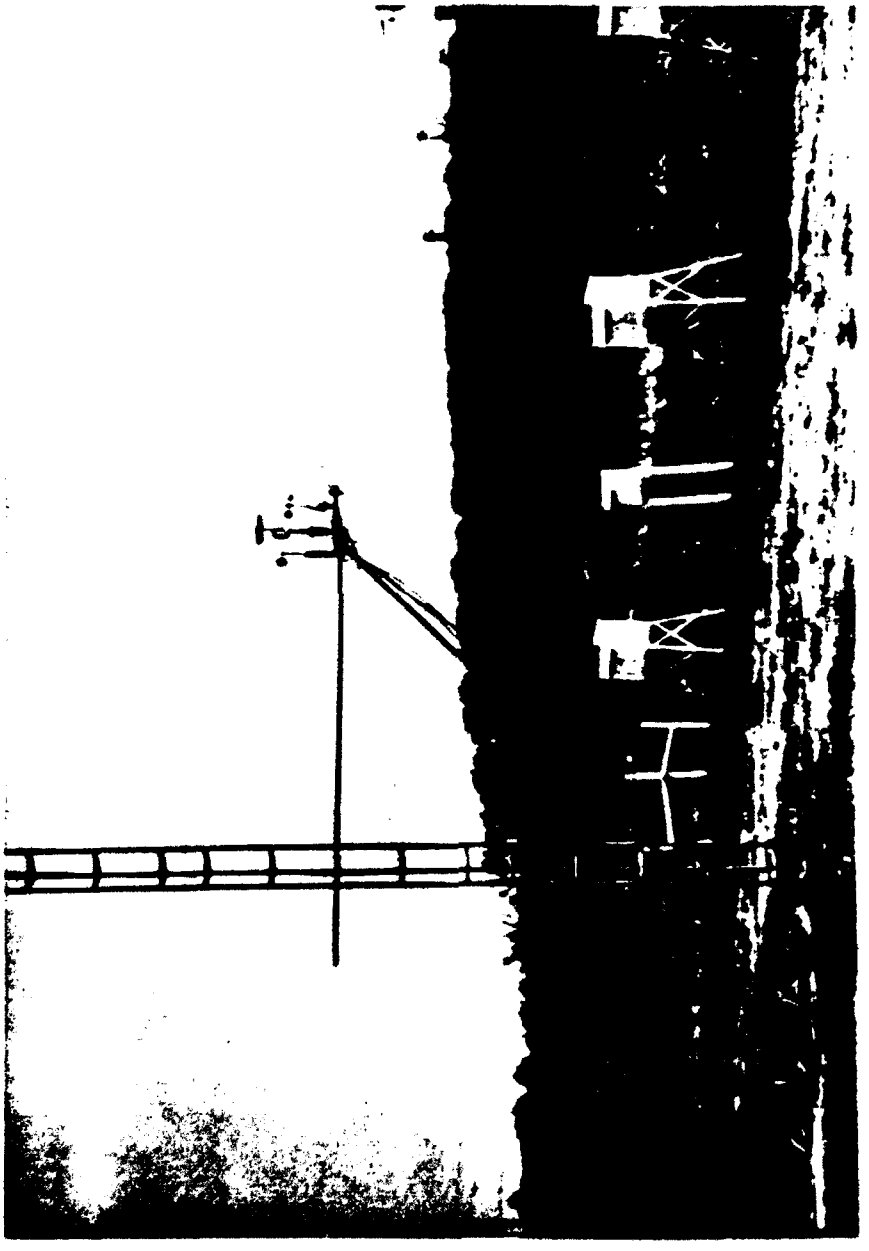

Figure 8

Figure 9. Same as Fig. 8, but with computer set-up included.

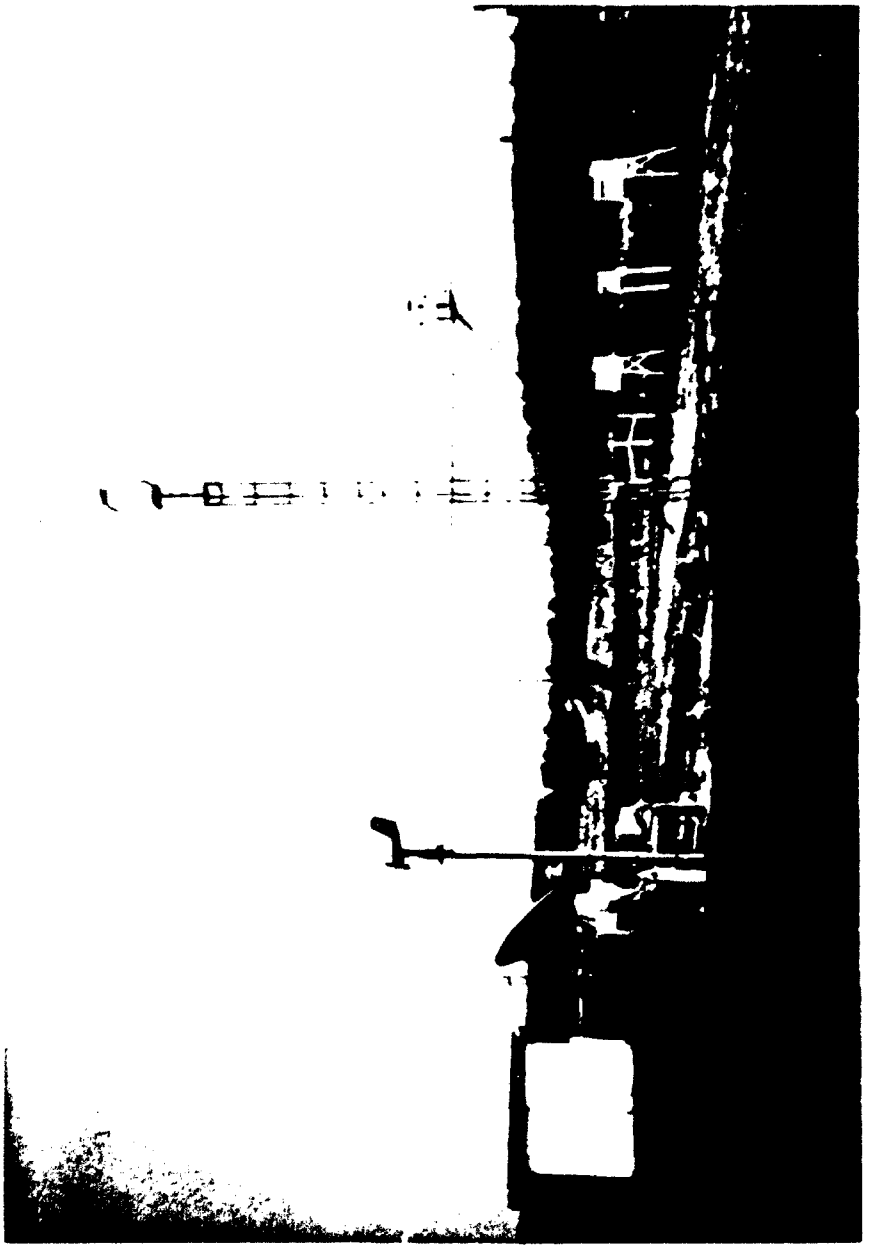

Figure 9

Figure 10. Instruments positioned on cross-bar: (left to right) cup anemometer, sonic anemometer probe, helicoid propeller anemometer, dual-annulus bivane.

Figure 10

a bubble-level.

The boom was aligned such that the sonic anemometer, which was the only fixed (i.e., irrotational) instrument, pointed towards the southwest (the prevalent wind direction for the experiment period) (Figures 11 & 12). Thus, with a mean flow between 180° and 270°, any wake effects induced by the tower or the instrumentation itself would be minimized. Experiments were not conducted on days when the mean direction was either outside this range or displayed a variable trend outside the desired range. Also, since the Analog-to-Digital[11] (A/D) board used could not ingest voltages in excess of ± 10 volts (vdc), this limited the maximum detectable horizontal wind component from the sonic anemometer to 20 m s^{-1}. Similarly, the maximum detectable vertical component was limited to 5 m s^{-1}.

4.1. Instrument Configuration

The primary concern with instrument configuration on the cross-bar was providing sufficient spacing between instruments without compromising the ability of all of the instruments to sample the same air parcel simultaneously (a parcel being defined as a finite mass of 'air' having uniform turbulent characteristics). In reality, this is not feasible; the fact the instruments cannot be exactly co-located precludes this possibility. With this limitation in mind, and since the length of the cross-bar was fixed, the instruments were subsequently positioned on the bar in a manner that would minimize turbulent effects between instruments. The three-cup anemometer and dual-annulus bivane were placed near the extreme ends of the bar, with the sonic anemometer and a helicoid propeller anemometer (not used in

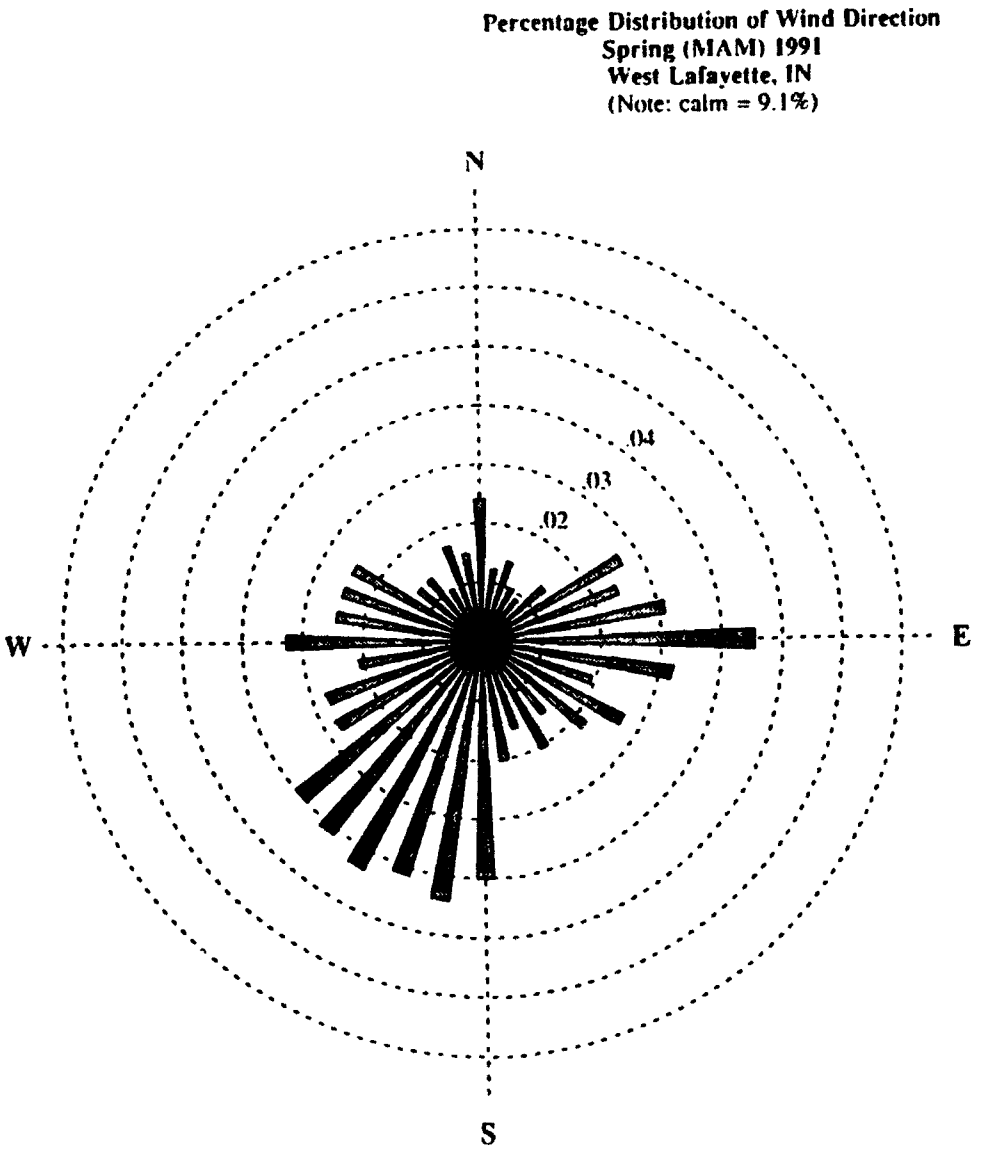

Figure 11. Wind rose of directional frequency for West Lafayette, IN, for Spring (March-May) 1991, similar to climatological norms (data and analysis provided by Dr. E.M. Agee).

Figure 12. As in Fig 11, for Summer (June-August) 1991, similar to climatological norms (data and analysis provided by Dr. E.M. Agee).

this experiment) placed inward from the edges (Figure 10). Although the spacing between instruments was not uniform, as they had different shapes and sizes, each was separated by approximately 45 cm from adjacent instruments.

For the final field test, the dual-annulus bivane was replaced with a gill or cruciform-tailed vane. This vane was considerably larger than its predecessor, necessitating the removal of the helicoid anemometer from the cross-bar to insure proper spacing between instruments. Since it was considerably heavier than any of the other instruments, the gill bivane was placed in the center of the cross-bar to prevent tilting. The sonic anemometer probe was subsequently moved to the end opposite from the cup anemometer.

4.2. Data Collection Procedure

Each instrument was connected to a nearby computer[12] for data acquisition (Figure 13). Output analog voltages from the instruments were recorded and subsequently transformed into digital format with the A/D computer board, exactly as in the wind tunnel tests. Each data set consisted of 15 minutes of data, sampled at a rate of five samples per second (i.e., 5 Hz), for 4501 total data points. The data was time-based and recorded using a second acquisition software package[13].

During the initial data collection period (30 April 1992), the following parameters were recorded: sonic anemometer u-, v-, and w-components, cup anemometer u-component, bivane vertical (ϕ) and horizontal (θ) angles, and the helicoid anemometer w-component. Subsequent data runs also included the virtual temperature from the

Figure 13. Computer and instrument wiring set-up for data collection for 30 April 1992 experiment. Each instrument is connected to the Analog-to-Digital (A/D) board in the rear of the computer.

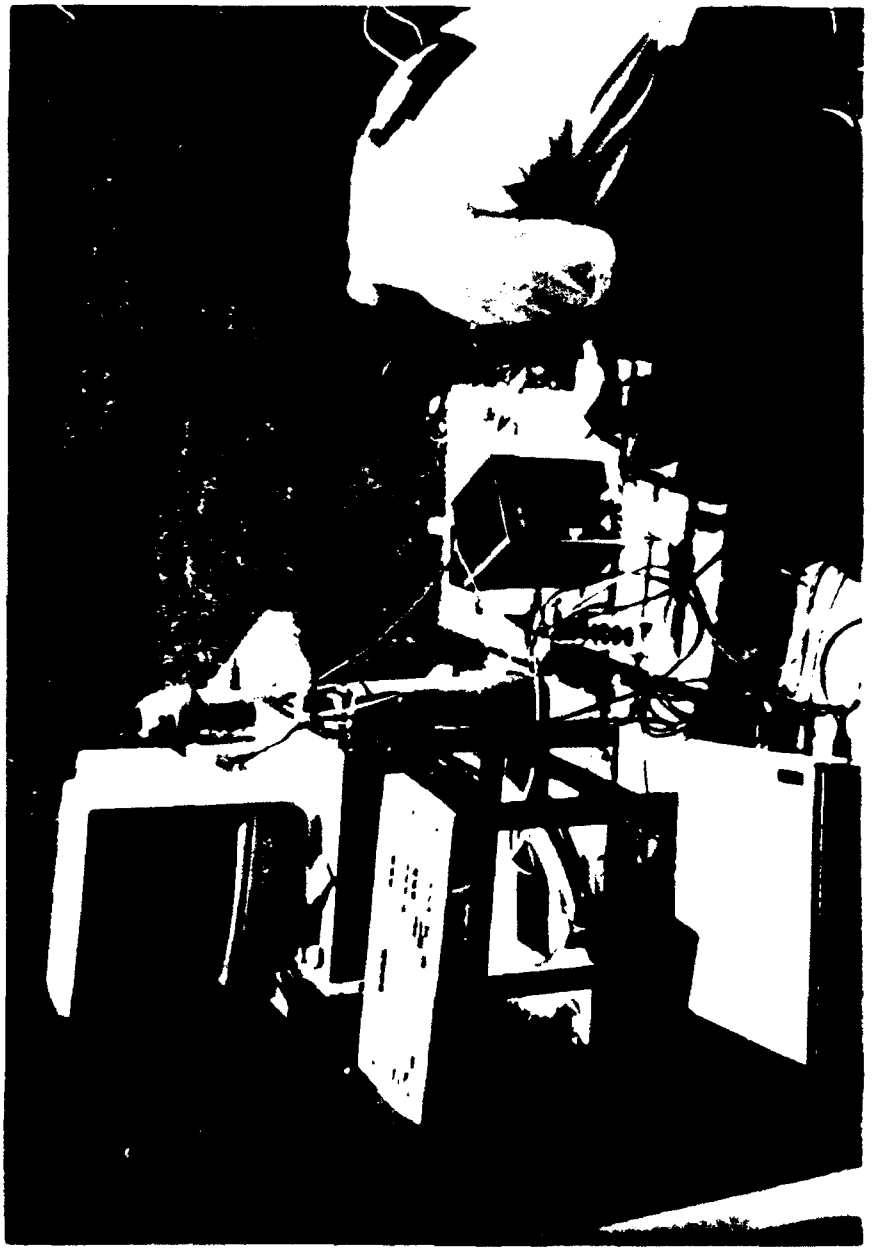

Figure 13

sonic anemometer.

To quantify the atmosphere's turbulent nature, the Monin-Obukov (M-O) stability parameter was estimated, given by

$$\frac{z}{L}, \tag{32}$$

where z is height and the Obukov length scale, L, is approximated by

$$L \simeq \frac{-(\overline{u'w'}^2)^{3/4}}{k(g/\bar{T}_v)(\overline{w'T_v'})} \tag{33}$$

where k is von Karman's constant (0.40), g is the gravitational constant (9.81 m s^{-1}), and T_v is the virtual temperature in degrees K. Note that $w'T_v'$ is measured with the sonic anemometer.

5. POST-COLLECTION DATA PROCESSING

Each base (i.e., unfiltered) data set was processed to convert instrument output voltages into components using the derived transfer functions. Converted components included the u-, v-, and w-components for the sonic anemometer, the u-component from the cup anemometer, and horizontal angle θ and vertical angle ϕ from the bivane.

Once these components were obtained, other required values were calculated. A total horizontal wind component was derived for the sonic anemometer by taking the square root of the sum of squares of the u- and v- components (Note: from this point forward, 'u' refers to the total horizontal component unless specifically stated otherwise).

From the horizontal and vertical components, an estimated instantaneous vertical angle for the sonic anemometer was computed:

$$\phi_{son}(t) = \tan^{-1}\left[\frac{w_{son}(t)}{u_{son}(t)}\right] \tag{34}$$

An estimated instantaneous w-component was derived using the u-component from the cup anemometer and the bivane vertical angle ϕ:

$$w_{est}(t) = u_{cup}(t)\tan(\phi_{biv}(t)) \tag{35}$$

Instantaneous sonic anemometer and estimated (derived from the

cup/bivane system) covariances from the vertical and horizontal components were also derived:

$$u'w'_{son}(t) = (\bar{U}_{son}-u(t)_{son})(\bar{W}_{son}-w(t)_{son}) \quad (36)$$

$$u'w'_{est}(t) = (\bar{U}_{cup}-u(t)_{cup})(\bar{W}_{est}-w(t)_{est}) \quad (37)$$

5.1. Temporal Analysis

A statistical analysis (including mean, variance, range, etc...) of the base (i.e., actual) time-series for measured and derived components was performed for each data run. A similar analysis was performed on the detrended base data (i.e., with the least-squares, best-fit regression line subtracted off). Additionally, statistical analyses were performed on filtered data (using a 21 point running average) and detrended filtered data for the first data set only. Filtering was not employed on either of the subsequent runs.

5.1.1. Momentum Flux Computations

To address the problem listed in 1.1. and check Chimonas' mathematical reasoning, four values of momentum flux were calculated using either the eddy-correlation or approximation methods. These were:

τ: the closest estimation of the 'true' momentum flux. τ was determined using sonic anemometer mean wind covariances in the eddy-correlation method (9);

τ_{MC-cb}: the MCAM (24) using the cup anemometer and bivane. τ_{MC-cb}

utilized mean values of u_{cup} and ϕ_{biv} and a derived bivane offset angle (20);

τ_{EC-cb}: an eddy-correlation estimation (9) using the cup anemometer and bivane. τ_{EC-cb} utilized the time-series mean of the instantaneous estimated covariance (37);

τ_{check}: a mathematical check of the MCAM (24), using time-series mean values of u and ϕ_{son} (34) from the sonic anemometer and a derived sonic vertical offset angle (using $\bar{u}_{son}$ and $\bar{w}_{son}$ in (20)).

To address the questions posed in 1.1., momentum flux values calculated for τ_{MC-cb} and τ_{EC-cb} were compared with corresponding values of τ. To check the mathematical and physical reasoning used by Chimonas' in his derivation of the CAM, flux values computed using the same instruments but different flux estimation methods (τ and τ_{check}, τ_{MC-cb} and τ_{EC-cb}) were compared.

5.2. Spectral Analysis

A spectral analysis was performed on the component used in the flux computations: actual and derived time-series for horizontal and vertical components, vertical angle, and covariance of horizontal and vertical wind components.

The procedure employed is similar to that given in Kaimal and Kristensen (1990). First, the base data was filtered with a 21-point running average to diminish aliasing (or folding). The middle 4096 (or 2^{12}; the largest number that could be processed with the software used) data points were then isolated, and the remaining data points were

discarded. The remaining filtered data was then detrended. A Fast Fourier Transform (FFT) was performed on the data, converting the temporal series to a frequency spectrum.

To ensure the transform was correctly accomplished, the area under each spectral curve was computed using a simple Reimann sums technique. The area of a linear-linear plot of power vs. frequency is equal to the variance of the pre-transformation temporal data set. Once this relationship was confirmed, each power spectrum was plotted to see if it followed the five-thirds law for turbulent diffusion.

6. RESULTS AND DISCUSSION

The results of the field experiments are presented here, with emphasis on three points: the response characteristics of the instruments and their effects on the flux calculations; a spectral analysis of the components used in the flux calculations; and the derived values of momentum flux using the different methods.

6.1. Specific Instrument Responses

To better understand the results of the approximation and eddy-correlation methods, the responses of the instrumentation used to obtain these values are examined. Since the generalized response characteristics of interest are common throughout all three data sets, the first set alone will be used to highlight features of note. A complete time-series from the first run for the u- and w-components, vertical angle ϕ, and cross-correlations of horizontal and vertical wind components from the sonic anemometer and the cup/bivane system are presented in a series of figures (each 900 seconds or 15 minutes) in length. These figures are shown in three 300 second panels, so that general response tendencies and features can be readily compared. Specific features of interest are subsequently highlighted in shorter intervals.

Although it is not physically possible for each instrument to sense the same parcel of air, general comparisons can be made if

turbulent features persist for sufficient duration. Using Taylor's Theory of 'Frozen Turbulence', which hypothesizes that eddies maintain their shape, structure, and turbulent properties while being advected, an attempt can be made to compare and contrast instrument response characteristics. Based on the mean horizontal wind speed from the first run (1.69 m s^{-1}), the distance constant for the cup anemometer (2.63 m; Snow et al., 1989), and the natural wavelength of the dual-annulus bivane (2.50 m; Coats, 1991), only features exceeding 6.0 seconds in length will be considered[14].

Generalized dynamic response characteristics (for zeroth-, first-, and second-order systems) of the various instruments are reviewed in the appendix at the end of this publication.

6.1.1. Horizontal Wind Component

Cup anemometer data from the first experiment are shown in Figures 14-16. Concurrent data from the sonic anemometer are shown in Figures 17-19.

The cup response is similar to that of a first-order system, and displays the expected linear response characteristics relative to the signal from the sonic anemometer. For example, Figure 20 shows the cup response clearly lags that of the sonic anemometer. A peak is clearly evident in the sonic trace at 184 seconds; the corresponding peak is not evident in the cup response for another three seconds beyond that point. The value if the peak is also attenuated: the sonic measured the peak wind of 3.8 m s^{-1}, while the maximum cup speed is approximately 0.5 m s^{-1} less.

Beyond the peak, as wind speed continues to decrease, the cup

Figure 14. Three-cup anemometer horizontal wind speed for 1202 EST, 30 April 1992: first five minutes (0-300 seconds).

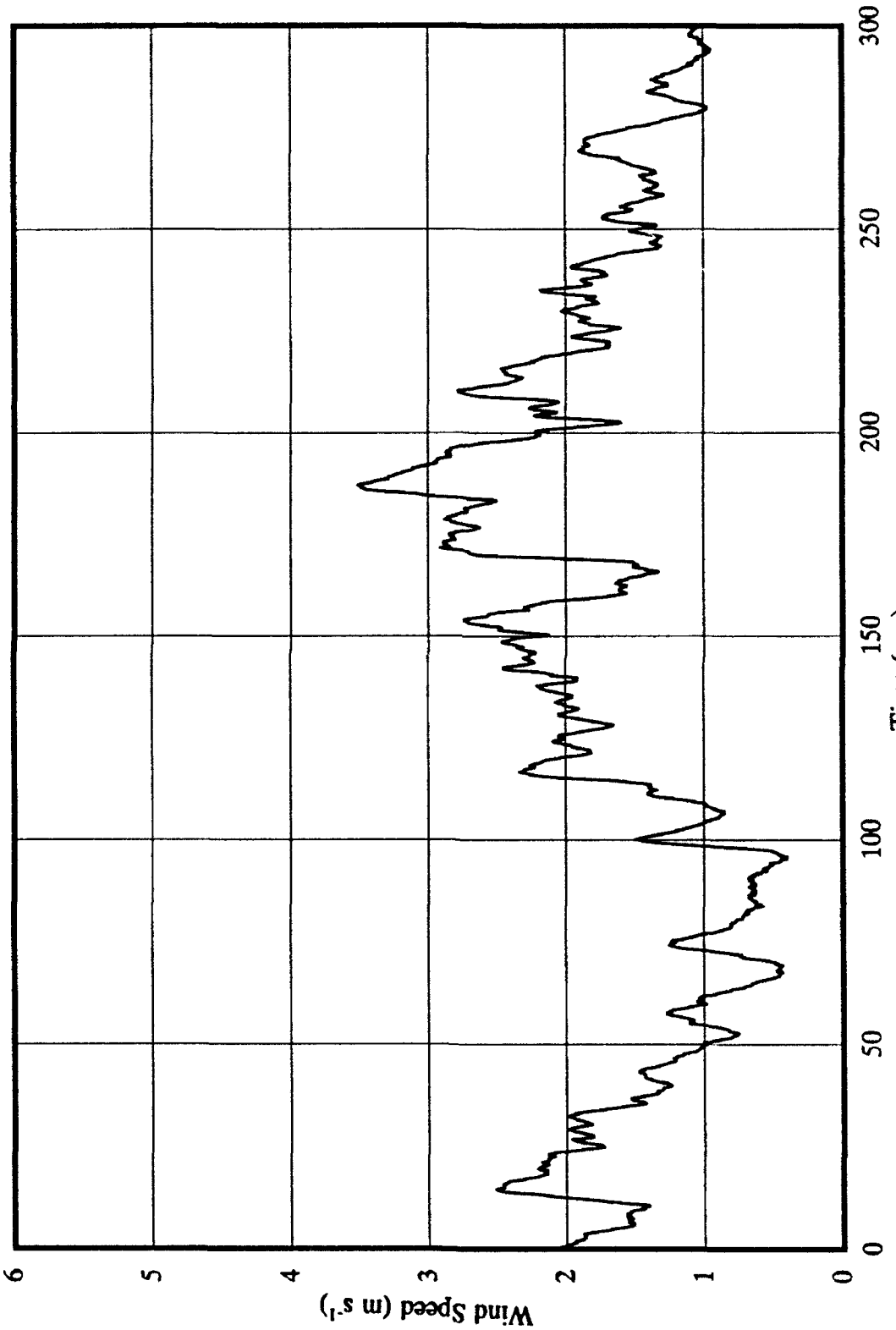

Figure 14

Figure 15. As in Fig. 14, middle five minutes (300-600 seconds).

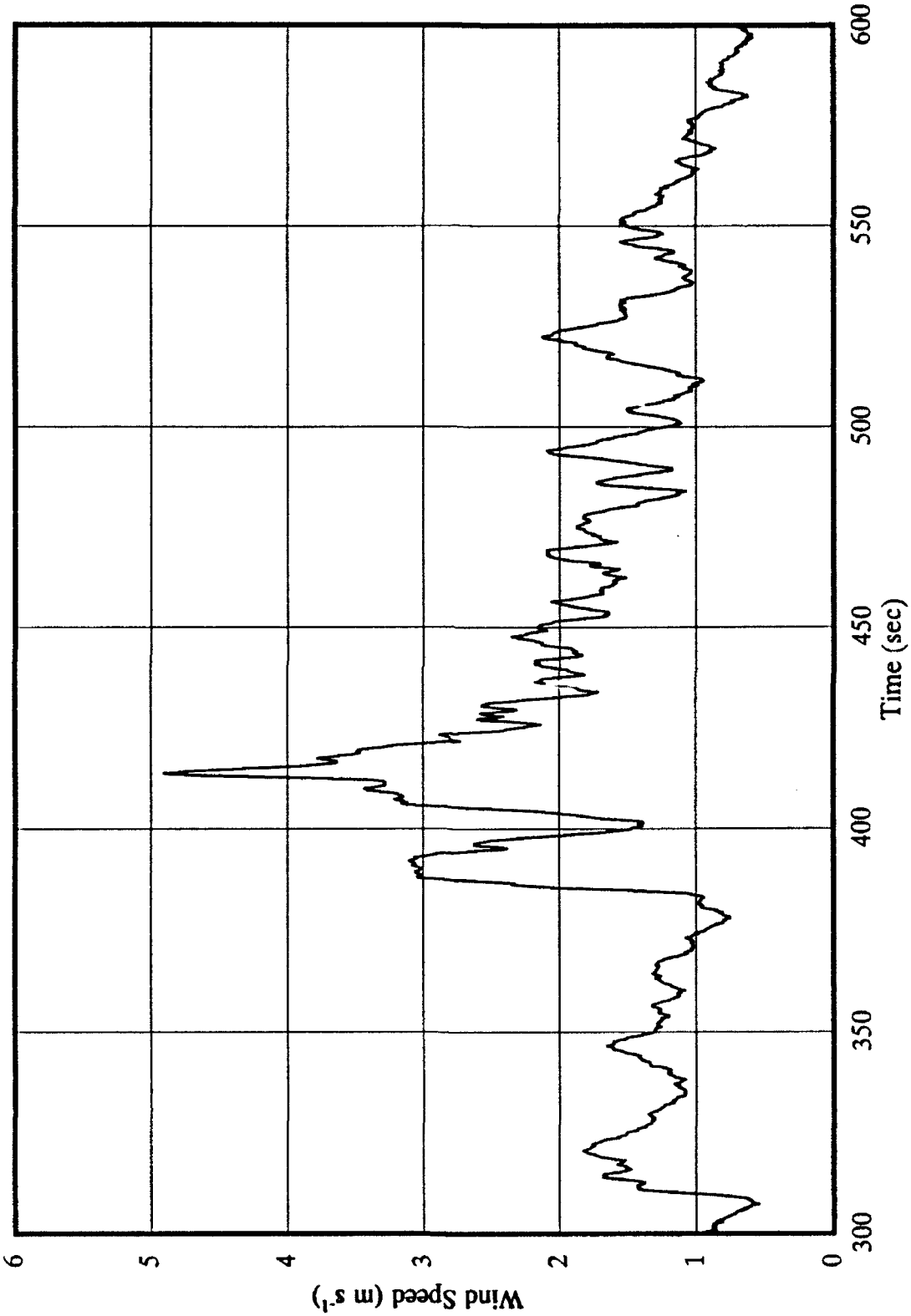

Figure 15

Figure 16. As in Fig. 14, final five minutes (600-900 seconds).

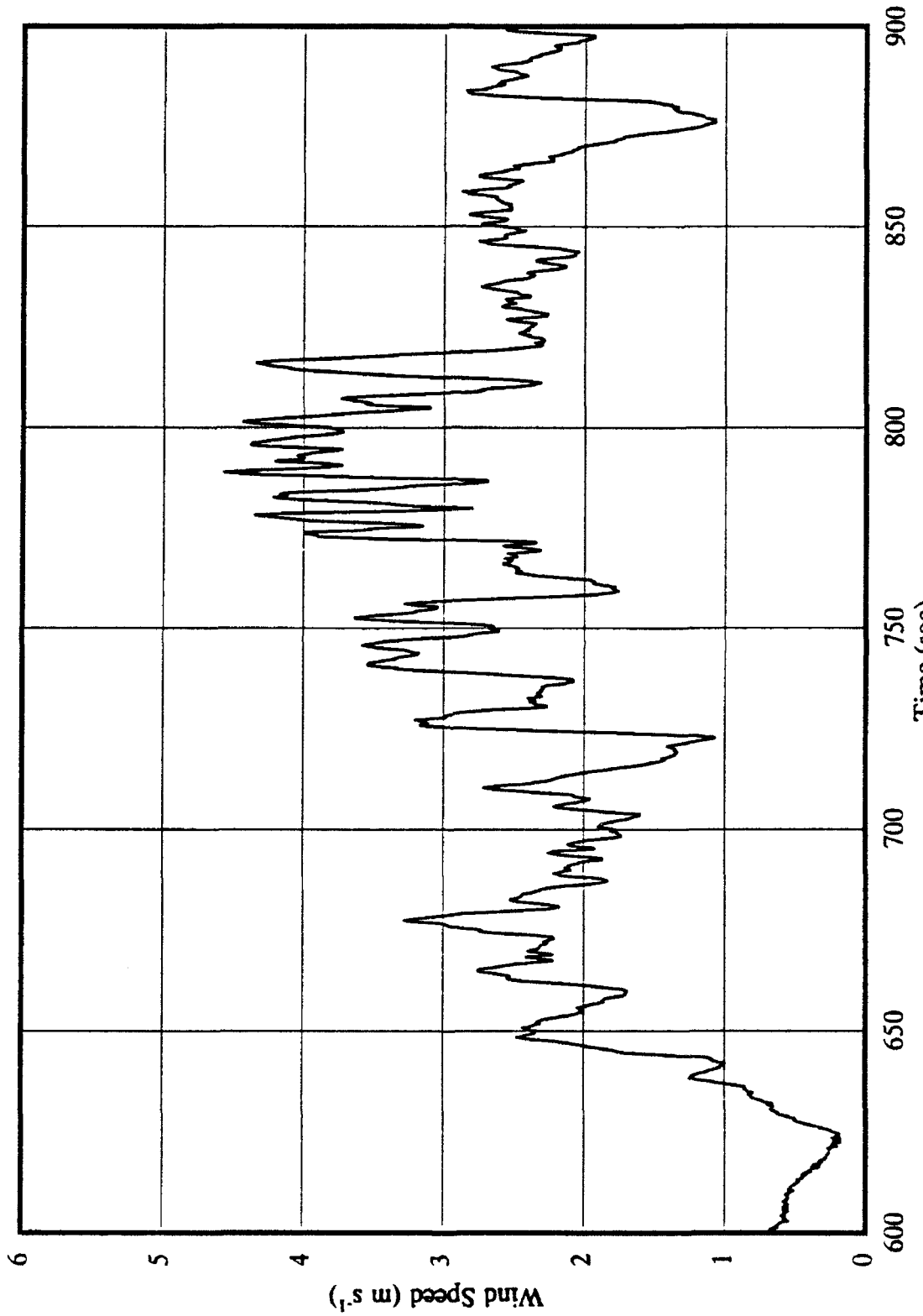

Figure 16

Figure 17. Sonic anemometer horizontal wind speed for 1202 EST, 30 April 1992: first five minutes (0-300 seconds).

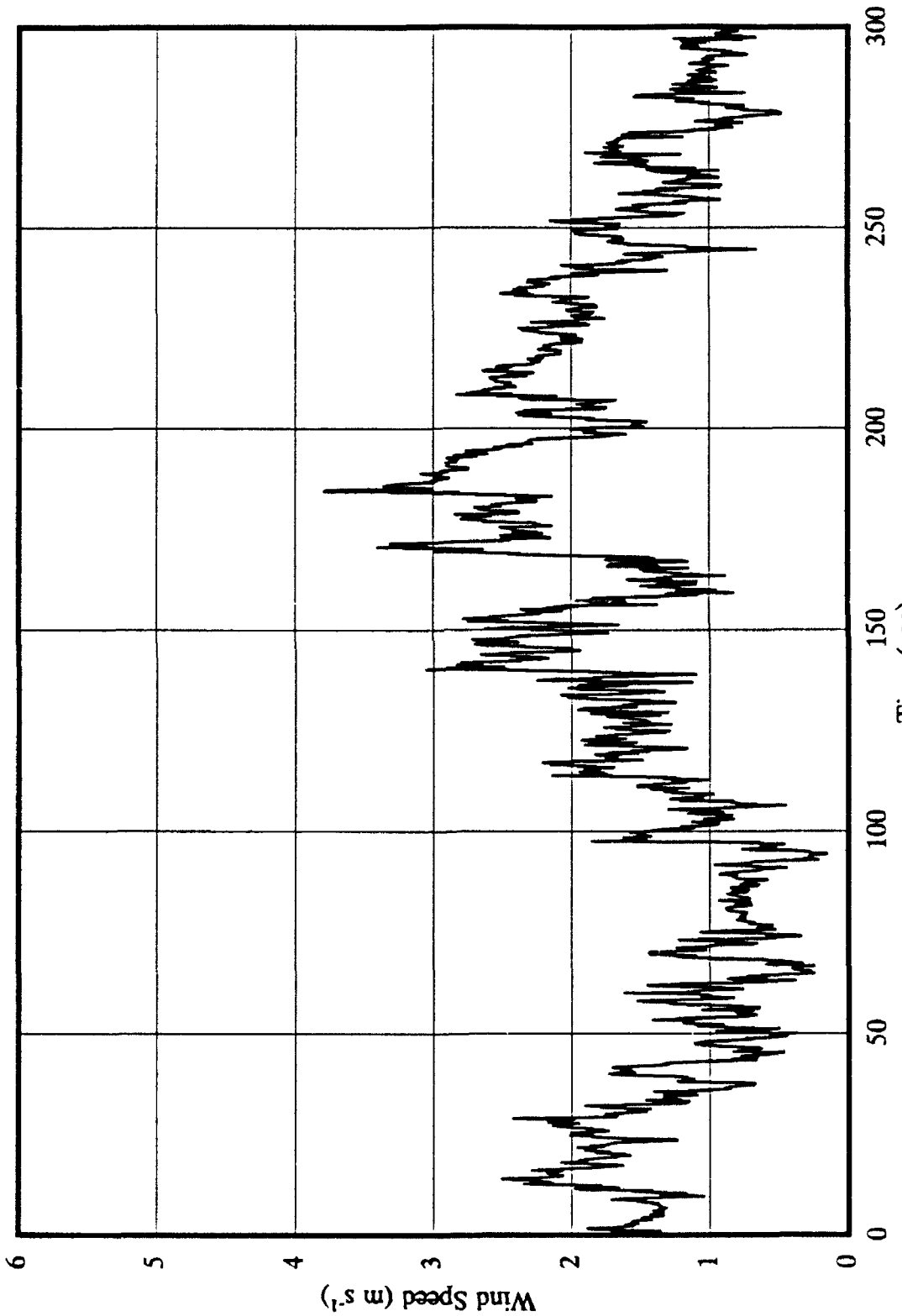

Figure 17

Figure 18. As in Fig. 17, middle five minutes (300-600 seconds).

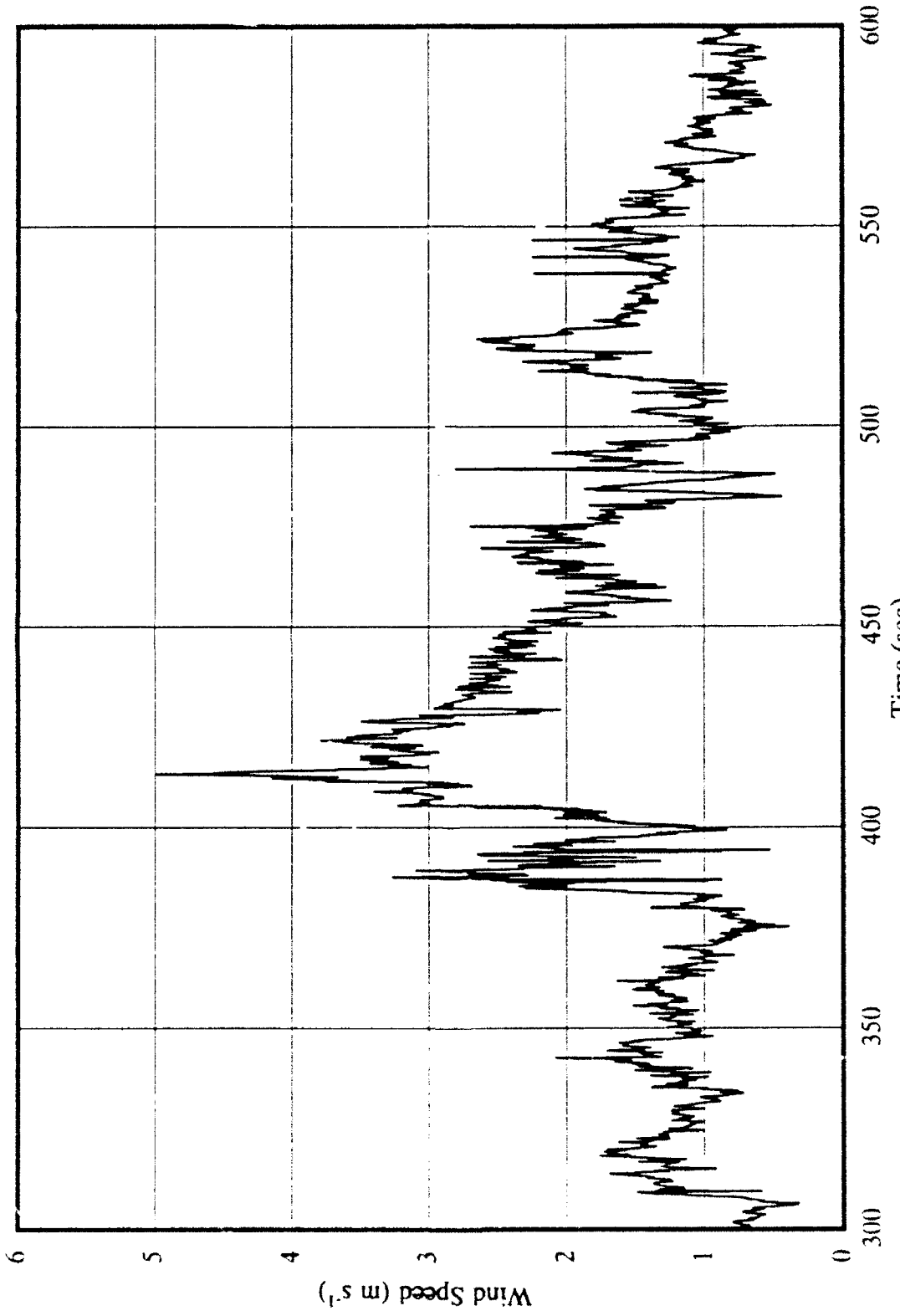

Figure 18

Figure 19. As in Fig. 17, final five minutes (600-900 seconds).

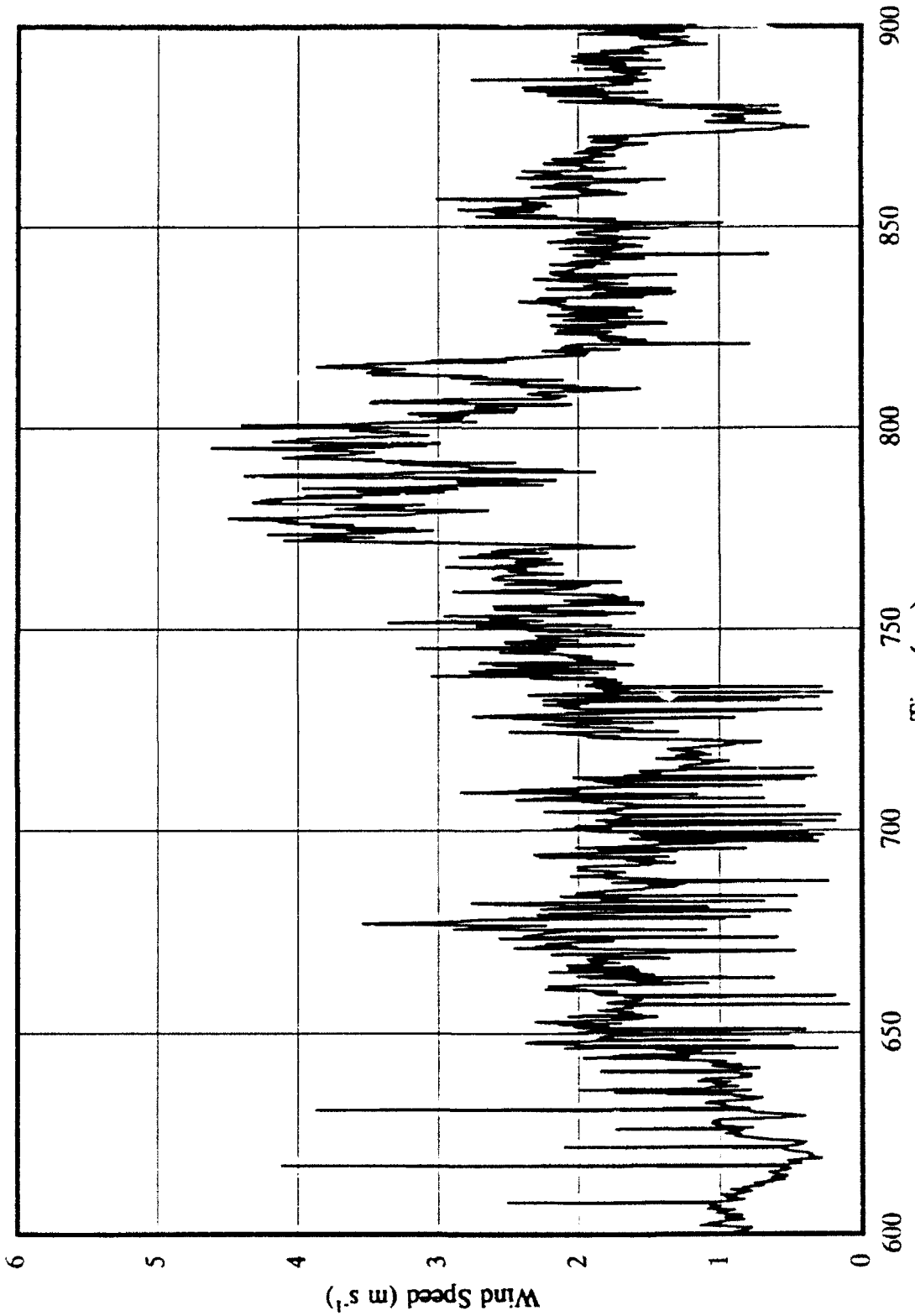

Figure 19

Figure 20. Comparison of sonic and three-cup anemometer horizontal wind speeds for 1202 EST, 30 April 1992: one minute (140-200 seconds).

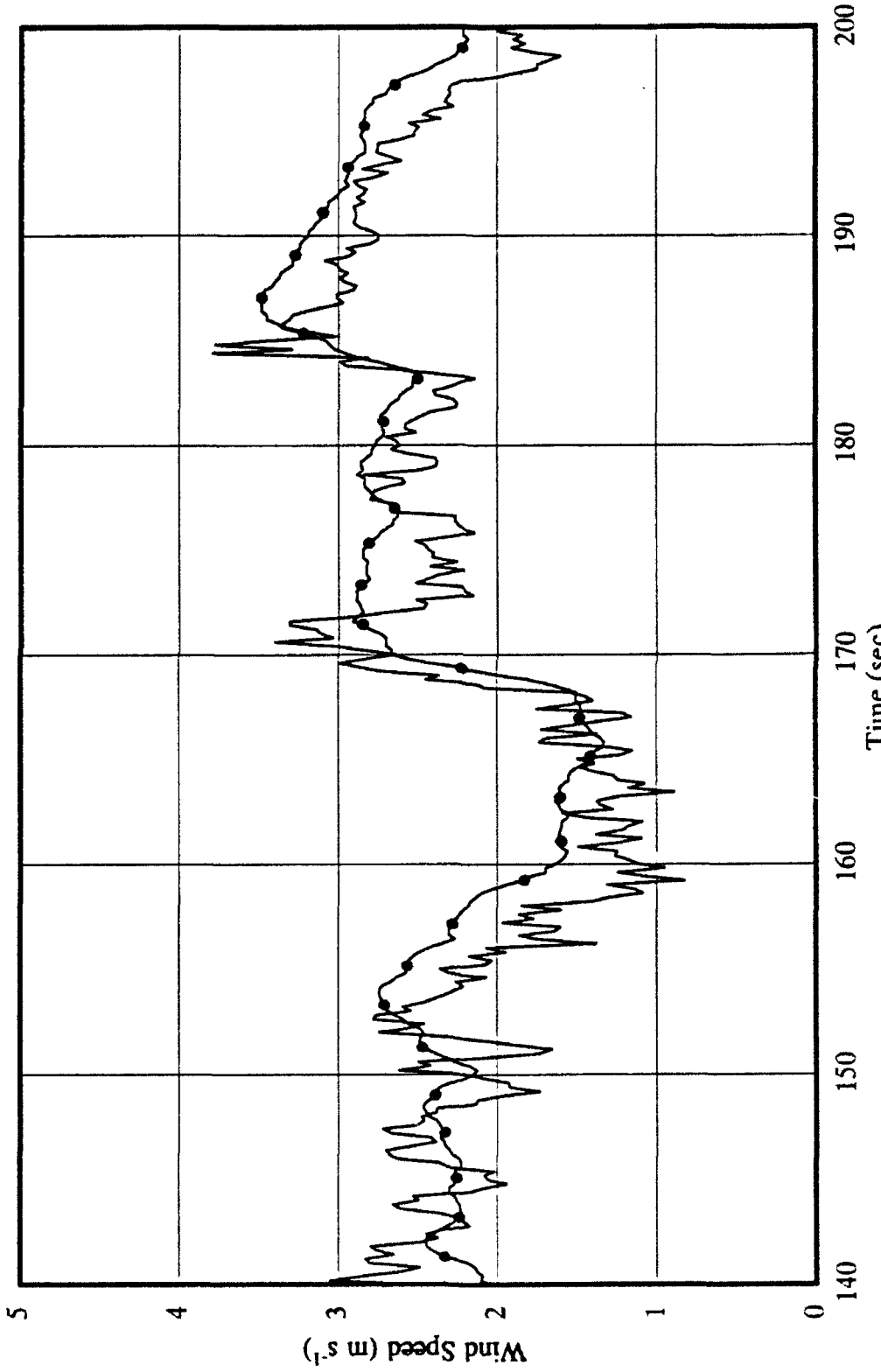
Wind Speed (m s-1)
5
4
3
2
1
0
140
150
160
170
180
190
200
Time (sec)
Sonic Anemometer
Three-Cup Anemometer

Figure 20

trace indicates a higher wind speed than the sonic anemometer. This is an example of the cup overspeeding. Overspeeding is a non-linear effect which cannot be accurately represented with a simple model. It occurs because the cup behaves like a flywheel; speeding up proportionally to the increased wind speed during the gust, but slowing down less rapidly during the lull. The result is, for a finite period of time, the anemometer indicates a higher speed than is truly occurring. This anomalously high speed continues until the increased angular momentum from the gust can be dissipated by frictional forces within the spinning shafts and bearings.

Although not easily seen independent of the effects of phase lag, overspeeding often occurs in turbulent flow (with the amount of overspeeding a function of the intensity of the turbulence). Time-series averages derived from a cup anemometer during gusty periods can overestimate the actual mean horizontal component by more than 20% (Busch and Kristensen, 1976).

Cup anemometers also display poor cosine response; even a properly-leveled cup will respond to a non-zero vertical wind component. Thus, during periods of increased vertical motion, the anemometer may again overestimate the magnitude of the horizontal component. Kaganov and Yaglom (1975) determined this overestimation can be as high as 6% during highly turbulent conditions.

Based on these results, one can anticipate that the mean horizontal component indicated by a cup anemometer during turbulent conditions may be erroneously high. This has an impact on the approximation, $\tau_{MC\text{-}cb}$, which utilizes $\bar{u}_{cup}$, and the eddy-correlation

estimation, τ_{EC-cb}, which uses u'_{cup}. In either case, the resultant flux estimations may be slightly greater due to the slightly higher average speed. Unfortunately, although we can recognize and expect this induced error, there is no standard procedure to determine its magnitude or to correct for it.

In comparison to the cup, the ability of the sonic anemometer to better respond to high-frequency perturbations is evident in Figure 21. Both detect a large eddy between 411 and 417 seconds; however, the sonic detects a number of smaller perturbations within the flow which the cup does not. While it may be that the cup and sonic anemometer are not seeing the exact same parcel during this period, the similarity of overall response implies there is sufficient justification for direct comparison. The abilities of the cup and sonic anemometer to resolve high-frequency fluctuations is further examined in section 6.3.2.

A curious feature is seen in the response of the cup as compared with the sonic anemometer in different mean speed regimes. Although none of the turbulent eddies appears to last sufficiently long to justify a direct comparison, a general pattern seems to emerge. Figure 22 shows a one minute comparison of the two u-components during a relatively low speed period. The mean of the sonic anemometer wind speed during this period is clearly less than 3.0 m s^{-1}, which is taken as the 'true' speed. Note that the speed indicated by the cup anemometer is consistently higher throughout the period. Examining Figure 23, a similar comparison from a subsequent time period, this pattern seems to hold for the first half of the displayed time-series, where the mean sonic speed is still less than 3.0 m s^{-1}. However,

Figure 21. As in Fig. 20, one-half minute (400-430 seconds).

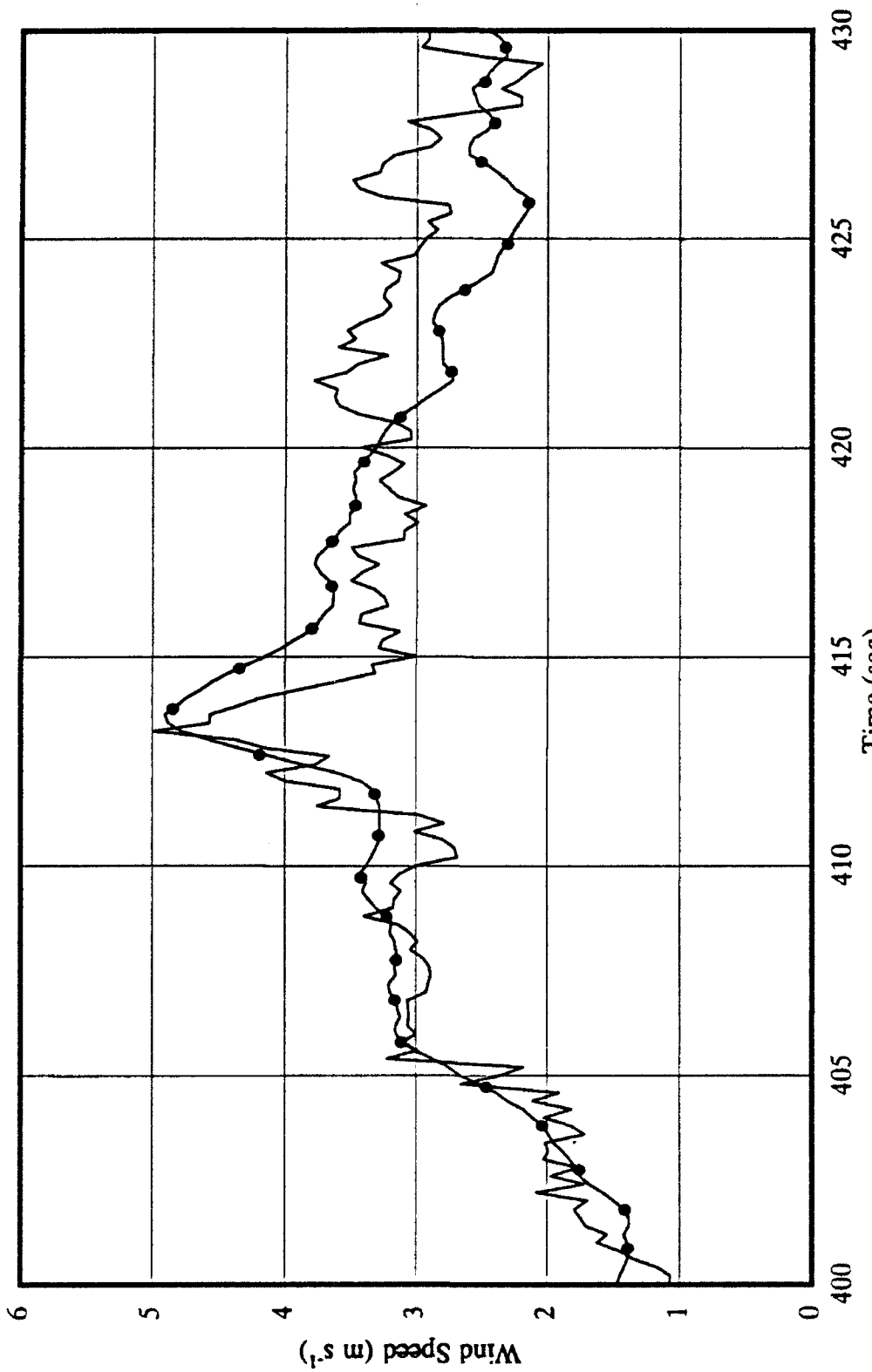
Wind Speed (m s-1)
0
1
2
3
4
5
6
400
405
410
415
420
425
430
Time (sec)
Sonic Anemometer
Three-Cup Anemometer

Figure 21

Figure 22. Comparison of sonic and three-cup anemometer horizontal wind speeds, with means less than 3.0 m s^{-1}, for 1202 EST, 30 April 1992: one minute (640-700 seconds).

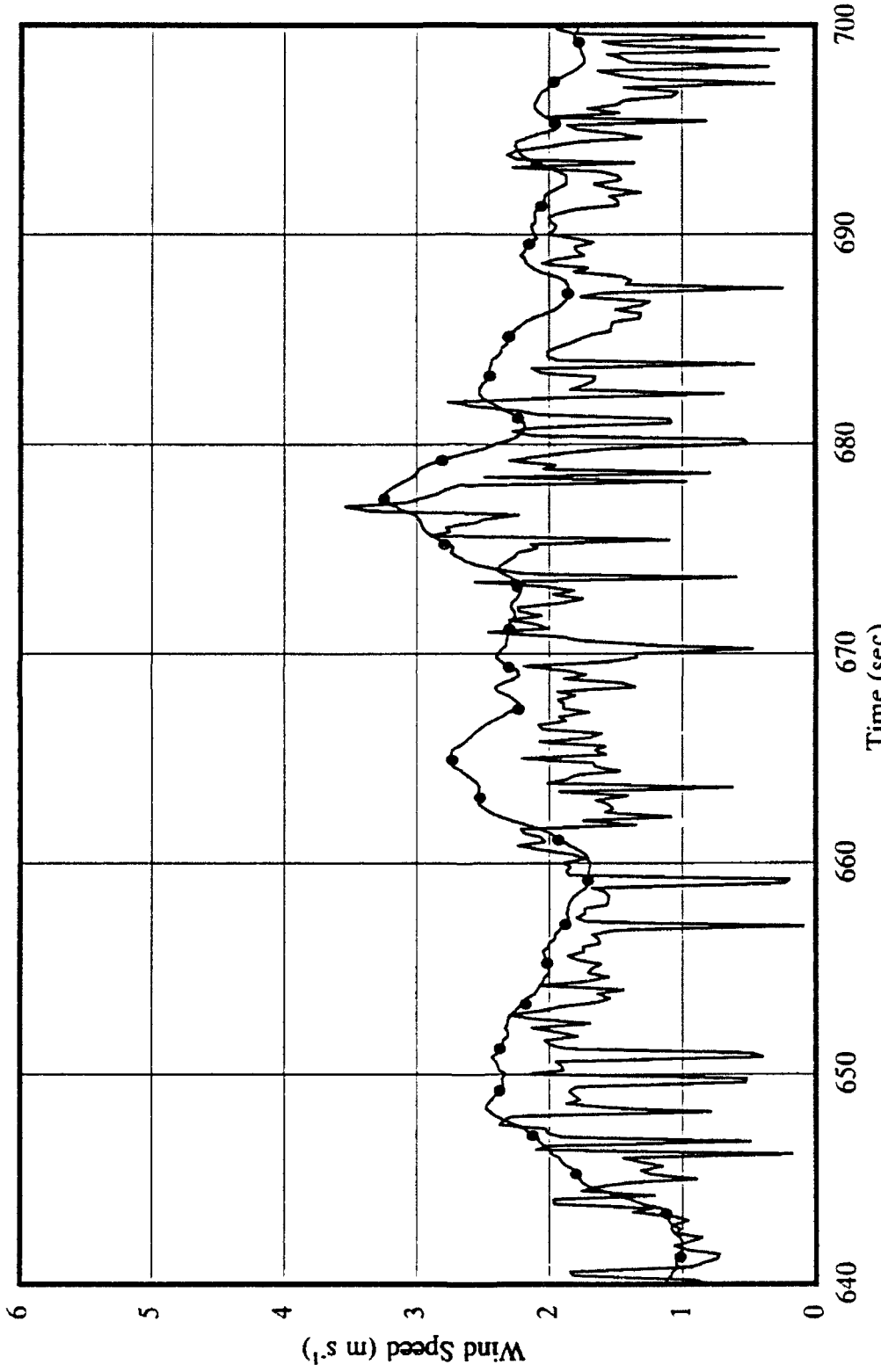
Wind Speed (m s-1)
0
1
2
3
4
5
6
640
650
660
670
680
690
700
Time (sec)
Sonic Anemometer
Three-Cup Anemometer

Figure 22

Figure 23. As in Fig. 22, with means greater than 3.0 m s^{-1}, one minute (740-800 seconds).

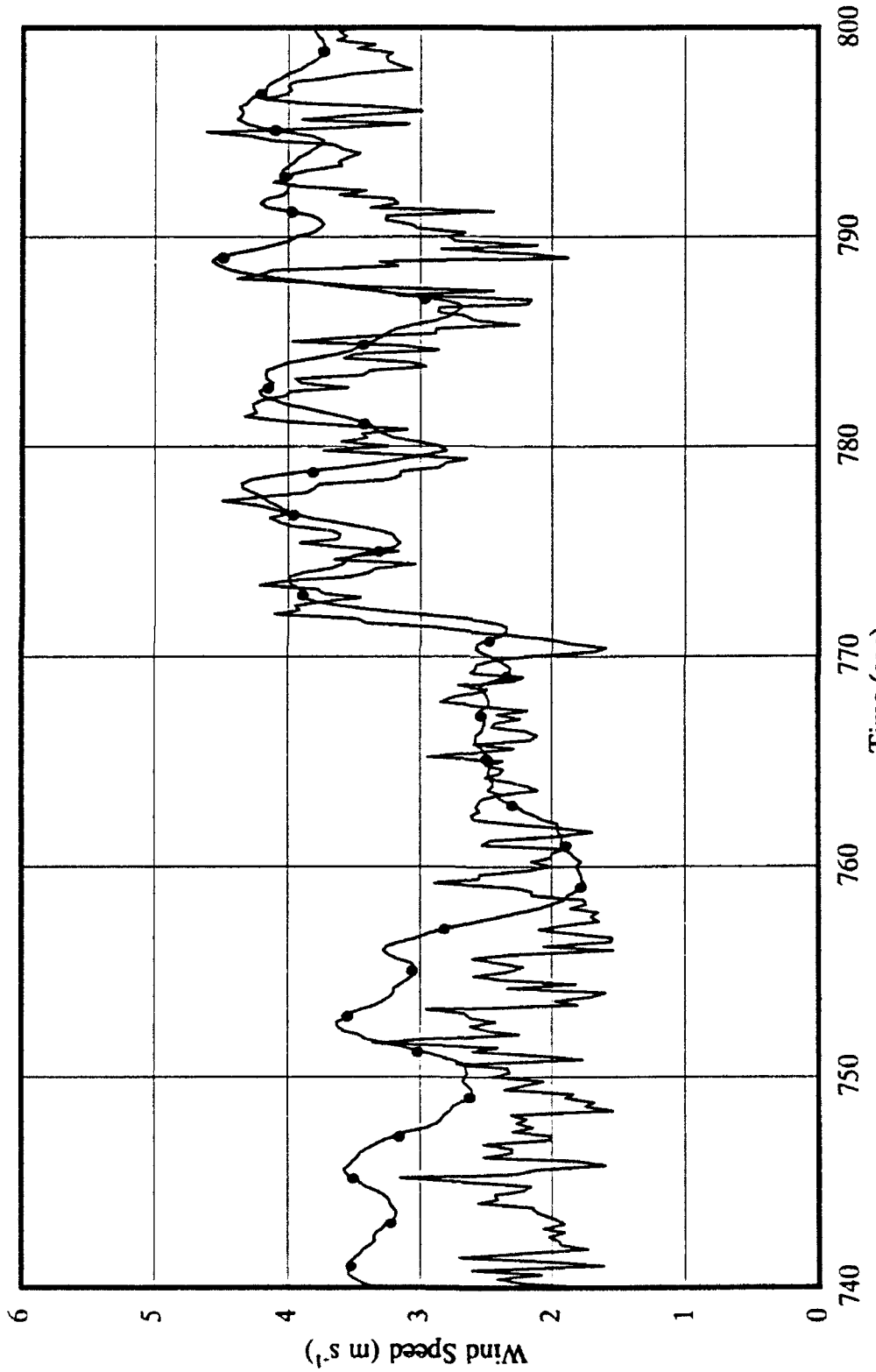
Wind Speed (m s-1)
0
1
2
3
4
5
6
740
750
760
770
780
790
800
Time (sec)
Sonic Anemometer
Three-Cup Anemometer

Figure 23

during the latter half of the interval, (772-800 seconds), the sonic mean speed exceeds that threshold. During this period, the indicated cup speed is much more congruent with the sonic anemometer. While it would be improper to use these figures to justify any specific response characteristics, they may suggest the cup anemometer responds more faithfully to the true wind at higher speeds. Of course, the level of turbulent flow will also affect the cup response, so a defendable hypothesis may not be possible.

6 1.2. Vertical Wind Component

The time-series from the first experiment for the vertical component, as measured by the sonic anemometer, is presented in Figures 24 through 26. The estimated time-series, derived from the bivane and cup anemometer (37), is found in Figures 27 through 29. This estimation is dependent on two instruments demonstrating less-than ideal response.

Examining the vertical components in Figure 30, a curious pattern is seen in the period between 155 and 158.5 seconds. The estimation appears to oscillate with a much greater magnitude than the sonic vertical velocity. This seems unusual in as much as amplitude attenuation would suggest that the estimation's magnitude would be lower than that of the sonic. To determine the cause of this over-estimation, data from the bivane and the cup anemometer are examined during this five-second interval. Figure 31 compares the vertical angle ϕ as measured from the bivane and as derived from the sonic anemometer. This figure clearly shows an over-estimation of the

Figure 24. Sonic anemometer vertical wind speed for 1202 EST, 30 April 1992: first five minutes (0-300 seconds).

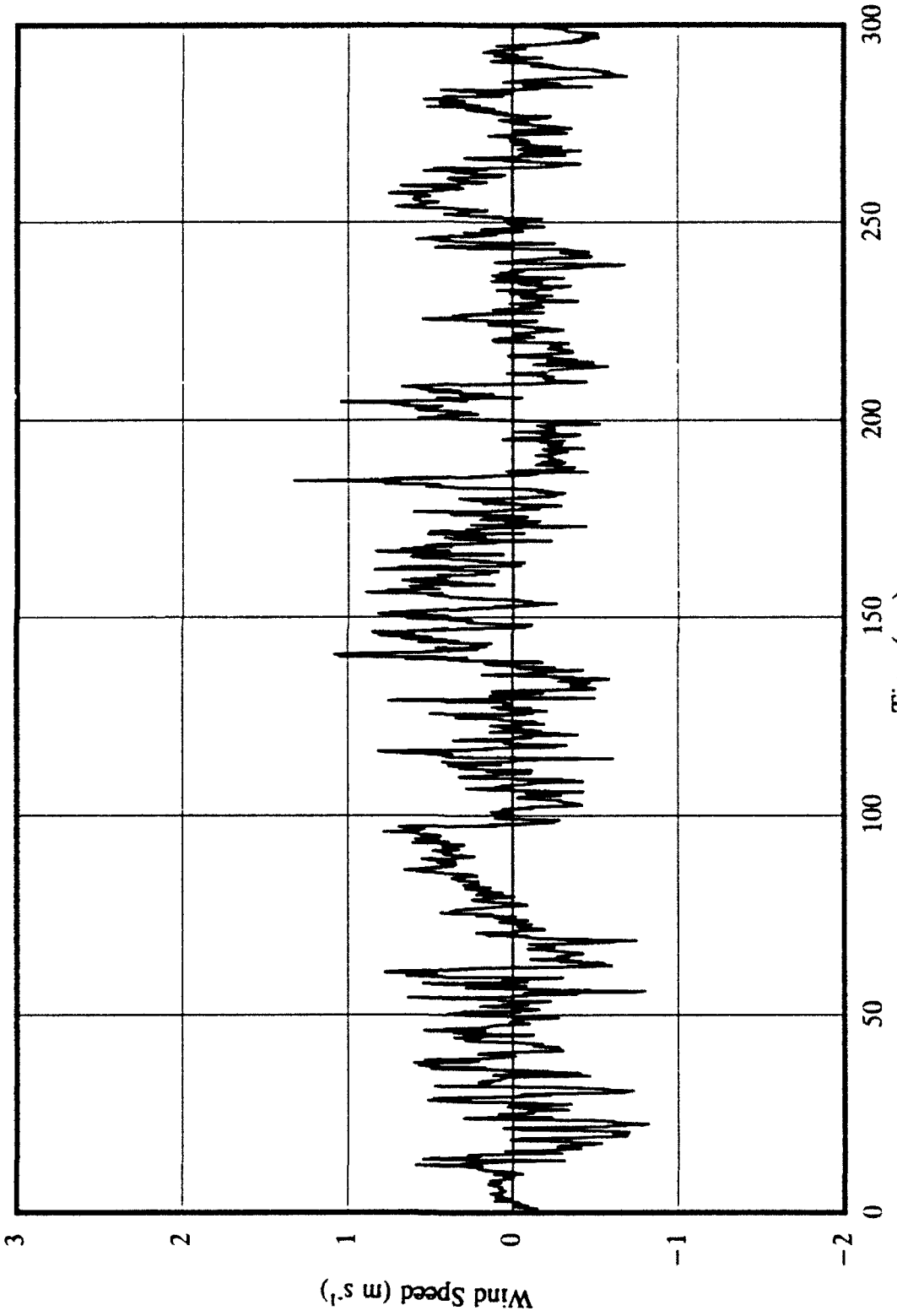

Figure 24

Figure 25. As in Fig. 24, middle five minutes (300-600 seconds).

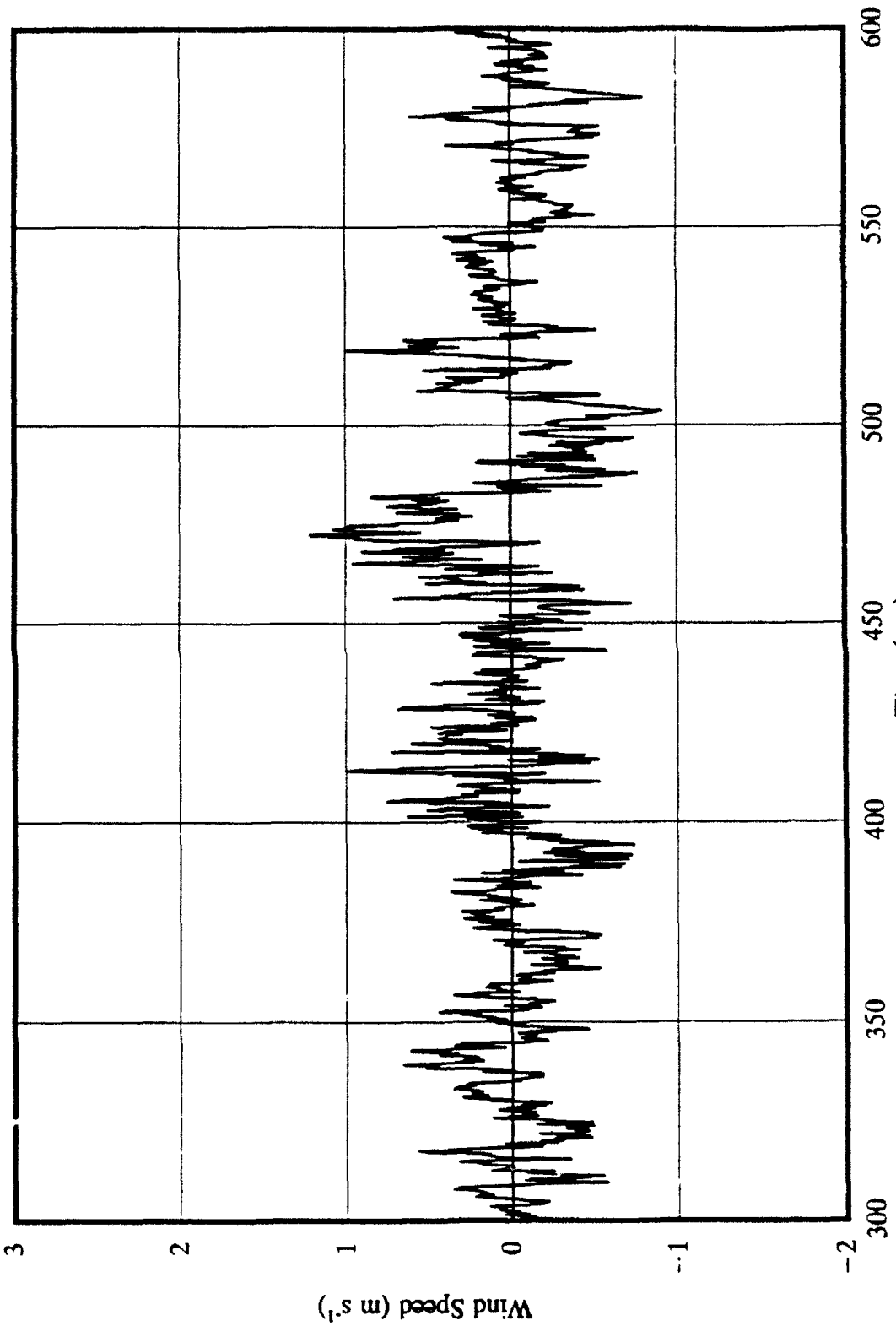

Figure 25

Figure 26. As in Fig. 24, final five minutes (600-900 seconds).

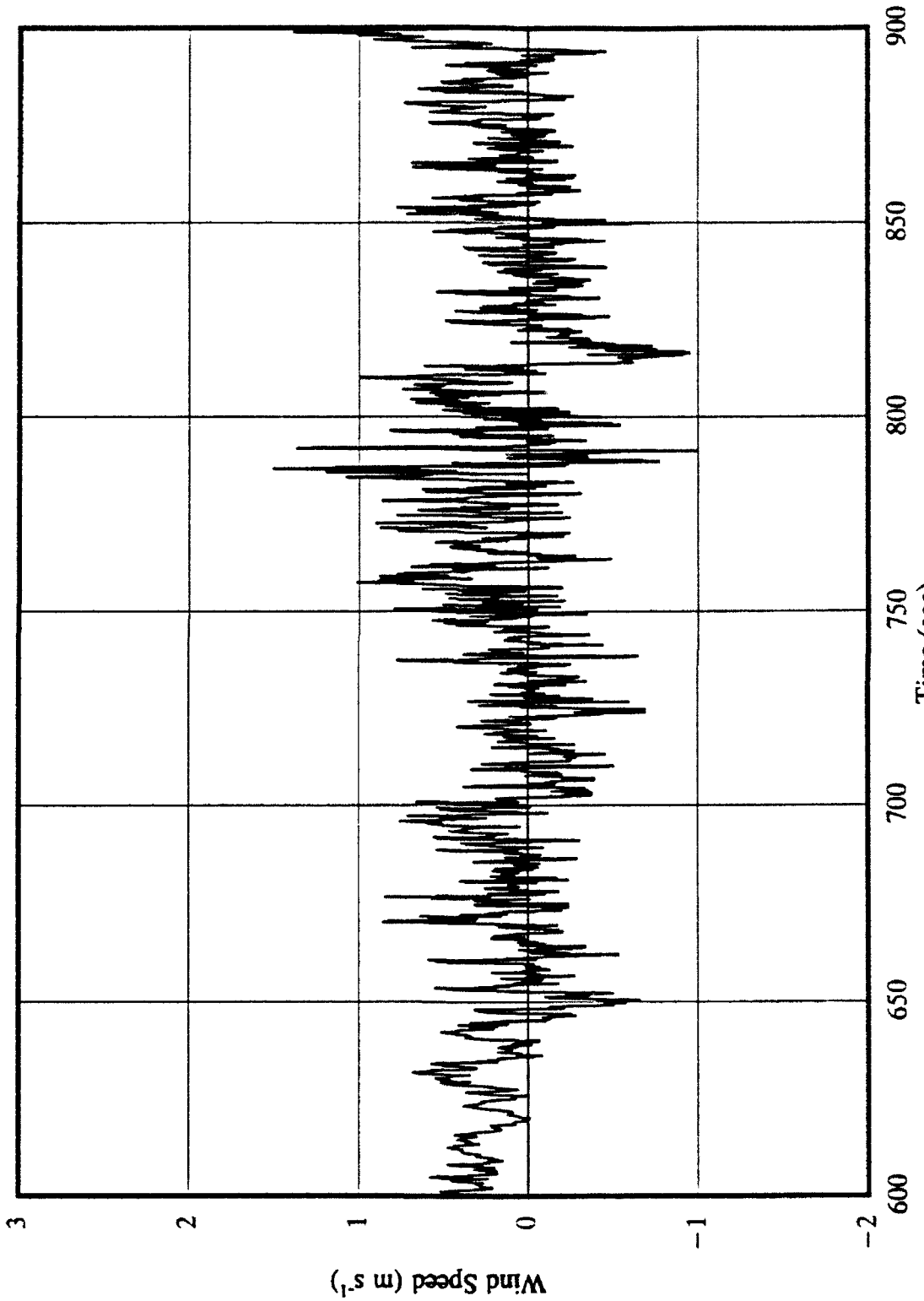

Figure 26

Figure 27. Estimated vertical wind speed for 1202 EST, 30 April 1992: first five minutes (0-300 seconds).

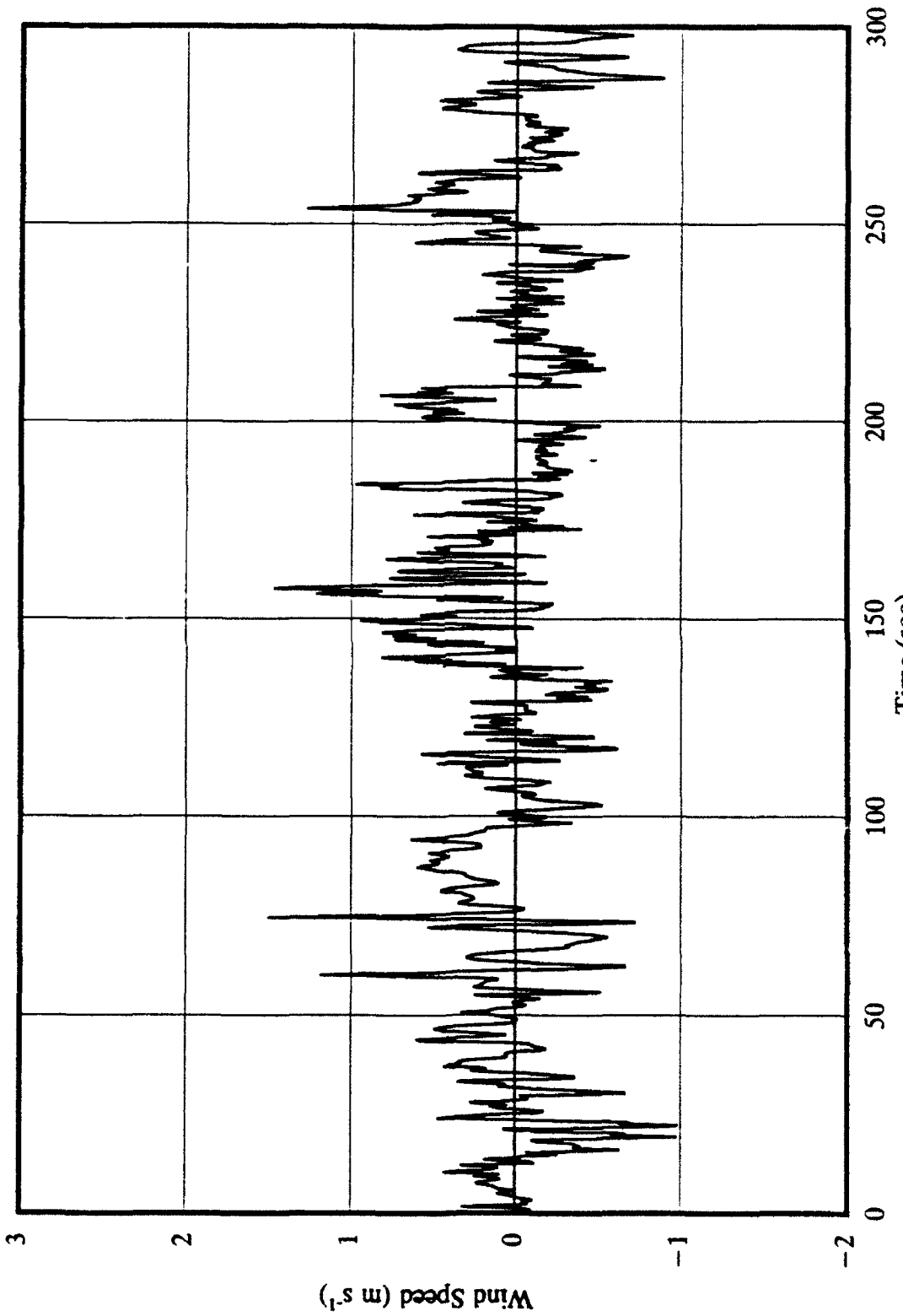

Figure 27

Figure 28. As in Fig. 27, middle five minutes (300-600 seconds).

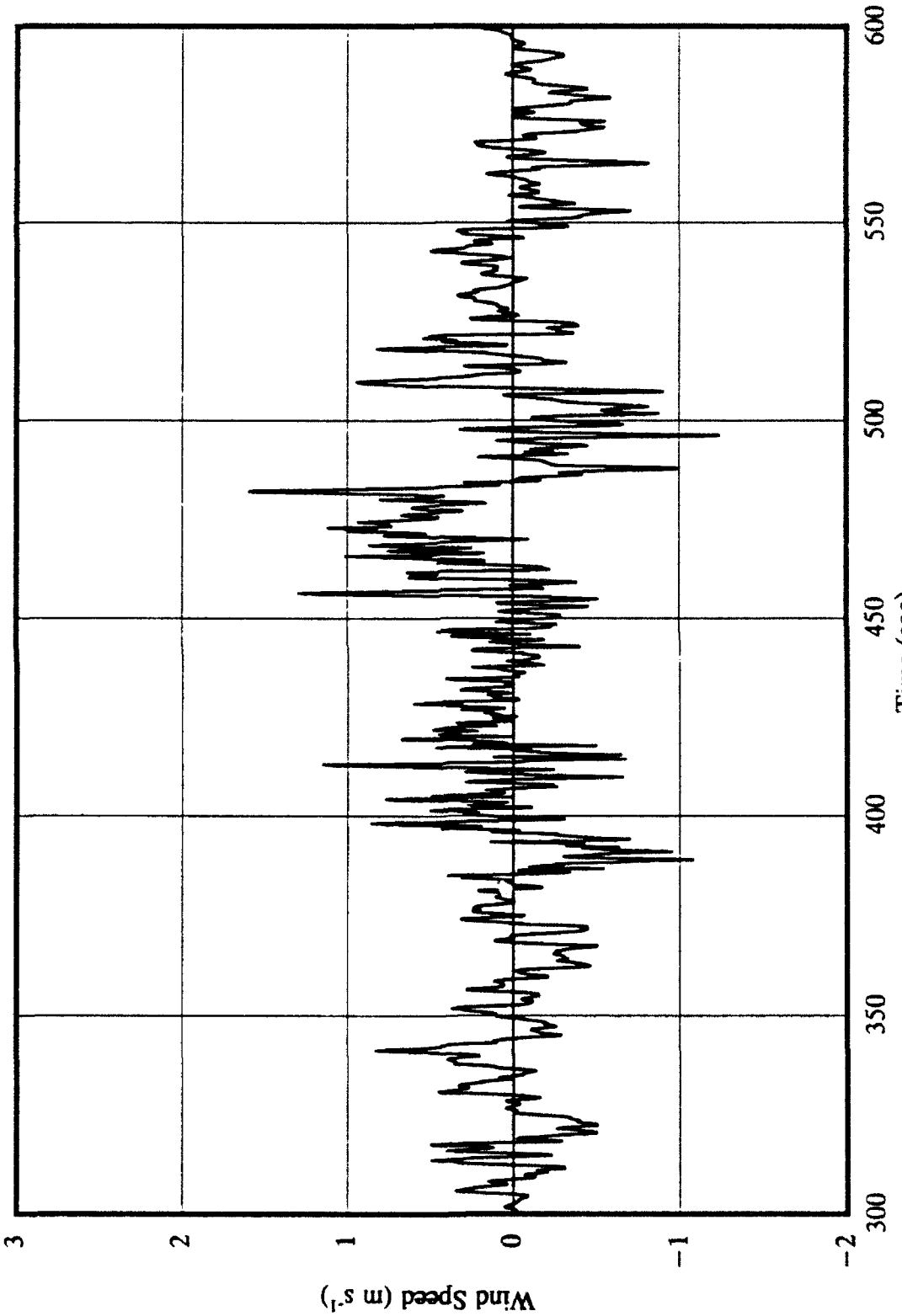

Figure 28

Figure 29. As in Fig. 27, final five minutes (600-900 seconds).

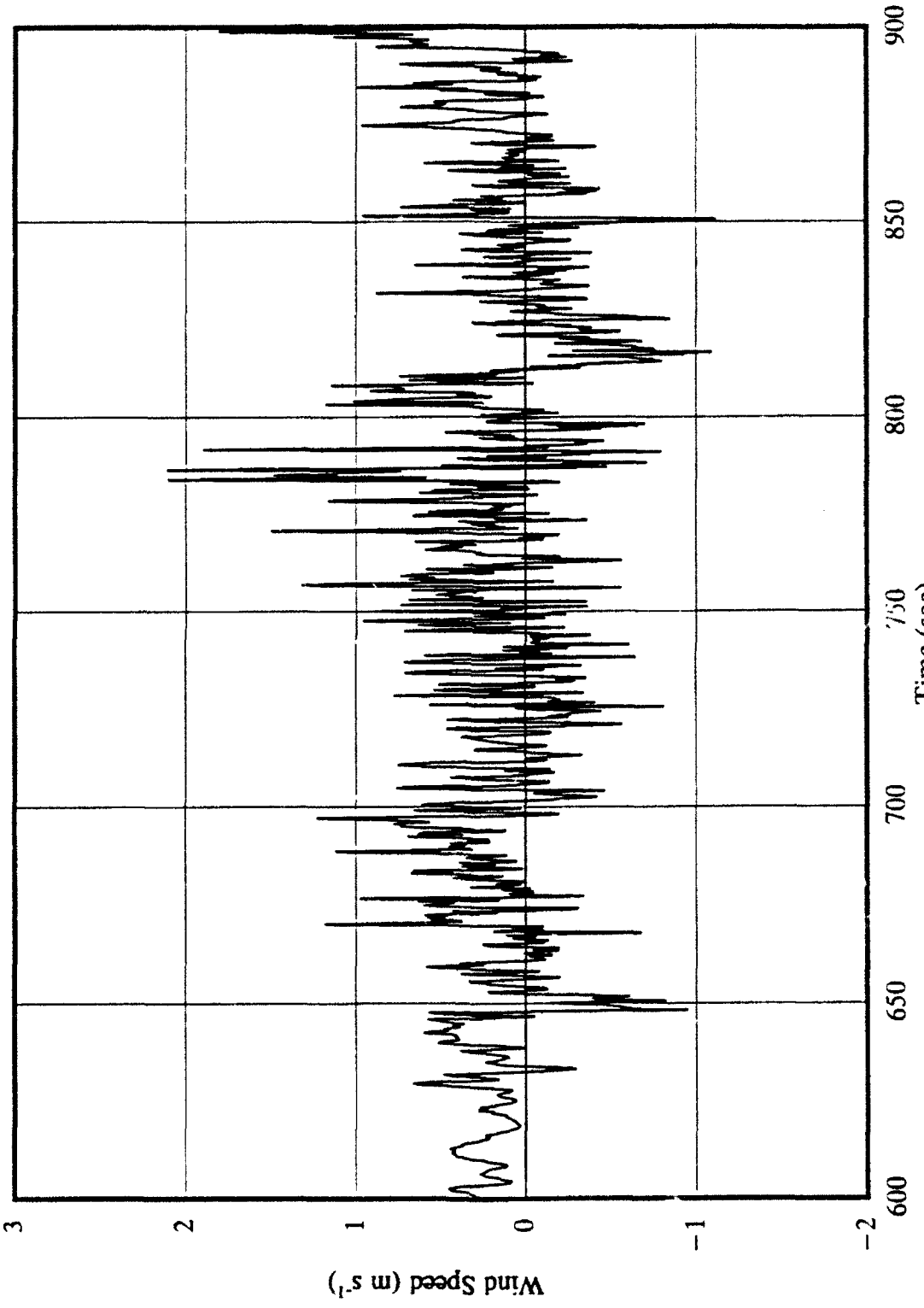

Figure 29

Figure 30. Comparison of sonic anemometer and estimated vertical wind speeds for 1202 EST, 30 April 1992: 150-170 seconds.

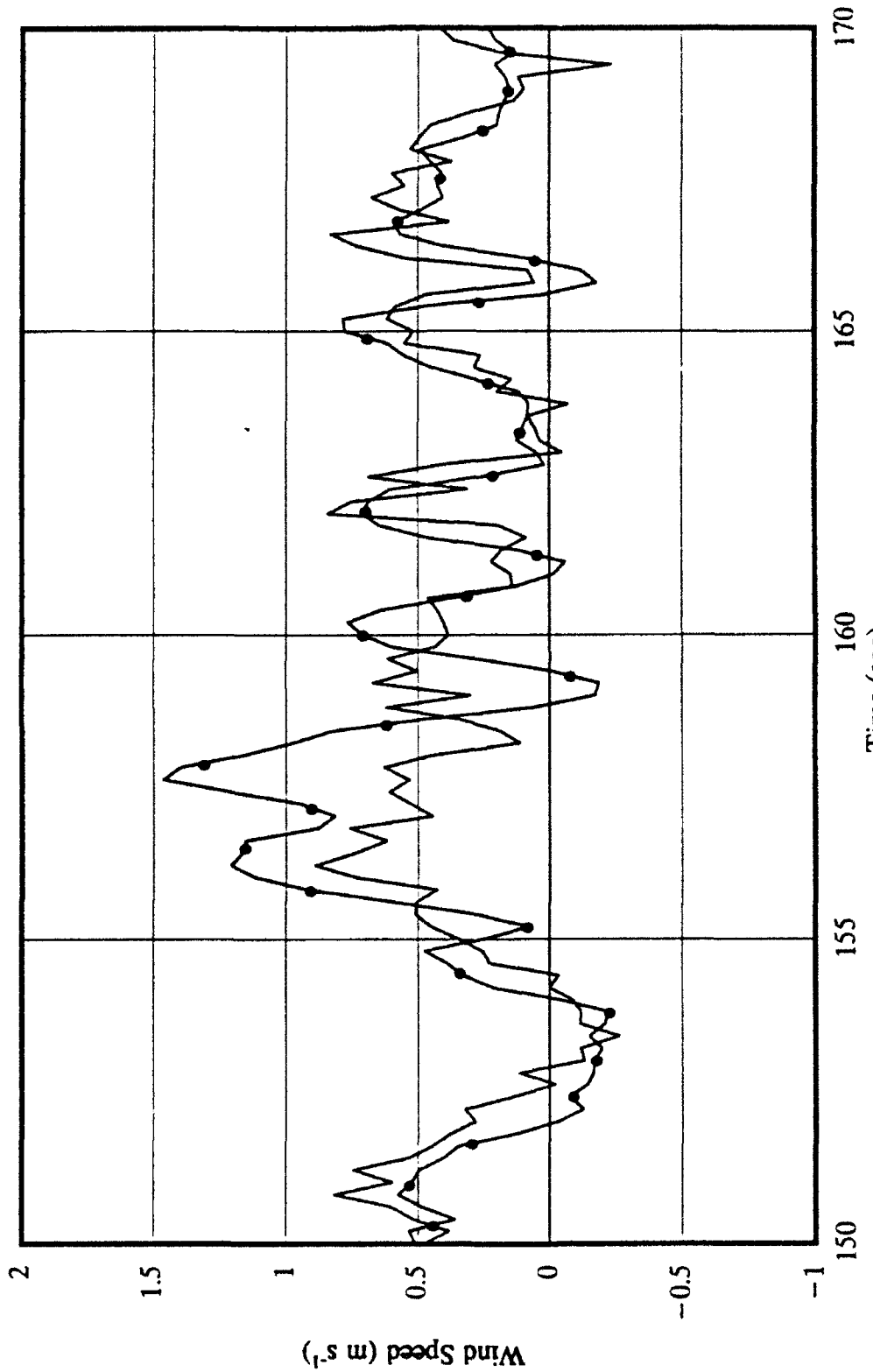
Wind Speed (m s-1)
2
1.5
1
0.5
0
-0.5
-1
150
155
160
165
170
Time (sec)
Sonic Anemometer (Measured)
Estimation (Derived)

Figure 30

Figure 31. Comparison of vertical angle from bivane and sonic anemometer for 1202 EST, 30 April 1992: 155-160 seconds.

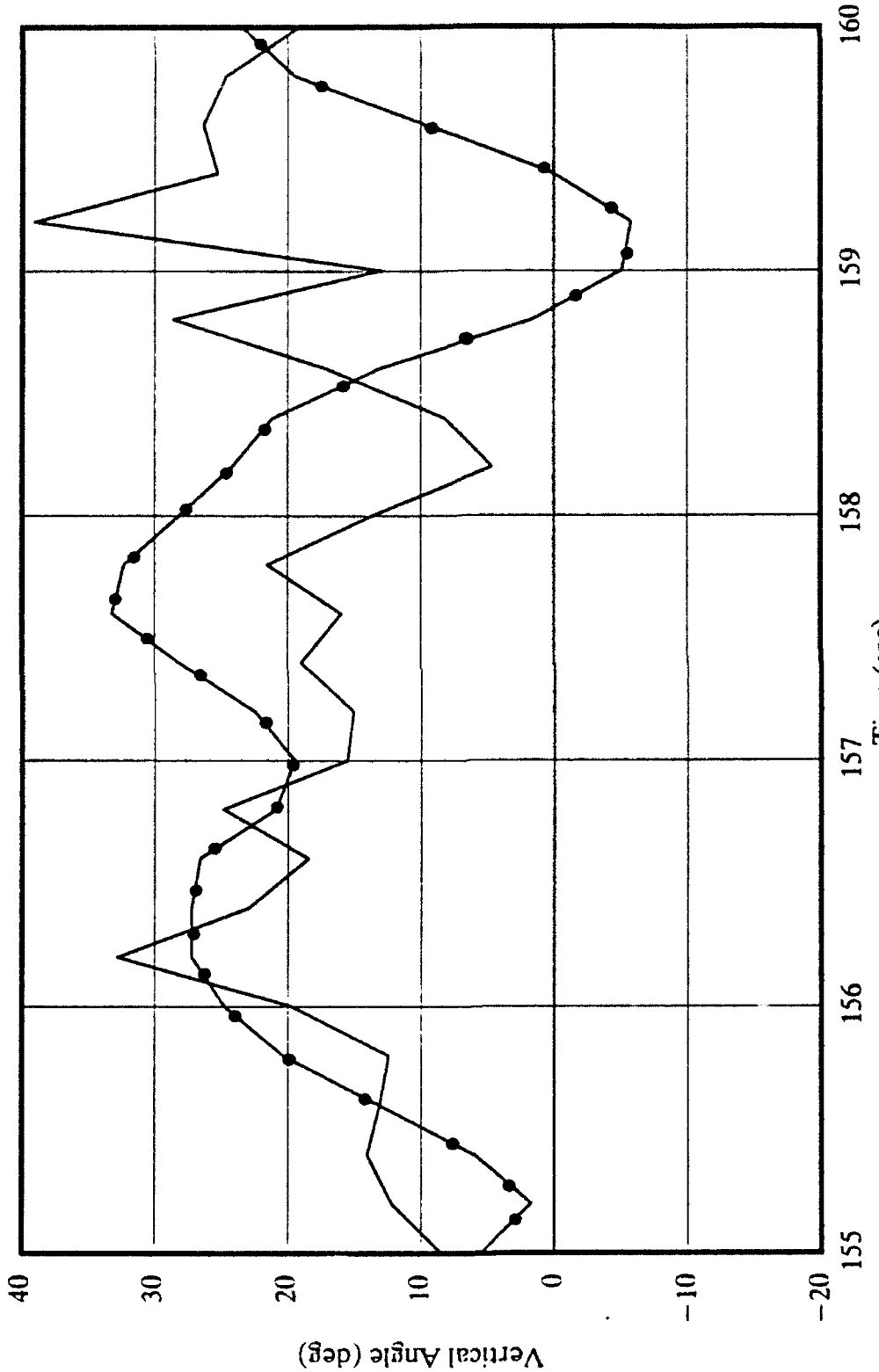
40
30
20
10
0
−10
−20
Vertical Angle (deg)
155
156
157
158
159
160
Time (sec)
Sonic Anemometer (Derived)
Bivane (Measured)

Figure 31

vertical angle from the bivane corresponding with the estimated w-component of interest. Figure 32 shows the sonic and cup anemometer u-components for the same period. No large discrepancy is found in the cup response (although the speed is consistently higher than that of the sonic anemometer). Thus, one may conclude that the bivane's response resulted in the over-estimated w-component.

After examining the estimated time series and the responses of the cup and bivane, it is apparent that care must be exercised in deriving a vertical component. The example presented above suggests the bivane would be the more likely contributor to significant estimation errors. If that hypothesis is correct, the selection of instruments with comparable distance constants, as employed in this problem, is necessary to minimize estimation error.

6.1.3. Vertical Angle

Using the horizontal and vertical components from the sonic anemometer, a vertical angle was derived as in (36). The time-series for this parameter from the first experiment is shown in Figures 33-35. The corresponding vertical angle measured by the bivane over the same period is shown in Figures 36-38.

Again, the length of most features makes small scale comparisons improper; however, there are several interesting features that can be seen. A selected comparison of the two time-series in Figure 39 shows the better high-frequency response of the sonic anemometer. The period between 270 and 285 seconds, however, appears to indicate the bivane's response to high-frequency fluctuations is substantially better than that of the cup when both are compared with the sonic anemometer.

Figure 32. Comparison of horizontal wind speed from cup and sonic anemometers for 1202 EST, 30 April 1992: 155-160 seconds.

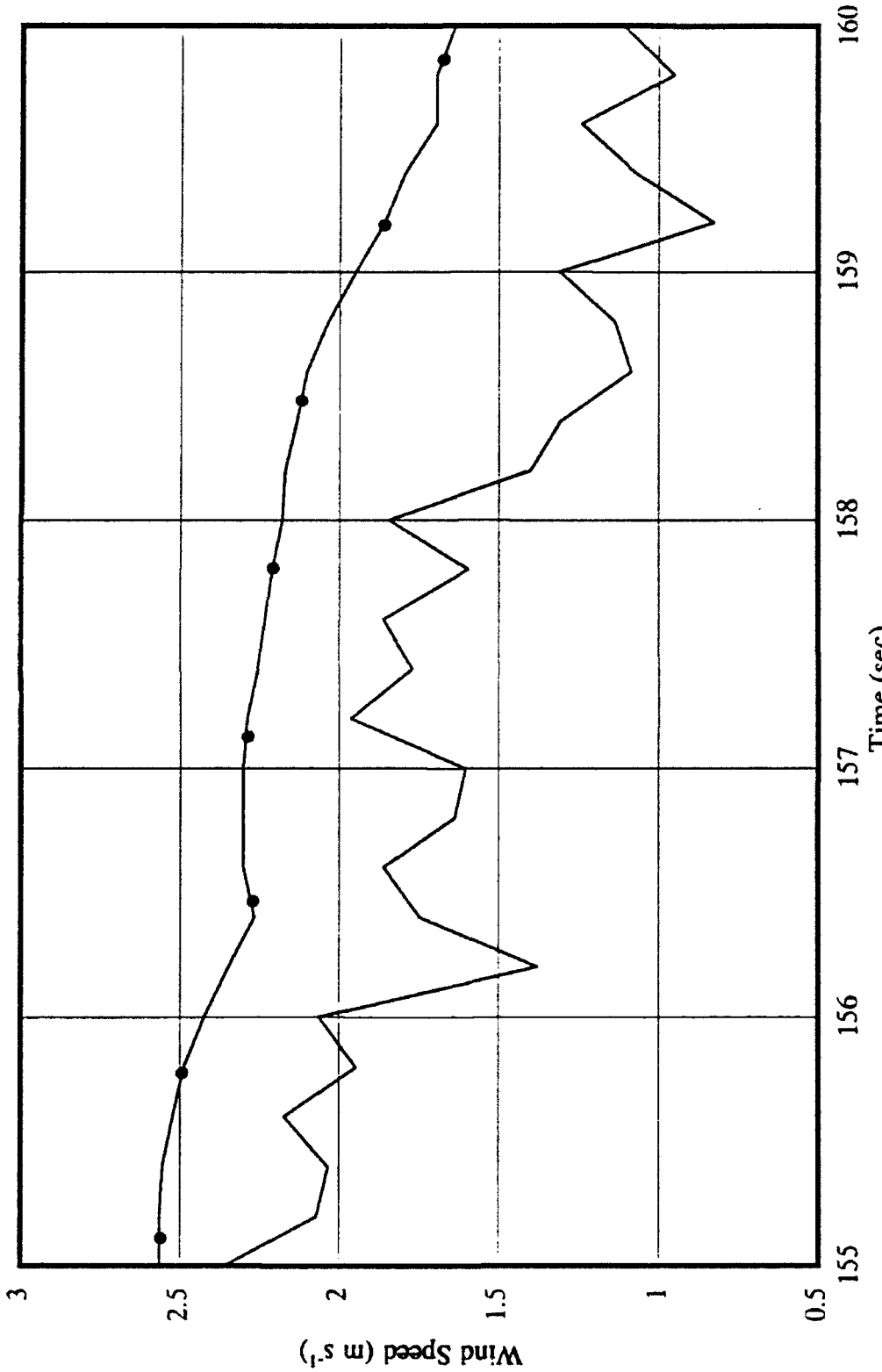
Wind Speed (m s-1)
3
2.5
2
1.5
1
0.5
155
156
157
158
159
160
Time (sec)
Sonic Anemometer
Three-Cup Anemometer

Figure 32

Figure 33. Sonic anemometer derived vertical angle for 1202 EST, 30 April 1992: first five minutes (0-300 seconds).

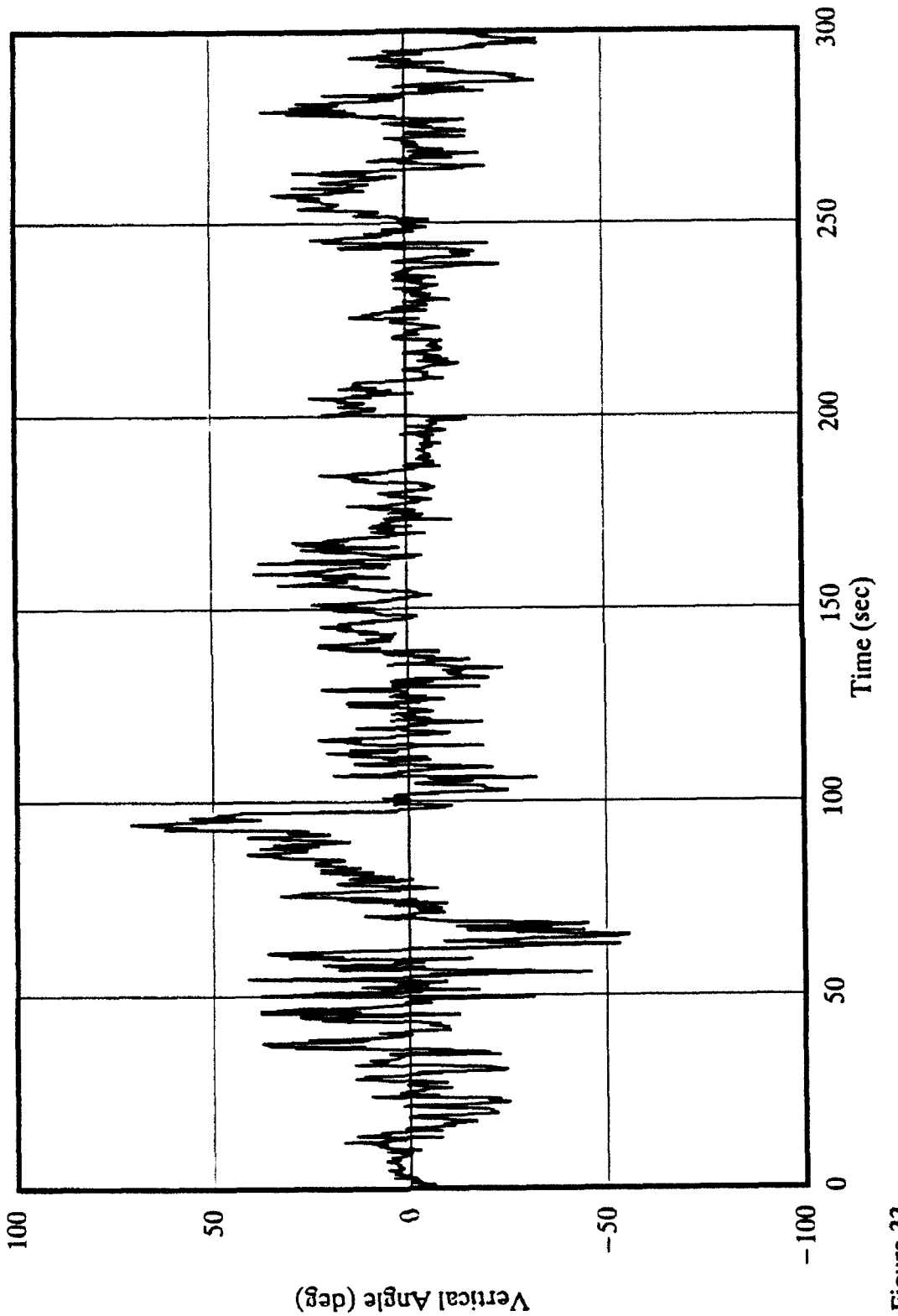
Vertical Angle (deg)
100
50
0
−50
−100
0
50
100
150
200
250
300
Time (sec)

Figure 33

Figure 34. As in Fig. 33, middle five minutes (300-600 seconds).

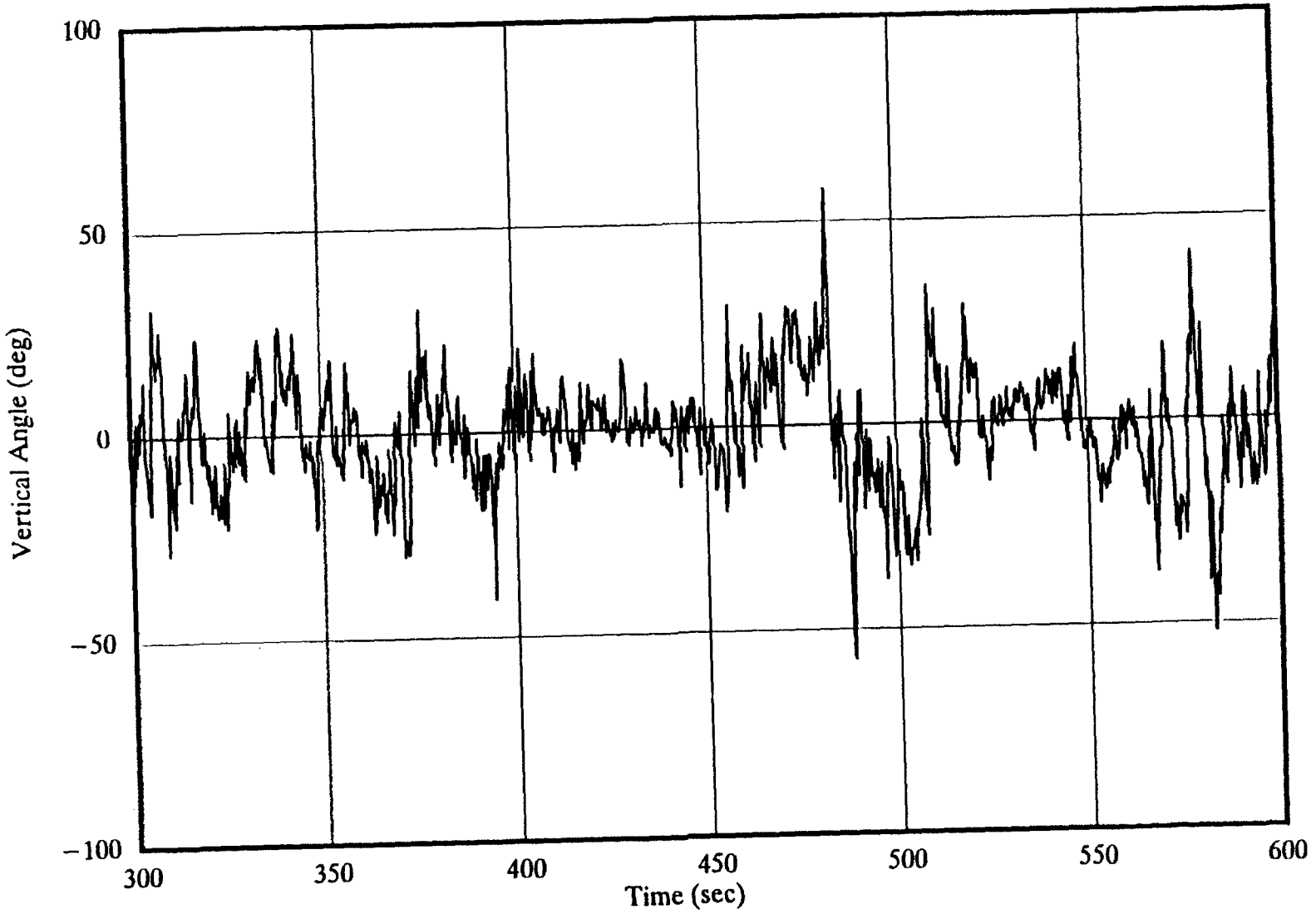
100
50
0
−50
−100
Vertical Angle (deg)
300
350
400
450
500
550
600
Time (sec)

Figure 34

Figure 35. As in Fig. 33, final five minutes (600-900 seconds).

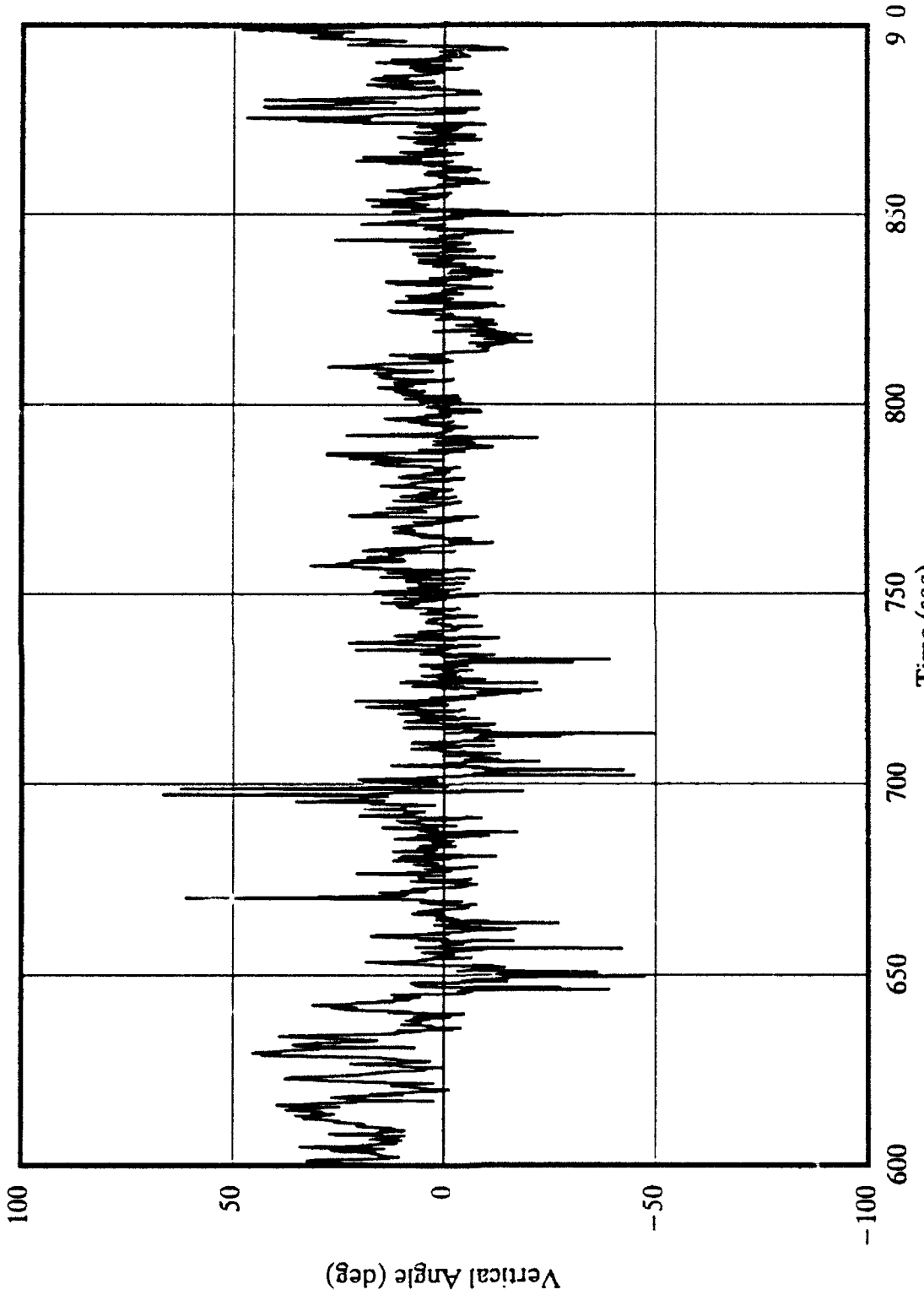
100
50
0
−50
−100
600
650
700
750
800
850
9 0
Time (sec)
Vertical Angle (deg)

Figure 35

Figure 36. Bivane vertical angle for 1202 EST, 30 April 1992: first five minutes (0-300 seconds).

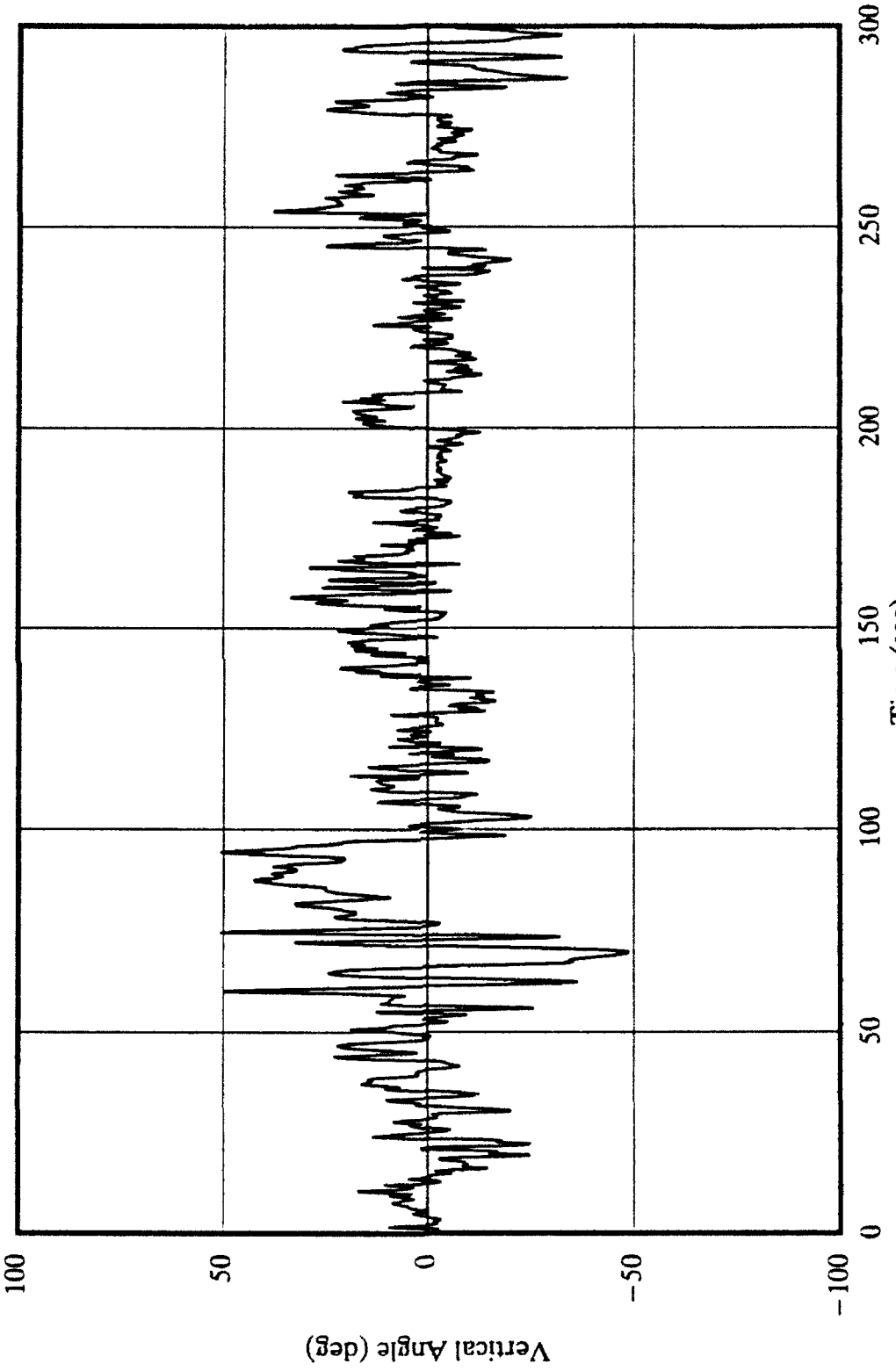
Vertical Angle (deg)
100
50
0
−50
−100
0
50
100
150
200
250
300
Time (sec)

Figure 36

Figure 37. As in Fig. 36, middle five minutes (300-600 seconds).

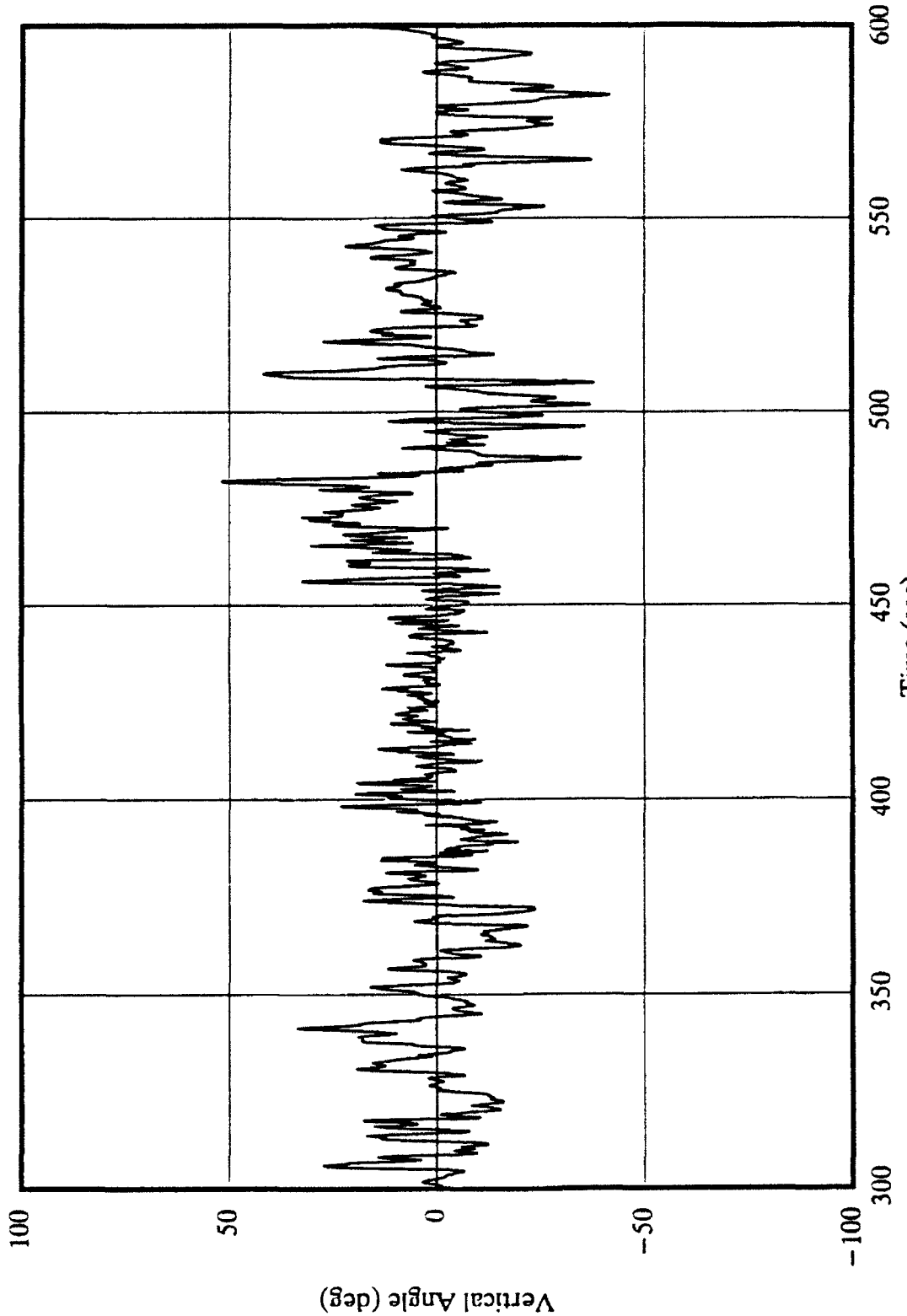
100
50
0
−50
−100
300
350
400
450
500
550
600
Time (sec)
Vertical Angle (deg)

Figure 37

Figure 38. As in Fig. 36, final five minutes (600-900 seconds).

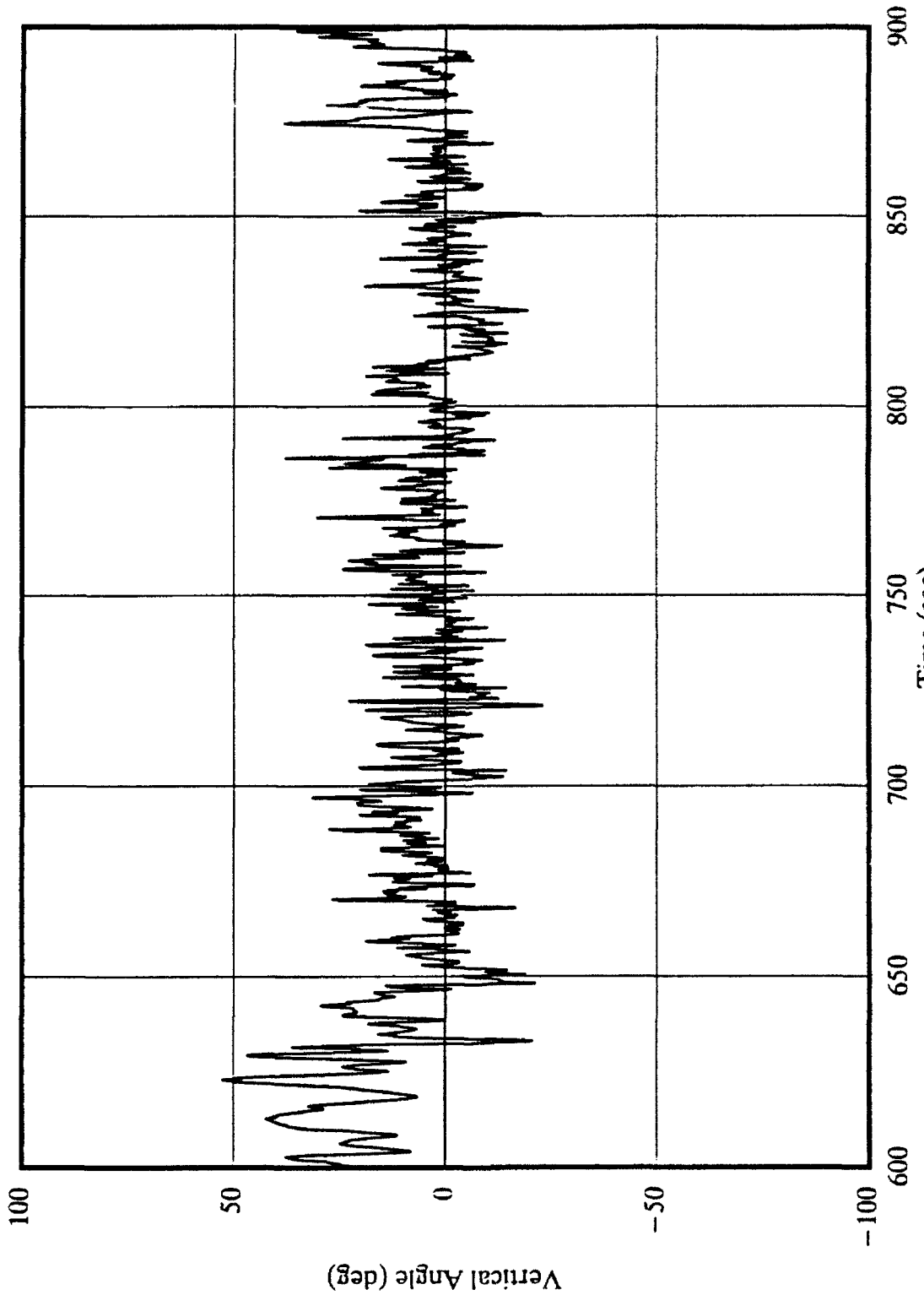
Vertical Angle (deg)
100
50
0
−50
−100
600
650
700
750
800
850
900
Time (sec)

Figure 38

Figure 39. Comparison of vertical angle from bivane and sonic anemometer from first field experiment, one-half minute (270-300 seconds).

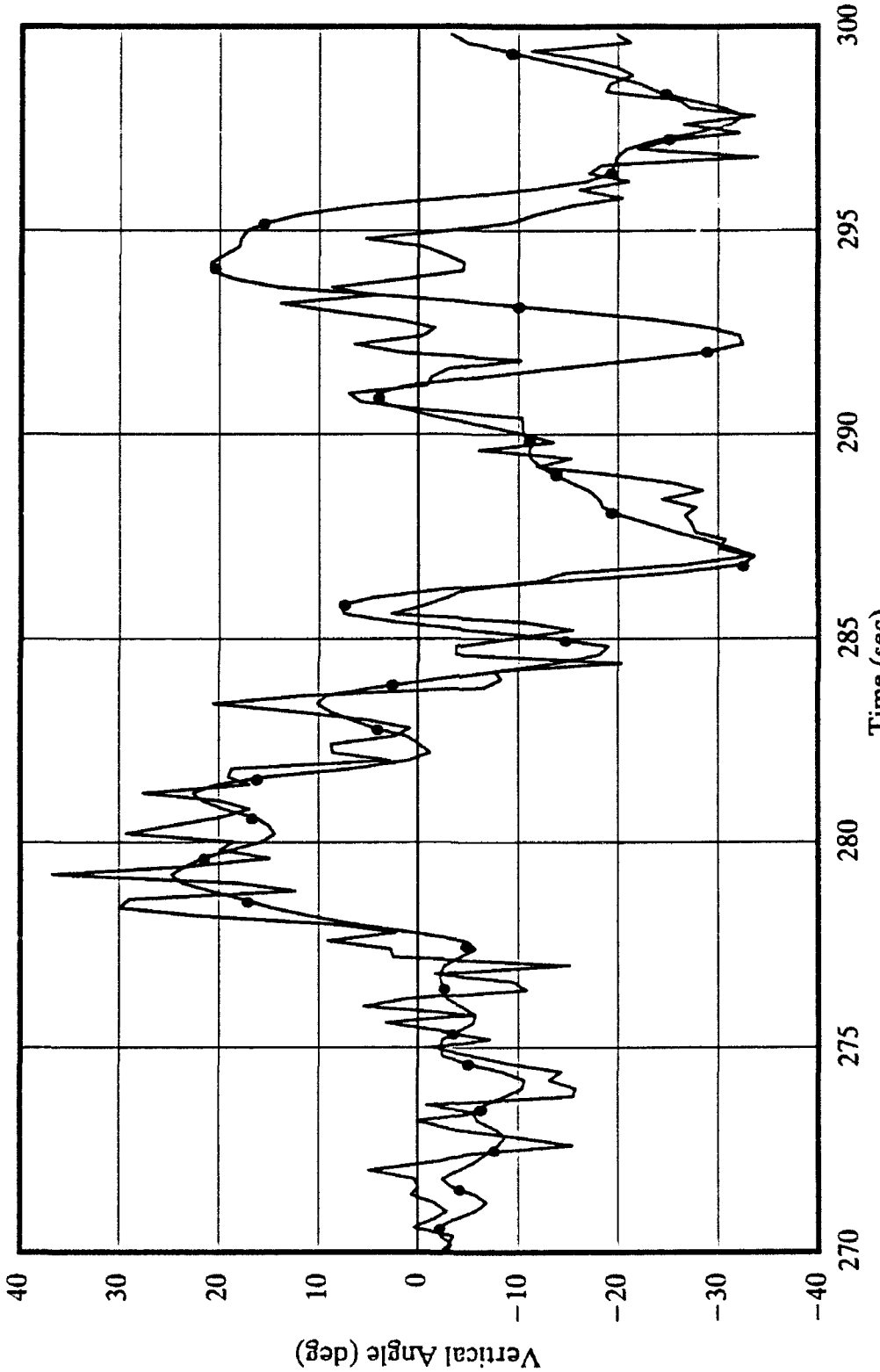
Vertical Angle (deg)
40
30
20
10
0
−10
−20
−30
−40
270
275
280
285
290
295
300
Time (sec)
Sonic Anemometer (Derived)
Bivane (Measured)

Figure 39

Figure 40. As in Fig. 39, one-half minute (680-710 seconds).

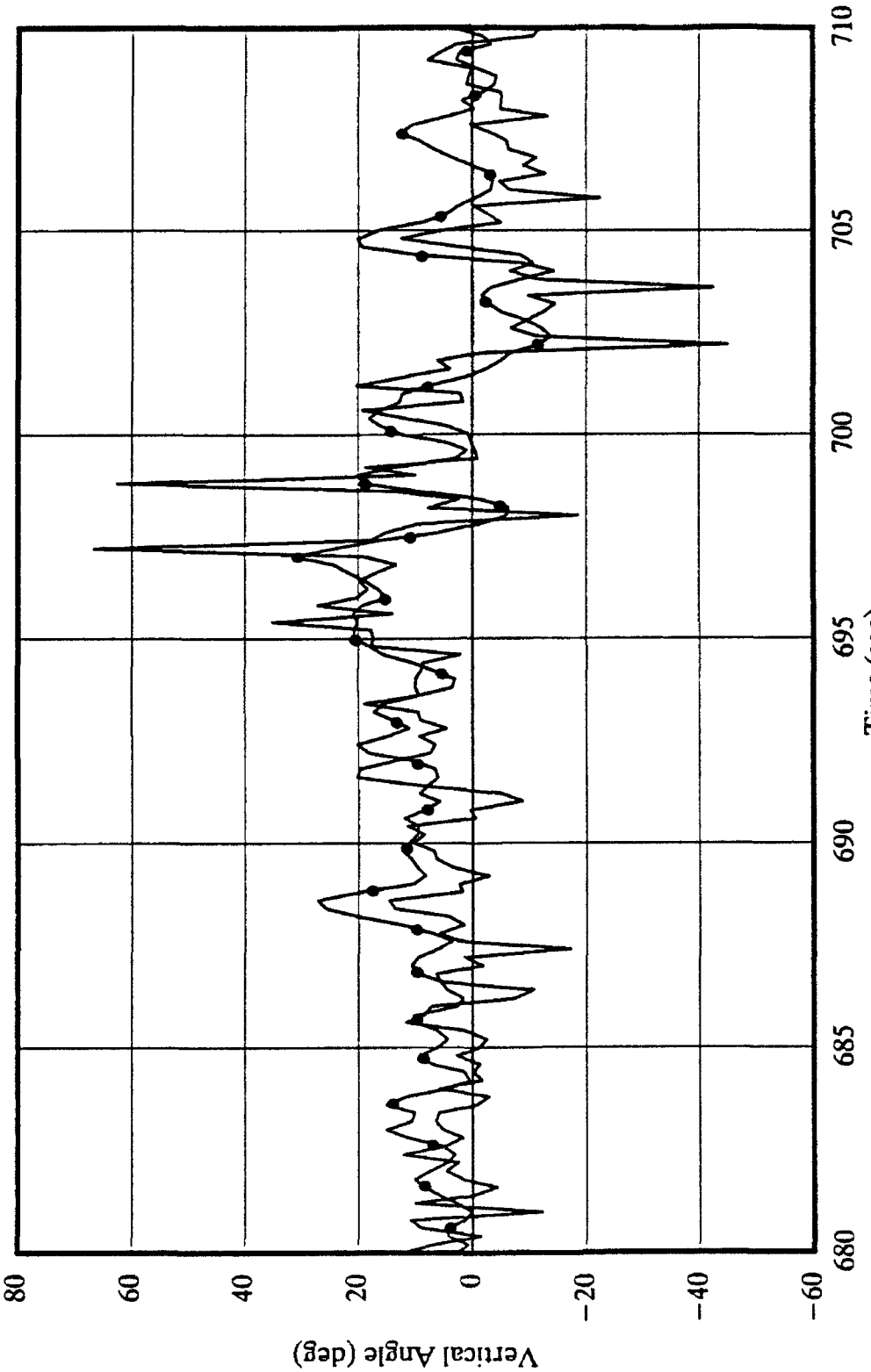
Vertical Angle (deg)
80
60
40
20
0
−20
−40
−60
680
685
690
695
700
705
710
Time (sec)
Sonic Anemometer (Derived)
Bivane (Measured)

Figure 40

The period between 290 and 300 seconds is characterized by a large oscillation in the bivane's response. This may be due in part to overshooting, a linear response characteristic of second-order systems. As detailed in the appendix, the response characteristics of a bivane can be modeled using a solution to such a system. Several other possible occurrences of overshooting occur in Figure 40 after 700 seconds, when the wind changes more rapidly.

6.1.4. Cross-Correlation of Wind Components

The time-series for cross-correlations of the instantaneous vertical and horizontal wind perturbations measured from the sonic anemometer is shown in Figures 41-43. A concurrent estimated covariance time-series derived from the cup anemometer and bivane signals is shown in Figures 44-46.

Comparison of the two time-series in Figure 47 indicates a peculiar pattern. Although there appears to be relative agreement with the two responses, the estimation actually appears to lead the sonic response. Logically, the sonic response should lead throughout the time-series, assuming all of the instruments are seeing the same parcels of air. This reversal suggests the duration and magnitude of most of the perturbations in either covariance time-series is too small for valid comparison.

The covariance time-series does, however, highlight the periods where momentum flux occurs. A common theory regarding momentum flux transfer is that it occurs during brief, highly-turbulent periods, or 'bursts'. These bursts, known as convective plumes, are indicated by

Figure 41. Sonic anemometer horizontal and vertical wind covariance for 1202 EST, 30 April 1992: first five minutes (0-300 seconds).

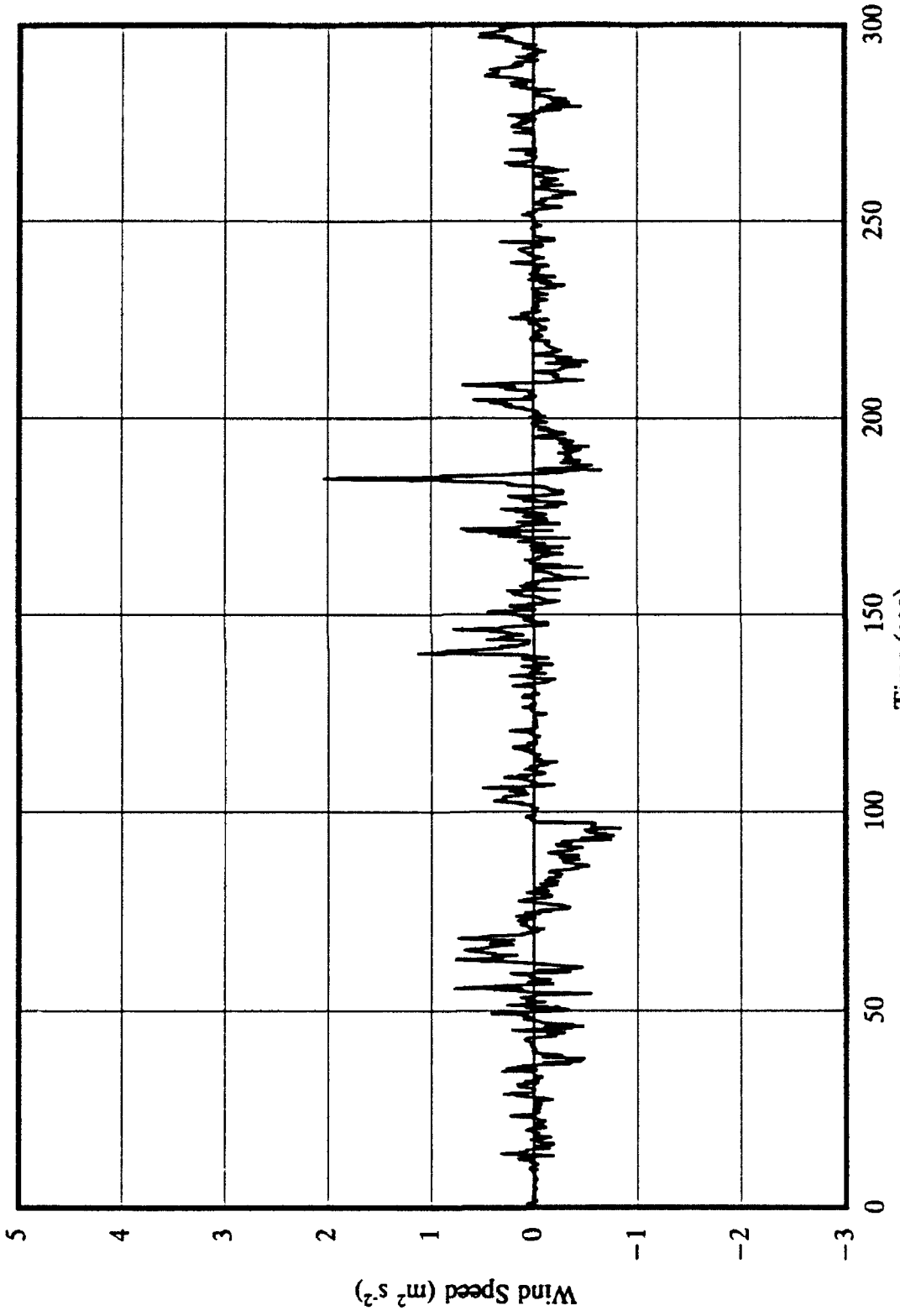

Figure 41

Figure 42. As in Fig. 41, middle five minutes (300-600 seconds).

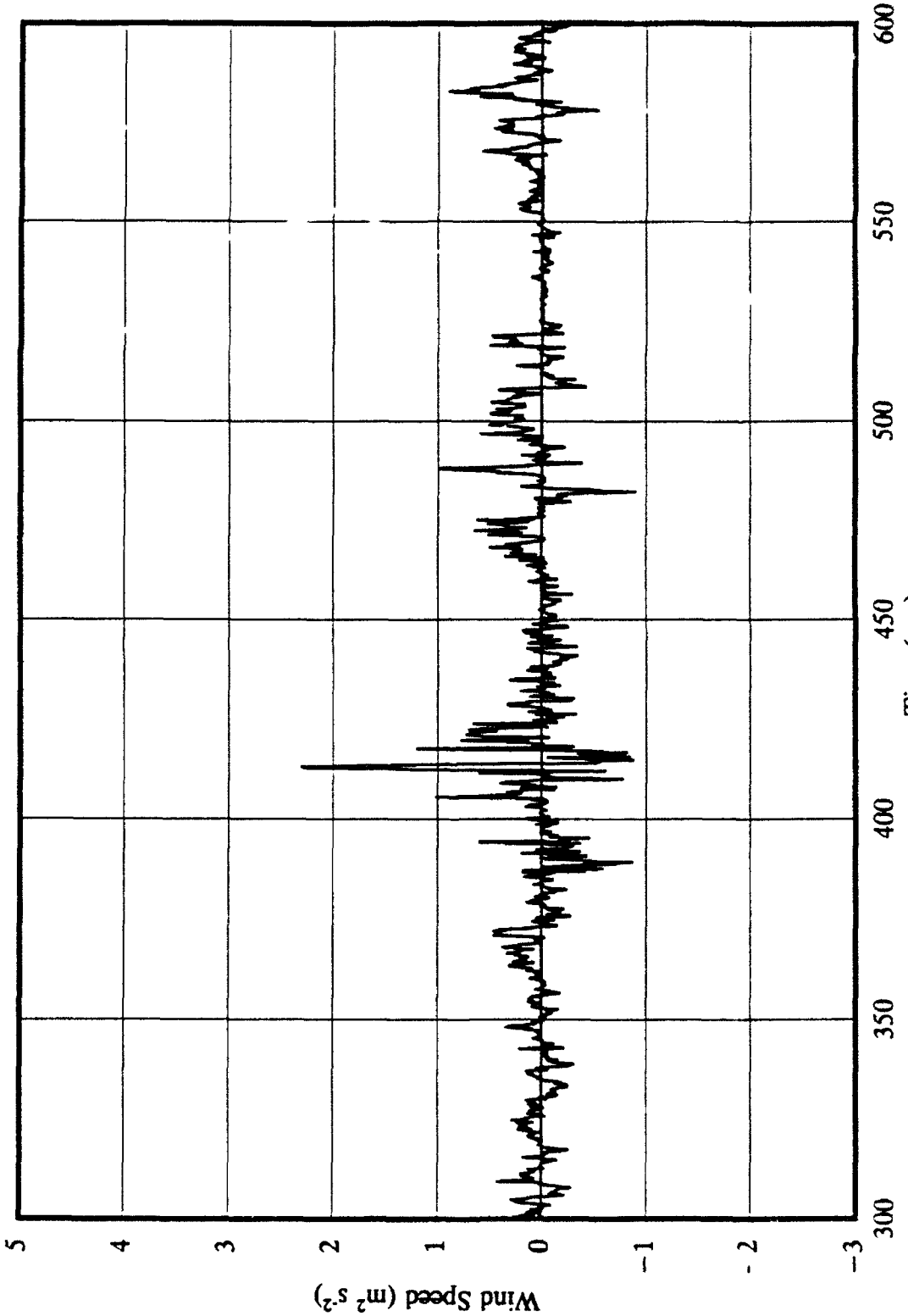
Wind Speed (m² s⁻²)
5
4
3
2
1
0
−1
- 2
−3
300
350
400
450
500
550
600
Time (sec)

Figure 42

Figure 43. As in Fig. 41, final five minutes (600-900 seconds).

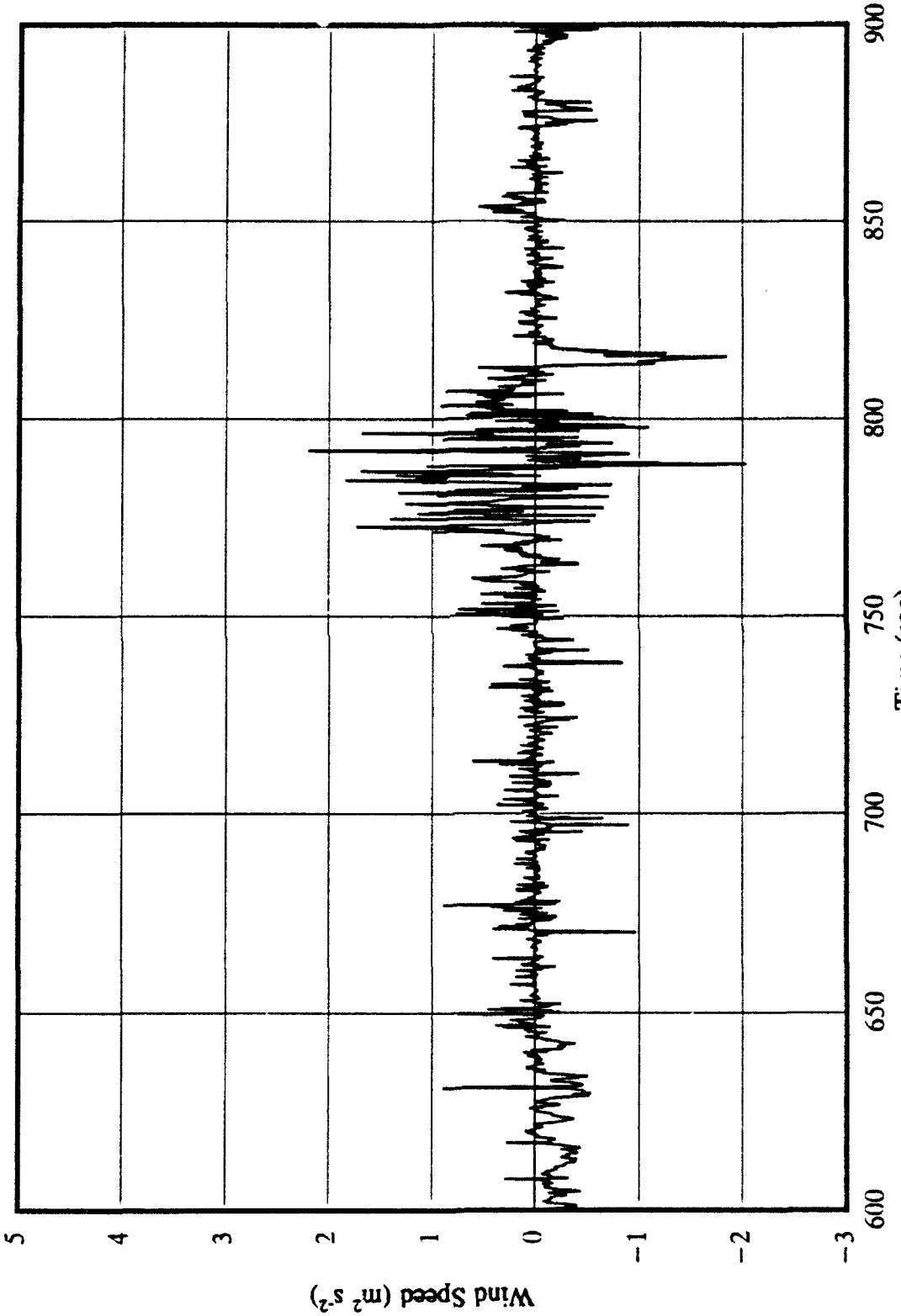
Wind Speed (m² s⁻²)
5
4
3
2
1
0
−1
−2
−3
600
650
700
750
800
850
900
Time (sec)

Figure 43

Figure 44. Estimated horizontal and vertical wind covariance for 1202 EST, 30 April 1992: first five minutes (0-300 seconds).

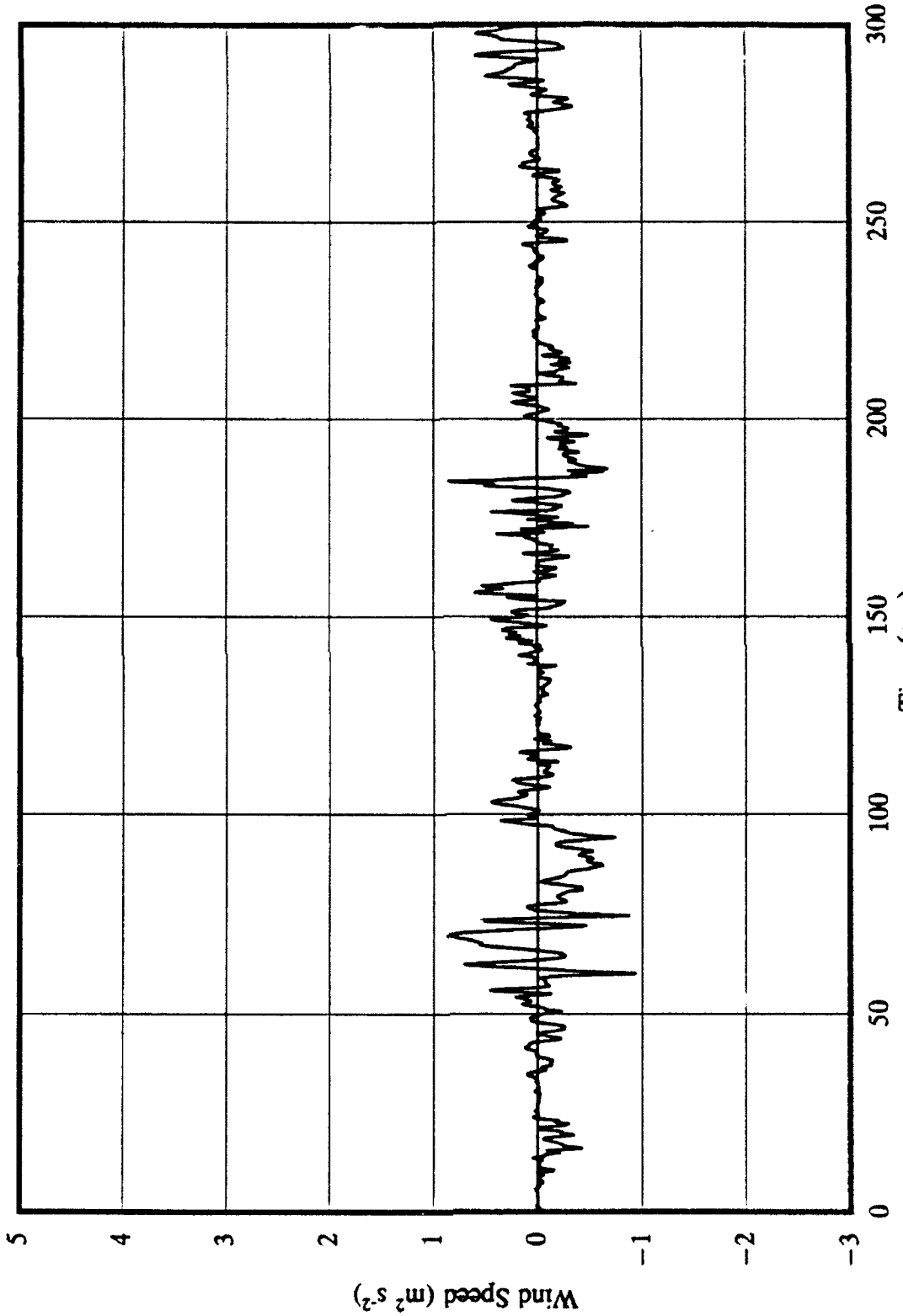

Figure 44

Figure 45. As in Fig. 44, middle five minutes (300-600 seconds).

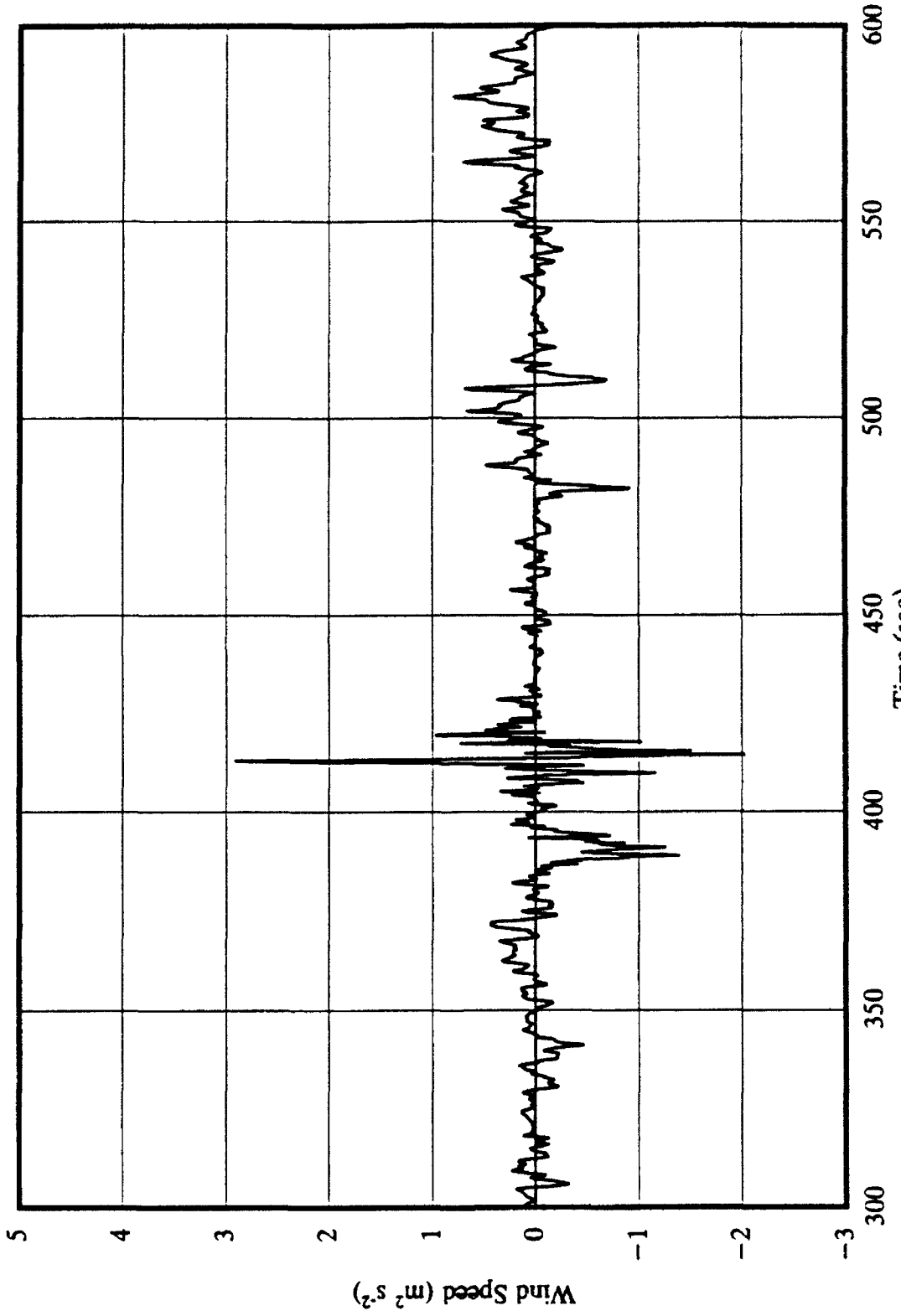
Wind Speed (m² s⁻²)
5
4
3
2
1
0
−1
−2
−3
300
350
400
450
500
550
600
Time (sec)

Figure 45

Figure 46. As in Fig. 44, final five minutes (600-900 seconds).

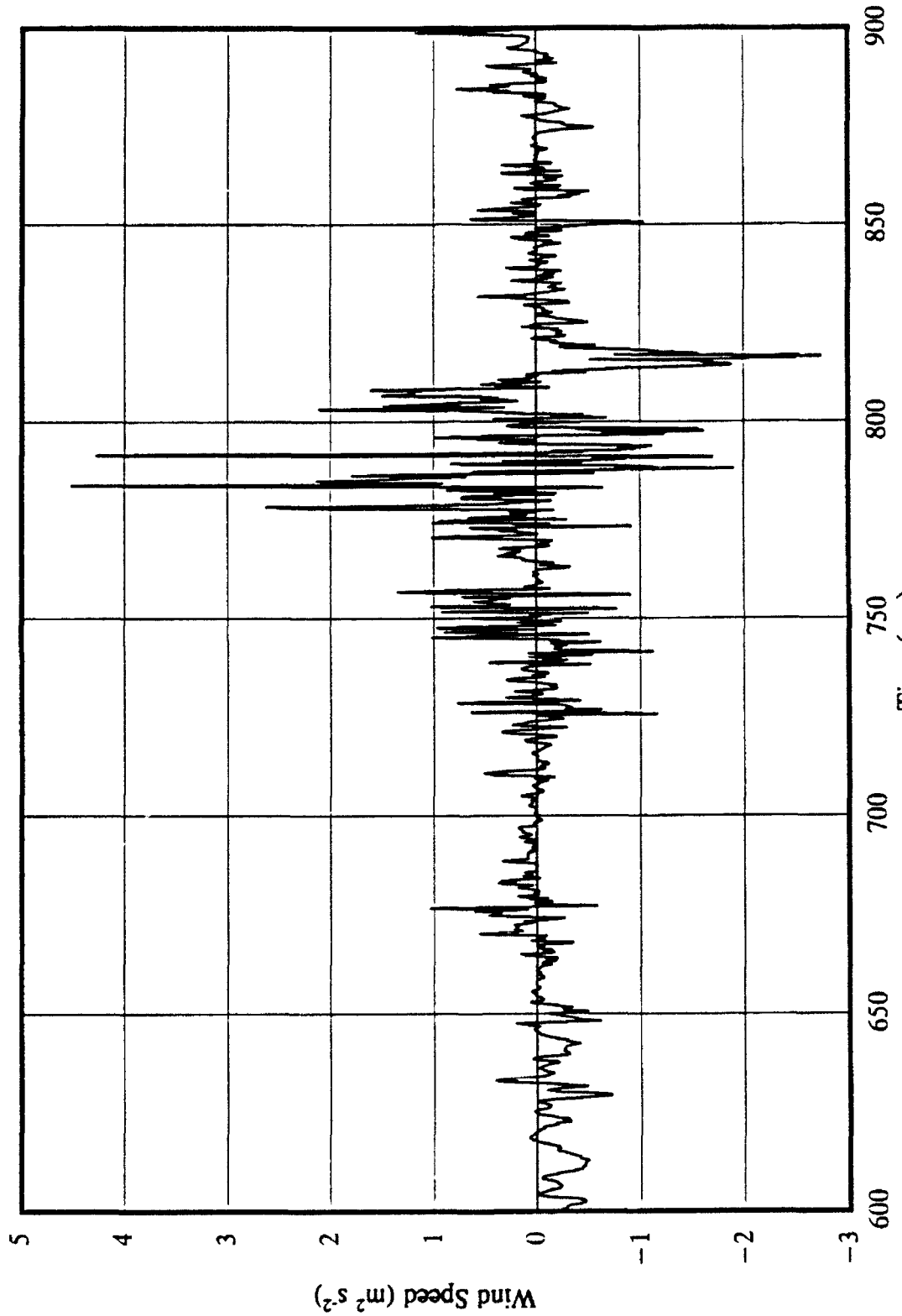
Wind Speed (m² s⁻²)
5
4
3
2
1
0
−1
−2
−3
600
650
700
750
800
850
900
Time (sec)

Figure 46

Figure 47. Comparison of estimated and sonic anemometer horizontal and vertical wind covariance for 1202 EST, 30 April 1992: 410-430 seconds.

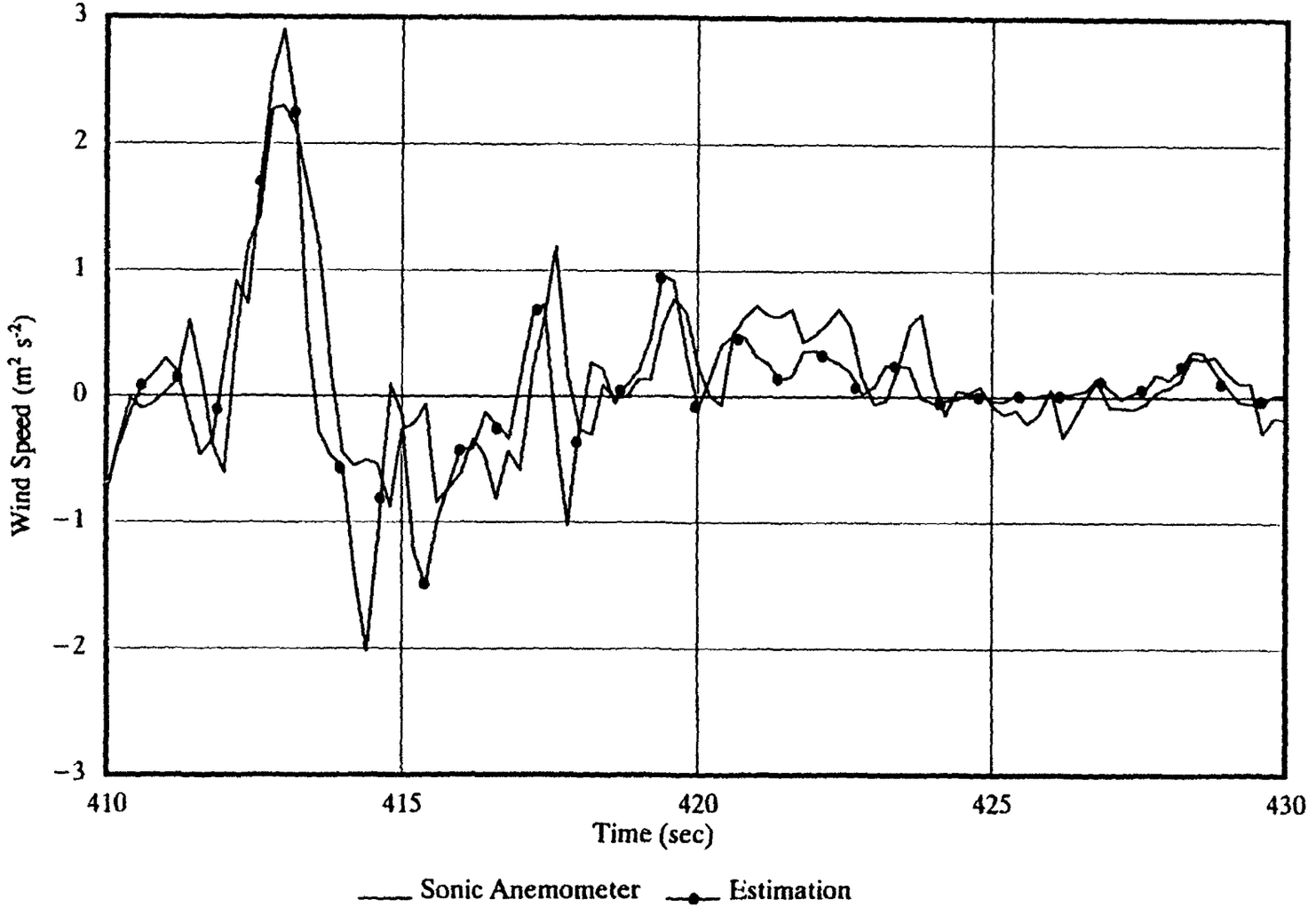
3
2
1
0
−1
−2
−3
Wind Speed (m² s⁻²)
410
415
420
425
430
Time (sec)
Sonic Anemometer
Estimation

Figure 47

the saw-toothed features seen in the w-component and vertical angle time-series (for example, Figure 24, between 60-95 seconds). If this theory is valid, a running sum of the covariances could possibly highlight these bursts.

Running sums for the sonic anemometer and estimated covariances are presented in Figures 48 through 50. There is a general trend of motion consistent with the vertical velocities, particularly for the convective plumes between 60 and 95 seconds (Figure 24), 370 to 390 seconds (Figure 25), and 800 to 830 seconds (Figure 26). This would suggest that periods of turbulent transfer may occur during these 'bursts' apparent in the covariance running sums. It is recommended that this hypothesis be subsequently studied in further detail with a more extensive data set.

6.2. Spectral Analysis

A spectral analysis is presented for each component used in the flux calculations. Discussion regarding the analyses is brief, and is simply intended to point out basic features of interest and discuss possible topics for future study.

The spectra tend to bend or 'change course' in each of the three major subdivisions, so each region can be approximated by drawing a series of three straight lines through the spectra. Starting with the lowest frequencies (found on the left-hand side of the horizontal axis), the first region is the zero slope region, the location of which is self-explanatory. The middle region is the buoyancy subrange, where the slope approaches -2.0. A gap is usually detected after the buoyancy subrange, characterized by a dip in the spectral curve. The

Figure 48. Running sum of sonic anemometer and estimated covariances of vertical and horizontal wind components for 1202 EST, 30 April 1992: first five minutes (0-300 seconds).

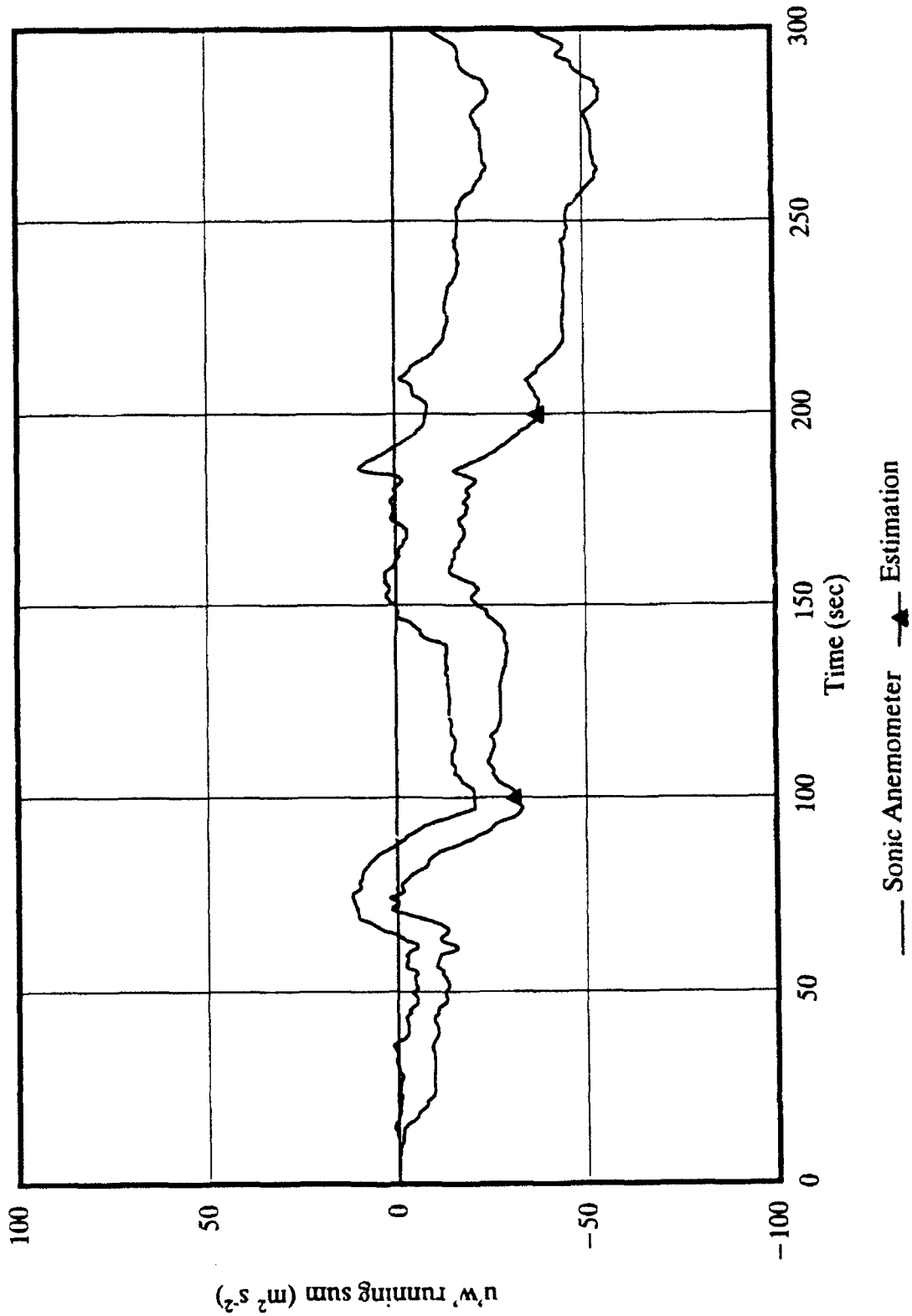
u'w' running sum (m² s⁻²)
100
50
0
−50
−100
0
50
100
150
200
250
300
Time (sec)
Sonic Anemometer
Estimation

Figure 48

Figure 49. As in Fig. 48, middle five minutes (300-600 seconds).

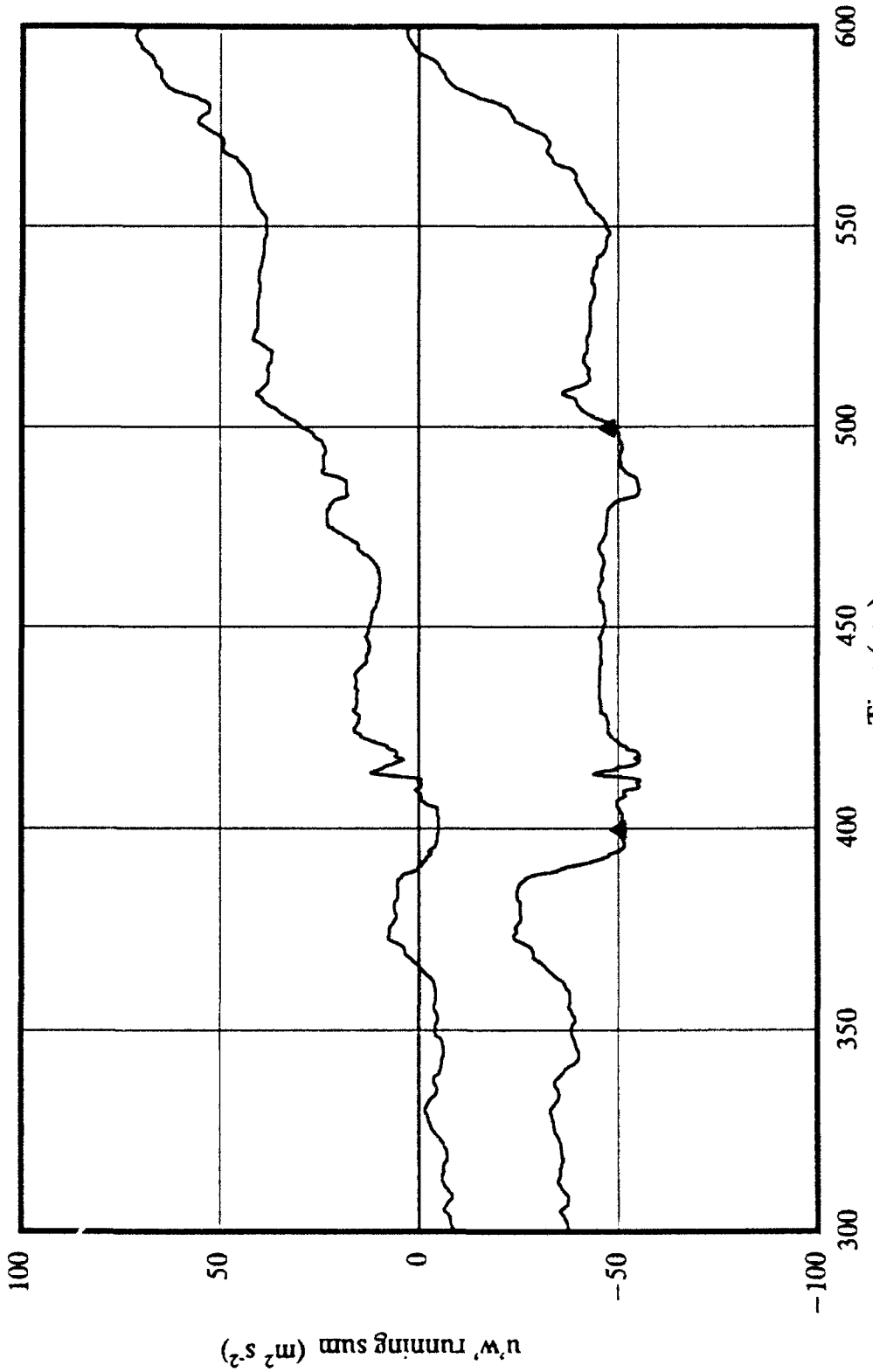
100
50
0
−50
−100
300
350
400
450
500
550
600
Time (sec)
u'w' running sum (m² s⁻²)
Sonic Anemometer
Estimation

Figure 49

Figure 50. As in Fig. 48, final five minutes (600-900 seconds).

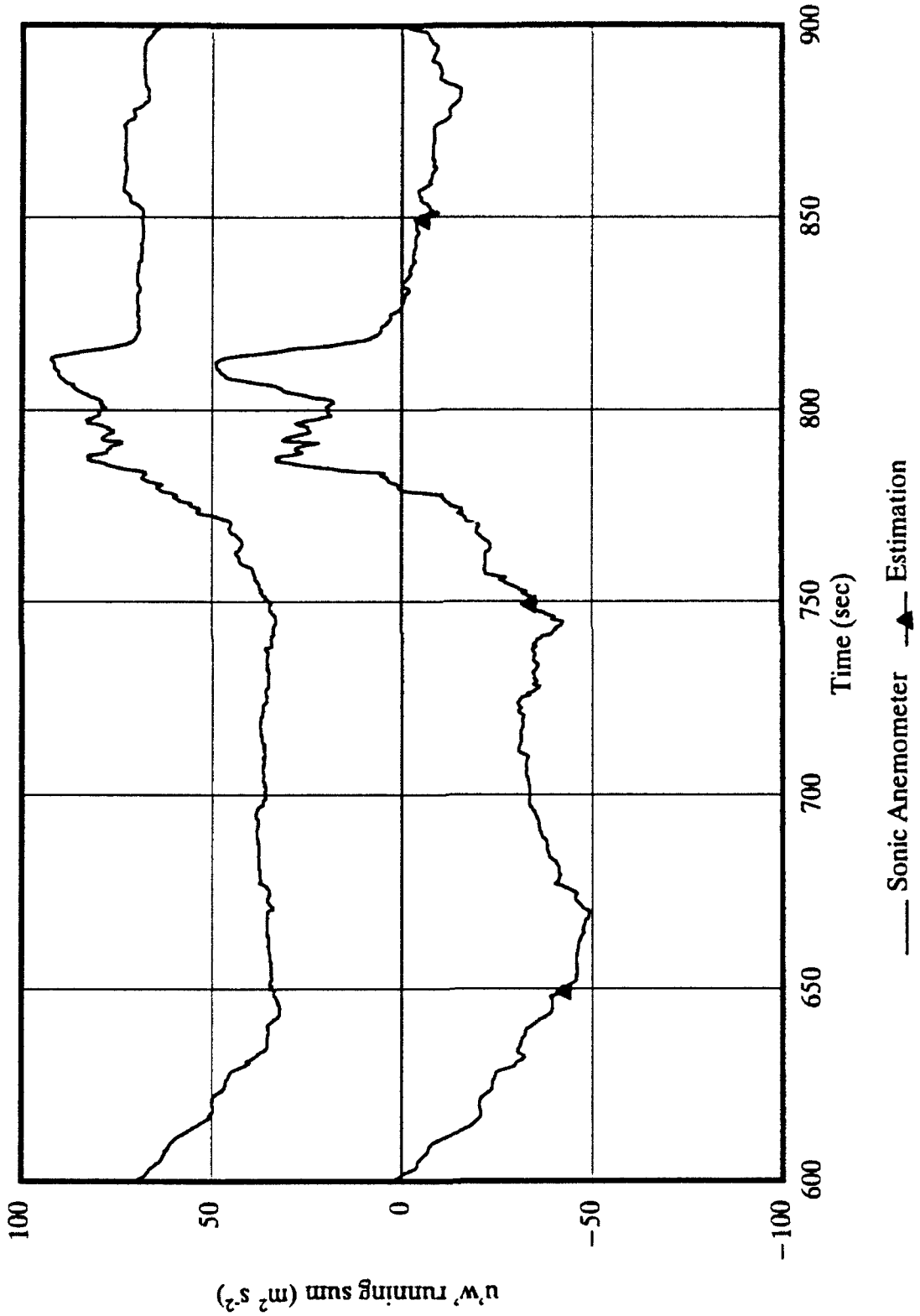
100
50
0
−50
−100
600
650
700
750
800
850
900
Time (sec)
u'w' running sum (m² s⁻²)
Sonic Anemometer
Estimation

Figure 50

inertial subrange is the right-most of the three regions, and is found after the dip. A major feature of interest is whether the spectra conform to the $-5/3^{rds}$ power law for turbulent components. This law, detailed in Stull (1988), states that components associated with turbulent transport have a slope of approximately -5/3 in the inertial subrange when the spectrum is plotted in the format shown. For convenience of comparison, a $-5/3^{rds}$ slope line is included adjacent to each spectra.

In addition, aliasing tendencies are noted. Aliasing, or folding, occurs in the inertial subrange when the data to be transformed was improperly filtered, or if the sampling rate is insufficient. In either case, contributions from higher frequency data is mistakenly plotted at lower frequencies (hence the term folding). Aliasing will cause the slope of this region to appear less steep than it should be.

The accuracy of each data set was verified by determining the area under the spectral curve. This area is by definition equal to the variance of the transformed data set prior to transformation (Stull, 1988). In each case presented below, this equality was proven, confirming the spectra were properly transformed.

The oscillating pattern noted for each spectra in the right-most region of the inertial subrange is a result of the pre-filtering done on the transformed data. The pattern of the oscillation is a function of the width of the filter, with a wider filter resulting in fewer oscillations. However, a delicate balance must be reached, as over-filtering distorts the slope in this region.

6.2.1. Horizontal Wind Component

The power spectrum for the sonic anemometer is shown in Figure 51; the corresponding spectrum for the cup anemometer is shown in Figure 52.

The sonic and cup spectra appear to have a slope somewhat less than -5/3 in the inertial subrange. Both spectra also exhibit significant aliasing, but the magnitude of the oscillations for the sonic anemometer is much greater than for the cup anemometer.

6.2.2. Vertical Wind Component

The power spectrum for the sonic anemometer is shown in Figure 53; the corresponding spectrum for estimation derived from the bivane and cup anemometer is shown in Figure 54.

The vertical component for the sonic anemometer also displays a slope less that -5/3. The estimation, however, does display a slope close to the expected value. Based on previous results, this would suggest that aliasing is a more serious problem with the sonic anemometer and cup anemometer than with the bivane.

6.2.3. Vertical Angle

The power spectrum for the derived vertical angle from the sonic anemometer is shown in Figure 55; the corresponding spectrum for the dual-annulus bivane is shown in Figure 56.

The vertical angle for the sonic anemometer has a slope significantly less than -5/3. This is not surprising given the spectral characteristics for the sonic's horizontal and vertical

Figure 51. Spectral analysis for sonic anemometer vertical component for 1202 EST, 30 April 1992.

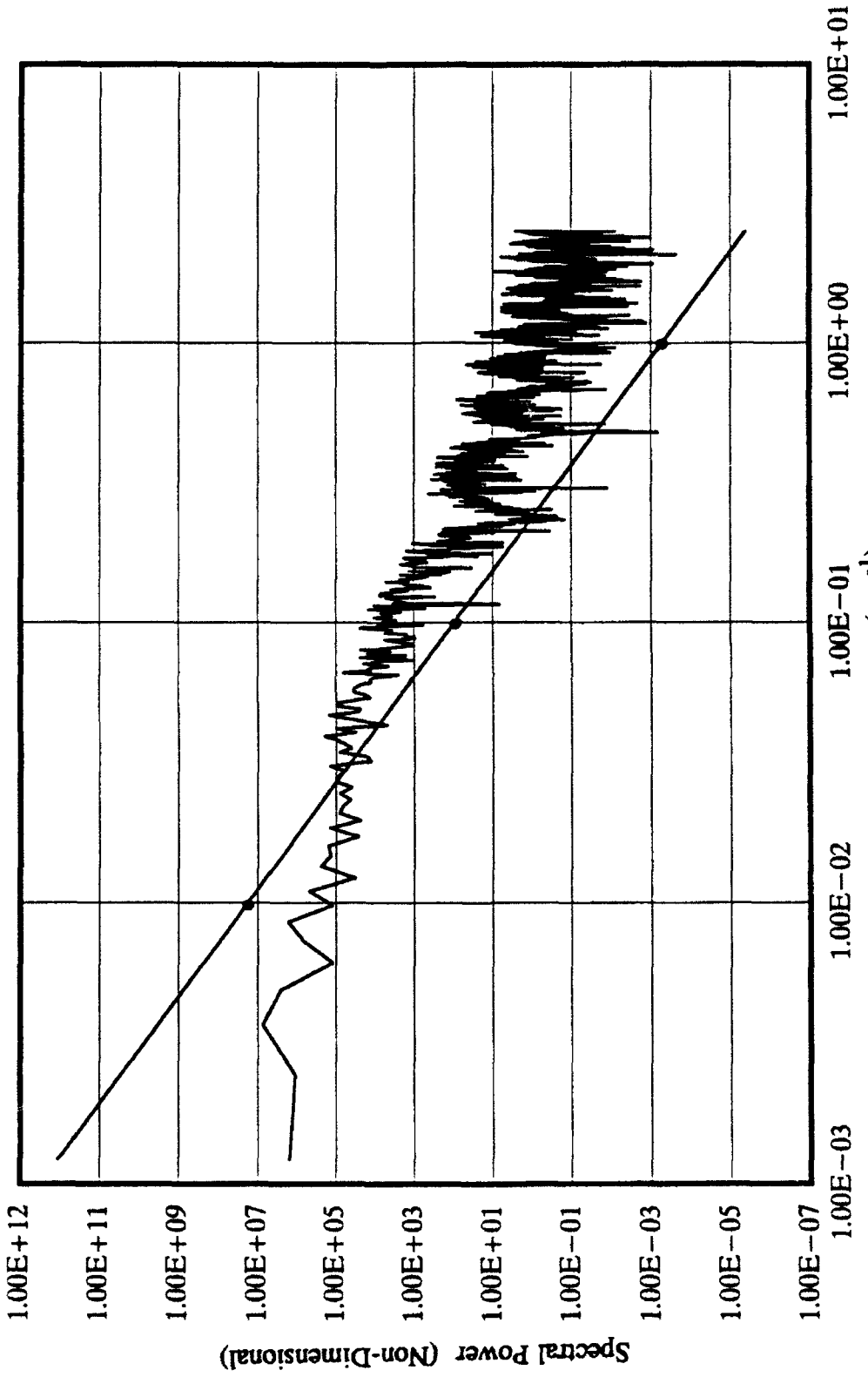
Spectral Power (Non-Dimensional)
1.00E+12
1.00E+11
1.00E+09
1.00E+07
1.00E+05
1.00E+03
1.00E+01
1.00E-01
1.00E-03
1.00E-05
1.00E-07
1.00E-03
1.00E-02
1.00E-01
1.00E+00
1.00E+01
Frequency (sec-1)
Power Spectrum
-5/3 Slope

Figure 51

Figure 52. As in Fig. 51, for cup anemometer horizontal component.

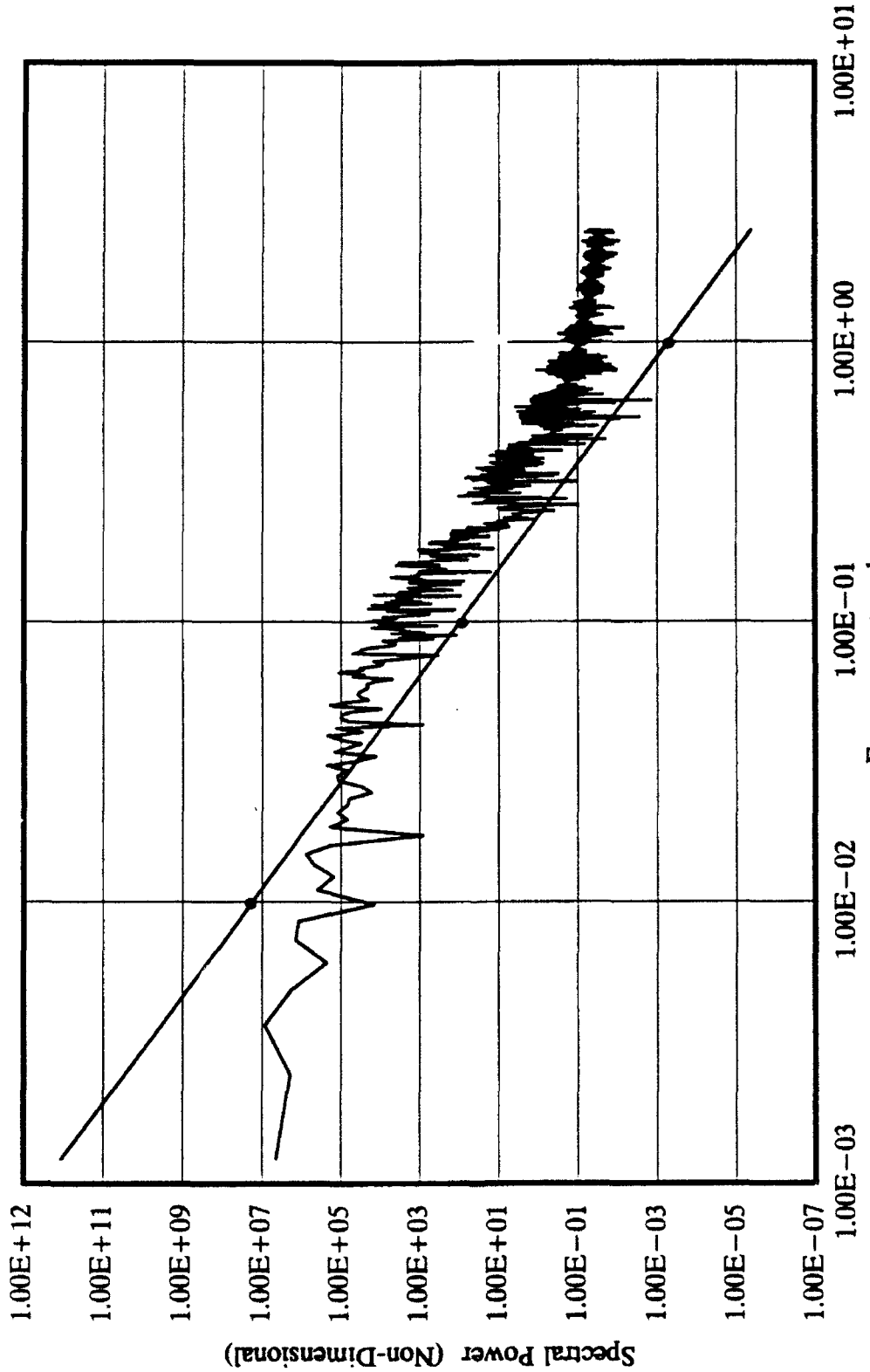
Spectral Power (Non-Dimensional)
1.00E+12
1.00E+11
1.00E+09
1.00E+07
1.00E+05
1.00E+03
1.00E+01
1.00E-01
1.00E-03
1.00E-05
1.00E-07
1.00E-03
1.00E-02
1.00E-01
1.00E+00
1.00E+01
Frequency (sec-1)
Power Spectrum
-5/3 Slope

Figure 52

Figure 53. As in Fig. 51, for sonic anemometer vertical component.

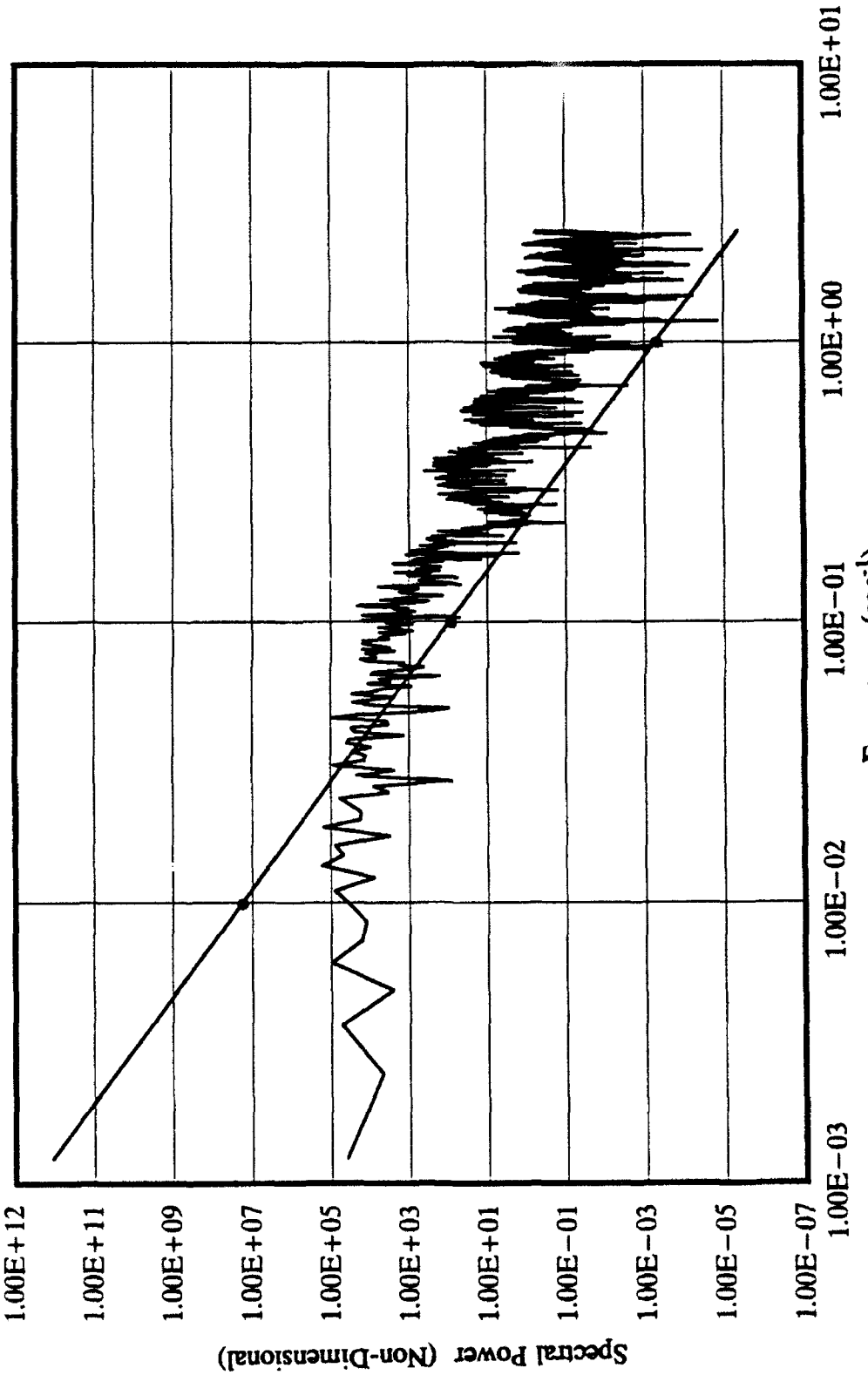
Spectral Power (Non-Dimensional)
1.00E+12
1.00E+11
1.00E+09
1.00E+07
1.00E+05
1.00E+03
1.00E+01
1.00E-01
1.00E-03
1.00E-05
1.00E-07
1.00E-03
1.00E-02
1.00E-01
1.00E+00
1.00E+01
Frequency (sec-1)
Power Spectrum
-5/3 Slope

Figure 53

Figure 54. As in Fig. 51, for estimated vertical component.

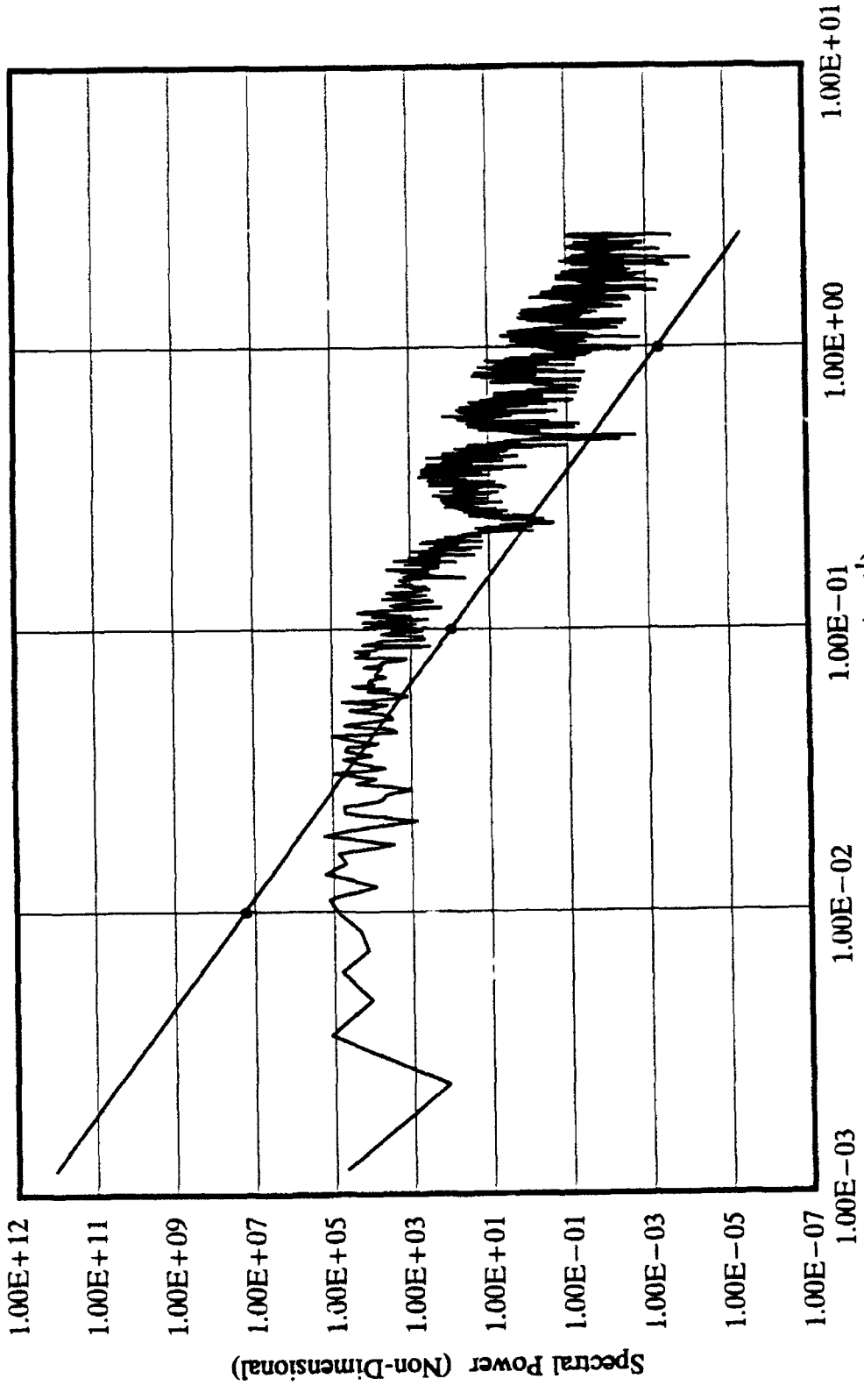
1.00E+12
1.00E+11
1.00E+09
1.00E+07
1.00E+05
1.00E+03
1.00E+01
1.00E-01
1.00E-03
1.00E-05
1.00E-07
Spectral Power (Non-Dimensional)
1.00E-03
1.00E-02
1.00E-01
1.00E+00
1.00E+01
Frequency (sec-1)
Power Spectrum
-5/3 Slope

Figure 54

Figure 55. As in Fig. 51, for sonic anemometer vertical angle.

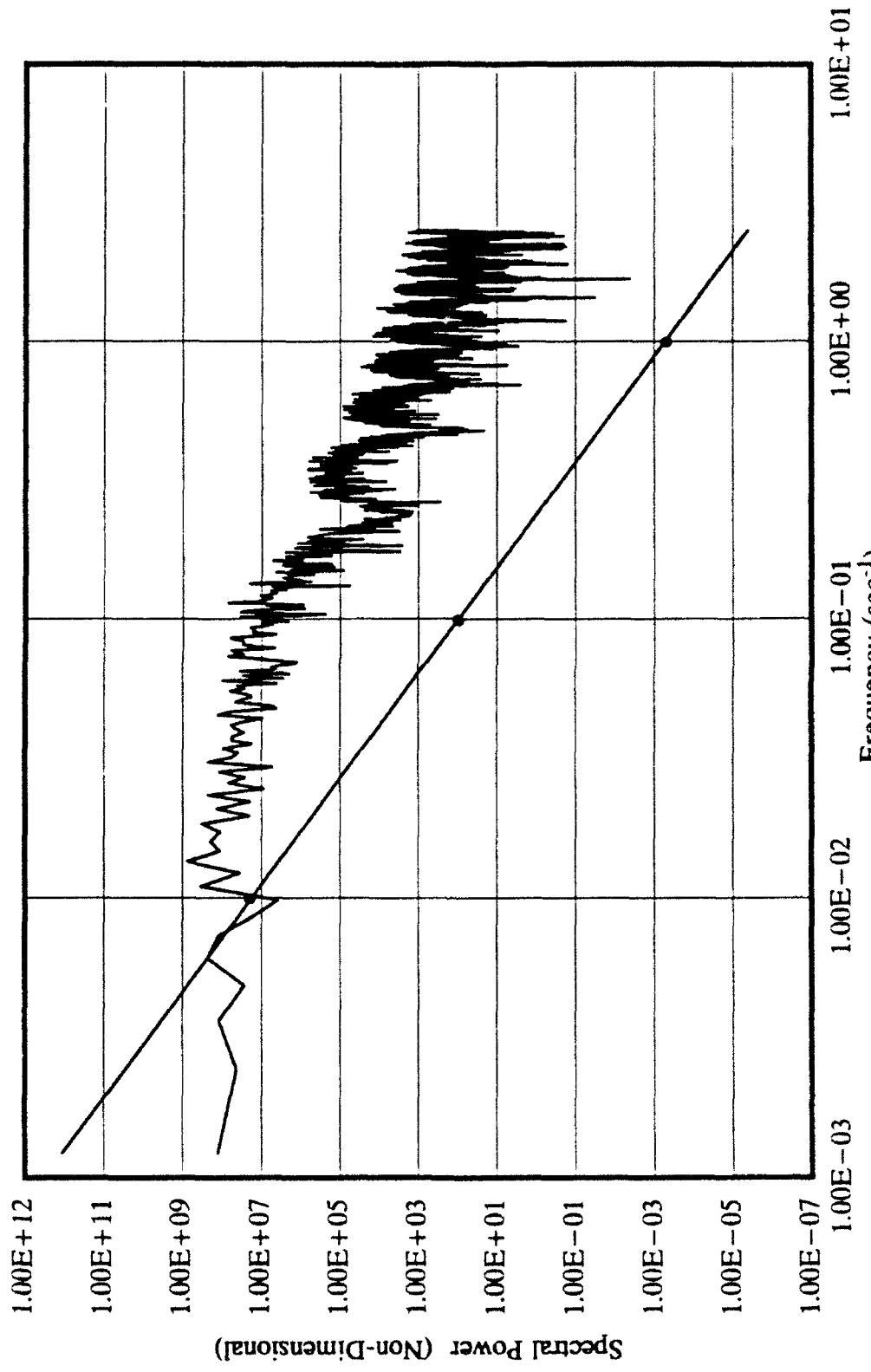
1.00E+12
1.00E+11
1.00E+09
1.00E+07
1.00E+05
1.00E+03
1.00E+01
1.00E-01
1.00E-03
1.00E-05
1.00E-07
Spectral Power (Non-Dimensional)
1.00E-03
1.00E-02
1.00E-01
1.00E+00
1.00E+01
Frequency (sec-1)
Power Spectrum
-5/3 Slope

Figure 55

Figure 56. As in Fig. 51, for dual-annulus bivane vertical angle.

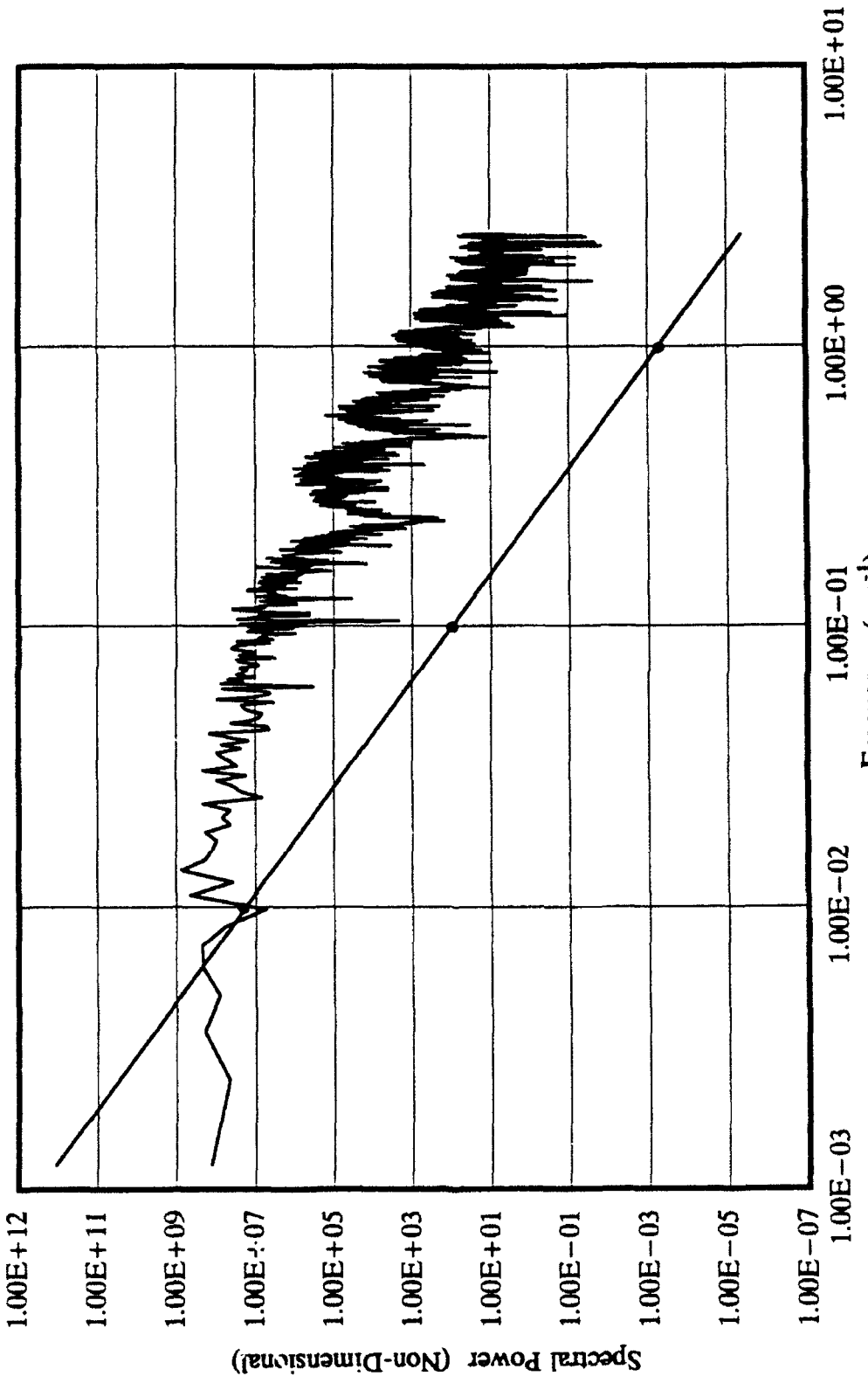
Spectral Power (Non-Dimensional)
1.00E+12
1.00E+11
1.00E+09
1.00E+07
1.00E+05
1.00E+03
1.00E+01
1.00E-01
1.00E-03
1.00E-05
1.00E-07
1.00E-03
1.00E-02
1.00E-01
1.00E+00
1.00E+01
Frequency (sec-1)
Power Spectrum
-5/3 Slope

Figure 56

components listed above. As suggested above, the bivane seems to exhibit a slope much closer to the desired value. The magnitude of the oscillations is also greater for the sonic anemometer, which may be a reflection of the fact that it measures more high-frequency perturbations.

6.2.4. Cross-Correlation of Wind Components

The power spectrum for the sonic anemometer covariance is shown in Figure 57; the corresponding spectrum for the estimation derived from the cup anemometer and dual-annulus bivane is shown in Figure 58.

These two spectra approximate the -5/3 slope. This suggests a definite connection between the desired slope and the covariance as a measure of turbulent transfer. Why the individual components comprising the covariances do not all conform to the desired slope as well is not known, and should be studied further.

It would appear the results seen in the covariances imply the data conform to the $-5/3^{rds}$ power law. However, significant aliasing appears to have distorted the slope in the inertial subranges of several components, particularly from the sonic anemometer. This result was noted by Kaimal and Kristensen (1990), who stated that this instrument seemed to be more prone to aliasing than other instruments used in turbulent measurements.

This discussion touches upon a small portion of data obtainable through spectral analysis. It is strongly recommended that further study be conducted, with emphasis placed on the following topics: (1) estimation of momentum flux through spectral analysis, (2)

Figure 57. As in Fig. 51, for sonic anemometer covariance of horizontal and vertical components.

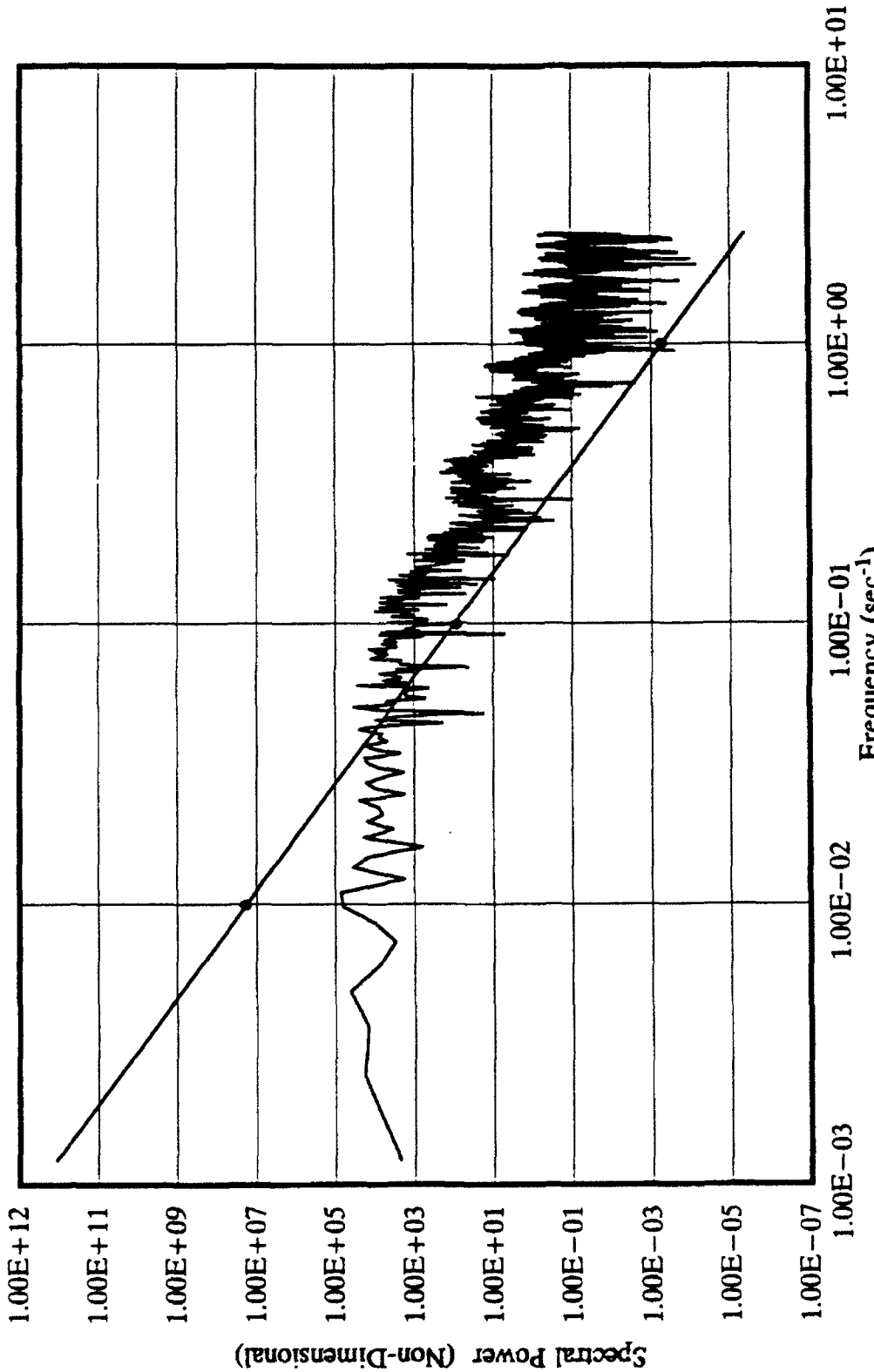
Spectral Power (Non-Dimensional)
1.00E+12
1.00E+11
1.00E+09
1.00E+07
1.00E+05
1.00E+03
1.00E+01
1.00E-01
1.00E-03
1.00E-05
1.00E-07
1.00E-03
1.00E-02
1.00E-01
1.00E+00
1.00E+01
Frequency (sec-1)
Power Spectrum
-5/3 Slope

Figure 57

Figure 58. As in Fig. 51, for estimated covariance of horizontal and vertical components.

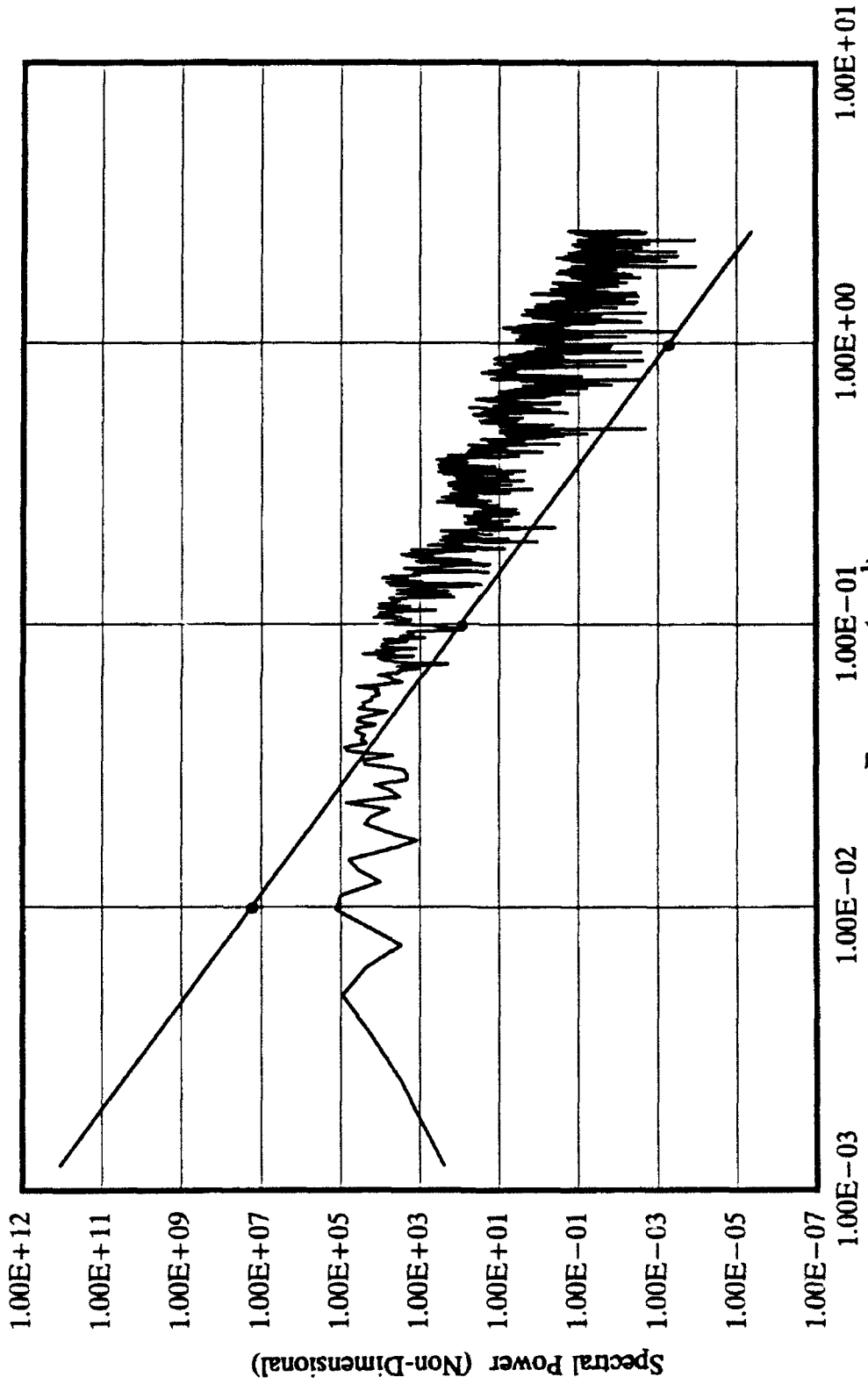
1.00E+12
1.00E+11
1.00E+09
1.00E+07
1.00E+05
1.00E+03
1.00E+01
1.00E-01
1.00E-03
1.00E-05
1.00E-07
Spectral Power (Non-Dimensional)
1.00E-03
1.00E-02
1.00E-01
1.00E+00
1.00E+01
Frequency (sec-1)
Power Spectrum
-5/3 Slope

Figure 58

determination of frequencies at which momentum is transferred, (3) determination of required sampling rates to prevent aliasing, (4) determination of proper pre-filtering widths to minimize aliasing without distortion of the slope of the inertial subrange, and (5) determination of buoyancy wave number using Taylor's hypothesis (after Finnigan et al., 1984).

6.3. Experimental Results

Criteria used for judging the validity of the flux estimation methods, (τ_{MC-cb} and τ_{EC-cb}) as compared with the 'true' value (τ) are: (1) whether the estimations are the same order of magnitude as τ, and (2) whether the direction of the flux is the same (as indicated by sign). Calculated results meeting both criteria are said to yield representative values of momentum flux.

6.3.1. Data Run 1 (30 April 1992)

The first data sample was taken shortly after local noon (1202 EST) on a clear, mid-spring day. There was abundant insolation, and surface ambient temperatures approached 25° C. An accurate Monin-Obukov stability parameter not obtainable, as virtual temperature measurements were not available. With the area under a large ridge of high pressure, strong subsidence was evident in the lack of any cloud development. Based on these observations, near-surface stability appeared to be neutral to perhaps slightly unstable (i.e., $z/L \simeq 0$).

Surface winds were predominantly from the southwest. Wind speeds remained light throughout the run, with both sonic and cup anemometer mean velocities less than 2.0 m s^{-1}. There were several periods of

relative gustiness; however, the maximum horizontal wind speed detected by the sonic anemometer was less than 5.0 m s^{-1}. Conversely, horizontal speeds approached calm conditions on several occasions, suggesting weak near-surface turbulent mixing.

6.3.1.1. Results

Momentum flux calculations for the first data run are given in Table 2. Statistical quantities for measured and derived components for both base (i.e., actual, unfiltered) and detrended (i.e., with the least-squares best-fit regression removed) data are presented in Tables 3 and 4, respectively.

The flux values for this run were an order of magnitude smaller than originally anticipated; the near-surface instability was initially estimated to be light-to-moderate, which should yield flux values of 10^{-1} N m^{-2} (Stull, 1988). Indeed, most of the values indicated a flux away from the surface. In reality, the momentum flux was likely essentially null during this run. If one considers the obvious strong stability of the lower troposphere, it seems logical that significant turbulent transfer in the ABL could be retarded well beyond solar noon (the approximate time of the experiment), when maximum insolation occurs.

Table 2. Momentum Flux Calculations for Data Run One, 1202 EST, 30 April 1992.

Calculation Method	Value ($N\ m^{-2}$)	Percent Difference From 'True' Flux
Eddy-Correlation From Sonic Anemometer ('true' value), τ	0.01699	-------
Approximation From Cup & Bivane, τ_{MC-cb}	-4.164×10^{-4}	-97.55
Eddy-Correlation From Cup & Bivane, τ_{EC-cb}	-0.05360	-415.48
Approximation From Sonic Anemometer (for check of Chimonas' math/physics only), τ_{check}	-0.01558	-191.70

Further evidence of the null flux result can be found in the means of both covariances, $\overline{u'w'}_{son}$ and $\overline{u'w'}_{est}$ (Table 4). Both give values well below the instrument's ability to accurately measure the components from which these values are derived from, and likely are instrument 'noise'. Similarly, the mean corrected vertical angles (i.e., with the offset angle subtracted) from both the bivane and sonic anemometer were less than 10^{-2} radians. These values are not within the sensitivity capability of either instrument, and also appear to be noise. With the respective covariances and vertical angles indicating little vertical transport, the only logical conclusion is that is that little or no vertical transport of momentum occurred during the run.

Having reached this determination, the fact that each method produced a flux value of essentially zero is an indication that all produced representative values. Thus, one can tentatively conclude

Table 3. Results and Statistical Data for Measured Quantities for Run One, 1202 EST, 30 April 1992, for Base and Detrended Data.

	u_{son} ($m\ s^{-1}$)	u_{cup} ($m\ s^{-1}$)	W_{son} ($m\ s^{-1}$)	ϕ_{biv} (deg)
BASE DATA				
Mean (μ)	1.695	1.852	0.061	3.125
Standard Deviation (σ)	0.755	0.849	0.325	13.346
Maximum Value	4.989	4.904	1.500	52.500
Minimum Value	0.155	0.178	-0.998	-48.667
Range of Values	4.834	4.726	2.498	101.167
Slope (β_0)	6.52×10^{-4}	1.01×10^{-3}	8.76×10^{-5}	2.11×10^{-3}
Intercept (β_1)	1.402	1.372	0.022	2.177
DETRENDED DATA ($\mu = \beta_0 = \beta_1 \equiv 0$)				
Standard Deviation (σ)	0.736	0.849	0.324	13.334
Maximum Value	3.317	4.904	1.141	49.010
Minimum Value	-1.602	0.178	-0.998	-50.991
Range of Values	4.919	4.726	2.498	100.001

Notes: (1) Slope and Intercept are from least-squares, best-fit regression. (2) Data for u_{son} is filtered to remove spurious data. (3) 'u' refers to the total horizontal wind component.

Table 4. Results and Statistical Data for Derived Quantities for Run One, 1202 EST, 30 April 1992, for Base and Detrended Data.

	w_{est} (m s^{-1})	$u'w'_{est}$ (m^2 s^{-2})	$u'w'_{son}$ (m^2 s^{-2})	ϕ_{son} (deg)
BASE DATA				
Mean (μ)	0.077	-0.0003	0.014	2.333
Standard Deviation (σ)	0.367	0.347	0.268	14.003
Maximum Value	2.105	4.507	2.298	70.814
Minimum Value	-1.236	-2.741	-2.023	-57.404
Range of Values	3.342	7.248	4.322	128.218
Slope (β_0)	1.24×10^{-4}	7.90×10^{-5}	3.03×10^{-5}	1.64×10^{-3}
Intercept (β_1)	0.021	-0.036	5.51×10^{-4}	1.597
DETRENDED DATA ($\mu = \beta_0 = \beta_1 = 0$)				
Standard Deviation (σ)	0.365	0.601	0.373	13.997
Maximum Value	1.986	5.111	2.505	69.063
Minimum Value	-1.319	-2.086	-1.711	-59.799
Range of Values	3.305	7.197	4.216	128.862

Note: Slope and Intercept are from least-squares best-fit regression

that the approximation, τ_{MC-cb}, and the eddy-correlation method using the cup/bivane system, τ_{EC-cb}, both yield reasonable momentum flux values for neutral to slightly unstable near-surface conditions in this case.

Post-collection data analysis detected a period of spurious data in the sonic anemometer horizontal component during the last third of the data run. These anomalies, manifested in data 'spikes', were found in 38 of the 4501 data points ($\simeq$ 0.8% of the data). The spikes, which were easily identified, were eliminated by replacing them with the average of the data points recorded immediately before and after. The corrected data was deemed acceptable for use because only a very small portion of the original data was contaminated. Indeed, the removal of the spikes had no discernible effect on the flux calculations, but did alter the minimum measured value and range for the component. After the spurious data were removed, these values were much more consistent with their counterparts from the cup anemometer.

6.3.2 Data Run 2 (12 August 1992)

The mechanical problem causing the data spikes in the sonic anemometer horizontal component resulted in a significant time gap between the first and second experiments. The unit was repaired but performed inconsistently (the output voltage range was not constant). Another unit was subsequently obtained and used for the second and third data runs.

The second data run was taken during mid-afternoon (1506 EST) on a cloudy, unstable day ($z/L \simeq -0.45$). The near-surface temperature

averaged nearly 28° C, about 3° C cooler than the climatological high temperature for the day. Abundant cumulus coverage left little doubt as to the instability in the ABL and lower troposphere. Near-surface winds were west-southwesterly and averaged nearly 1.0 m s^{-1} higher than during the first experiment. The risk of precipitation prevented further data collection under more turbulent conditions following the experiment period.

6.3.2.1. Results

Momentum flux calculations for the second data run are given in Table 5. Statistical quantities for measured and derived components for both base and detrended data are presented in Tables 7 and 8, respectively.

The near-surface instability characterizing this run was reflected in the flux calculations, which were an order of magnitude greater than the first run. The most striking feature, however, is the relative equality of the computations. All values indicated a downward-directed flux of momentum, which should be expected based on the means of vertical velocities, vertical angles, and covariances listed in Tables 7 and 8.

Of particular interest is the accuracy of the eddy-correlation using the cup and bivane (τ_{EC-cb}). This implies either the cup anemometer, or bivane, or both, have sufficient high-frequency response for a direct cross-correlation calculation. If the respective time-series for u_{cup} and ϕ_{biv} are filtered using a 21-point running average, the component having the better high-frequency response will show the greatest decrease in variance (by percentage). These results

are shown in Table 6.

Table 5. Momentum Flux Calculations for Data Run Two, 1506 EST, 12 August 1992.

Calculation Method	Value (N m^{-2})	Percent Difference From 'True' Flux
Eddy-Correlation From Sonic Anemometer ('true' value), τ	0.15814	-------
Approximation From Cup & Bivane, τ_{MC-cb}	0.09179	41.95
Eddy-Correlation From Cup & Bivane, τ_{EC-cb}	0.11352	28.22
Approximation From Sonic Anemometer (for check of Chimonas' math/physics only), τ_{check}	0.15028	4.97

Table 6. Comparison of Variance Change For Cup Anemometer Wind Speed and Bivane Vertical Angle For Base and Filtered Data, Run One.

Component	Variance for Base Data	Variance for Filtered Data	Percent Change
Bivane Vertical Angle, ϕ_{biv}	178.101°	111.562°	-37.36%
Cup Anemometer Wind Speed, u_{cup}	0.7203 m s^{-1}	0.7345 m s^{-1}	1.97%

Clearly, the bivane has the better high-frequency response. It would appear that the dual-annulus bivane, with its light-weight, space-age construction, responds with sufficient alacrity to high-

Table 7. Results and Statistical Data for Measured Quantities for Run Two, 1506 EST, 12 August 1992, for Base and Detrended Data.

	u_{son} ($m\ s^{-1}$)	u_{cup} ($m\ s^{-1}$)	w_{son} ($m\ s^{-1}$)	ϕ_{biv} (deg)
BASE DATA				
Mean (μ)	2.311	2.456	-0.091	-1.377
Standard Deviation (σ)	0.779	0.732	0.450	11.048
Maximum Value	5.447	4.857	1.600	36.227
Minimum Value	0.533	1.108	-1.700	-44.641
Range of Values	4.913	3.839	3.300	80.868
Slope (β_0)	1.02×10^{-3}	1.09×10^{-3}	-1.98×10^{-4}	-1.44×10^{-3}
Intercept (β_1)	1.869	1.982	-0.006	-0.758
DETRENDED DATA ($\mu = \beta_0 = \beta_1 = 0$)				
Standard Deviation (σ)	0.736	0.678	0.448	11.042
Maximum Value	3.012	2.262	1.758	38.138
Minimum Value	-2.160	-1.799	-1.551	-42.727
Range of Values	5.028	4.061	3.309	80.866

Notes: (1) Slope and Intercept are from least-squares best-fit regression. (2) 'u' refers to the total horizontal wind component.

Table 8. Results and Statistical Data for Derived Quantities for Run Two, 1506 EST, 12 August 1992, for Base and Detrended Data.

	w_{est} ($m\ s^{-1}$)	$u'w'_{est}$ ($m^2\ s^{-2}$)	$u'w'_{son}$ ($m^2\ s^{-2}$)	ϕ_{son} (deg)
BASE DATA				
Mean (μ)	-0.089	-0.095	-0.1319	-0.914
Standard Deviation (σ)	0.489	0.397	0.360	12.407
Maximum Value	2.035	2.126	2.125	59.065
Minimum Value	-1.989	-2.984	-2.669	-51.499
Range of Values	4.024	5.110	4.795	110.565
Slope (β_0)	1.24×10^{-4}	-1.29×10^{-4}	-3.86×10^{-5}	4.96×10^{-3}
Intercept (β_1)	-0.035	-0.038	-0.115	1.218
DETRENDED DATA ($\mu = \beta_0 = \beta_1 = 0$)				
Standard Deviation (σ)	0.488	0.396	0.360	12.345
Maximum Value	2.165	2.250	2.262	59.365
Minimum Value	-1.854	-2.873	-2.527	-49.391
Range of Values	4.020	5.123	4.789	108.756

Note: Slope and Intercept are from least-squares best-fit regression.

frequency fluctuations to yield representative flux values when paired with a cup anemometer having a distance constant well matched to the vane's natural wavelength.

The relative equality between τ and τ_{check} indicates Chimonas' physical and mathematical reasoning relating the component means for u and ϕ and the cross-correlations of the u- and w-components is sound. The relative equality of τ_{MC-cb} and τ_{EC-cb} is further evidence of this.

Based on the results from run two, both estimation methods, τ_{MC-cb} and τ_{EC-cb} produce representative values for momentum flux, tentatively indicating the use of either method is acceptable.

6.3.3. Data Run 3 (13 August 1992)

The third data run was taken at approximately the same time as the previous experiment (1525 EST). Unlike the previous day, however, the sky was clear, and the wind speeds were a little more variable (although mean speeds were comparable). A cold-front had passed through the area during the previous evening, resulting in a slightly cooler mean near-surface temperature of 26° C. The cloudless sky was similar to the first data run, suggesting strong subsidence again existed throughout the troposphere. The Monin-Obukov stability factor was $\simeq$ -0.60, indicating near-surface instability was slightly more pronounced than during the previous run.

The mechanical failure of an the dual-annulus necessitated an instrument change. The bivane experienced a electronics failure, and was replaced with a larger, slower-responding (Coats, 1991) cruciform-tailed vane[13]. To accommodate the new vane and minimize shadowing effects, the helicoid anemometer was removed from the cross-bar, and

the separation between adjacent instruments was increased to approximately 0.8 meters.

Although this replacement meant all of the field tests would not be undertaken with the same equipment, it provided the opportunity to contrast the effects of the different vanes on flux calculations for experiments with relatively similar near-surface stabilities, as seen during runs two and three.

6.3.3.1. Results

Momentum flux calculations for the third data run are given in Table 9. Statistical quantities for measured and derived components for base and detrended data are presented in Tables 10 and 11, respectively.

Overall, the flux values are similar to the second data run, indicating a downward-directed flux of momentum. This result is not unexpected, as the near-surface stabilities were similar (even though the synoptic conditions had changed greatly). The second and third experiments were conducted at about the same time of day, although this would not appear to be a significant factor taken by itself.

The only significant difference between data runs two and three is the values of τ_{MC-cb} and τ_{EC-cb} with respect to the true value, τ. In the second experiment, these two values are smaller than the actual flux, τ; in the third, both are larger. The reason for this difference can be traced to the different bivanes used.

Table 9. Momentum Flux Calculations for Data Run Three, 1525 EST, 13 August 1992.

Calculation Method	Value (N m^{-2})	Percent Difference From 'True' Flux
Eddy-Correlation From Sonic Anemometer ('true' value), τ	0.19435	-------
Approximation From Cup & Bivane, τ_{MC-cb}	0.28894	48.54
Eddy-Correlation From Cup & Bivane, τ_{EC-cb}	0.27084	39.23
Approximation From Sonic Anemometer (for check of Chimonas' math/physics only), τ_{check}	0.19897	2.28

Examining both runs all other parameters used in the flux calculations (the mean vertical and horizontal components, mean vertical angles measured by the sonic anemometer, and the horizontal components measured by the cup anemometer) were nearly identical. However, in the second run, the mean vertical angle from the dual-annulus bivane (corrected for leveling error) is less than the corresponding mean from the sonic anemometer. This pattern is reversed in the third run; the corrected mean angle from the cruciform-tailed bivane is greater than that of the sonic anemometer (Table 12).

This difference is a consequence of the larger, more massive cruciform vane's lesser ability to detect high-frequency fluctuations in the vertical component. Again, this is readily seen if the respective time-series of vertical angle for each vane is filtered with a 21-point running average, thus removing high-frequency perturbations.

Table 10. Results and Statistical Data for Measured Quantities for Run Three, 1525 EST, 13 August 1992, for Base and Detrended Data.

	u_{son} ($m\ s^{-1}$)	u_{cup} ($m\ s^{-1}$)	w_{son} ($m\ s^{-1}$)	ϕ_{biv} (deg)
BASE DATA				
Mean (μ)	2.341	2.536	-0.097	-0.101
Standard Deviation (σ)	0.927	0.948	0.586	18.318
Maximum Value	5.675	6.550	1.710	56.489
Minimum Value	0.028	0.664	-2.350	-54.864
Range of Values	5.647	5.886	4.060	111.353
Slope (β_0)	-5.89×10^{-4}	-8.48×10^{-4}	1.47×10^{-5}	5.49×10^{-3}
Intercept (β_1)	2.606	2.917	-0.104	-2.570
DETRENDED DATA ($\mu = \beta_0 = \beta_1 = 0$)				
Standard Deviation (σ)	0.915	0.922	0.586	18.263
Maximum Value	3.464	3.878	1.800	55.129
Minimum Value	-2.124	-1.650	-2.255	-56.541
Range of Values	5.679	5.528	4.056	111.712

Notes: (1) Slope and Intercept are from least-squares best-fit regression. (2) 'u' refers to the total horizontal wind component.

Table 11. Results and Statistical Data for Derived Quantities for Run Three, 1525 EST, 13 August 1992, for Base and Detrended Data.

	w_{est} ($m\ s^{-1}$)	$u'w'_{est}$ ($m^2\ s^{-2}$)	$u'w'_{son}$ ($m^2\ s^{-2}$)	ϕ_{son} (deg)
BASE DATA				
Mean (μ)	-0.099	-0.228	-0.162	-0.648
Standard Deviation (σ)	0.661	0.768	0.620	17.155
Maximum Value	1.939	5.116	3.761	82.092
Minimum Value	-2.302	-8.522	-4.878	-88.295
Range of Values	4.241	13.638	8.639	170.388
Slope (β_0)	2.49×10^{-5}	-3.03×10^{-4}	-1.42×10^{-4}	1.32×10^{-3}
Intercept (β_1)	-0.111	-0.089	-0.097	-1.244
DETRENDED DATA ($\mu = \beta_0 = \beta_1 = 0$)				
Standard Deviation (σ)	0.661	0.764	0.619	17.151
Maximum Value	2.043	5.286	3.947	82.492
Minimum Value	-2.198	-8.345	-4.739	-87.867
Range of Values	4.241	13.631	8.685	170.359

Note: Slope and Intercept are from least-squares best-fit regression.

Accordingly, the variance of a data set with a greater percentage of high-frequency fluctuations should be reduced more when filtered.

Table 12. Corrected Mean Vertical Angles for Dual-Annulus Bivane (Run Two) and Cruciform-Tailed Bivane (Run Three), As Opposed to Sonic Anemometer Mean Vertical Angles.

	Run Two	Run Three
Dual-Annulus Bivane:		
$\bar{\phi}_{son}$	1.3431°	----------
$\bar{\phi}_{biv}$	0.7269°	----------
Difference: $\bar{\phi}_{biv} - \bar{\phi}_{son}$	-0.6162°	----------
Cruciform-Tail Bivane:		
$\bar{\phi}_{son}$	----------	1.7394°
$\bar{\phi}_{biv}$	----------	2.1451°
Difference $\bar{\phi}_{biv} - \bar{\phi}_{son}$	----------	+0.4057°

Table 13 shows the percentage difference between variances of the two vanes when the base data are filtered. The variance for the dual-annulus bivane changes by a greater percentage, indicating a greater percentage of high-frequency data is filtered out of that vane's response. Additionally, the larger tail implies the vane must 'see' a larger parcel of air to produce a comparable response. These factors could result in a slightly higher corrected mean value for ϕ_{biv}, leading to a slightly higher derived value for both τ_{MC-cb} and τ_{EC-cb}.

The second and third experiments suggest values for both τ_{MC-cb}

and τ_{EC-cb} may slightly underestimate the 'true' flux when a dual-annulus bivane is used; conversely, these values may overestimate the 'true' flux when a cruciform vane is used. However, each estimation appears to yield reasonable values which are representative of the 'true' flux, and supports the validity of the respective estimation methods.

Table 13. Percentage Change in Variance for Base and Filtered Base Data, Dual-Annulus and Cruciform-Tailed Bivanes, Runs One Through Three.

	Variance of Unfiltered Base Data	Variance of Filtered Base Data	Percent Difference Unfiltered - Filtered Data
Run Two			
Dual-Annulus Bivane	$122.058^{\circ 2}$	$41.887^{\circ 2}$	-62.620%
Run Three			
Cruciform-Tail Bivane	$335.549^{\circ 2}$	$173.659^{\circ 2}$	-48.246%

Returning to a point noted in 6.3.1.1.; the fact that significant near-surface instability existed during the third run, but not in the first (although synoptic conditions were similar), tends to confirm the assertions that: (1) sufficient time and insolation were required to overcome the strong subsidence existing in the troposphere; and (2) under such conditions, significant turbulence can be delayed until after the time of maximum insolation, with the delay time a function of both the amount of insolation and the magnitude of the subsidence.

7. CLOSING REMARKS

7.1. Final Discussion

The results from the experiments show a direct relationship between momentum flux and bivane vertical deflection. Based on the running sum of the covariances in Figures 48-51, momentum flux does not occur in a time-extensive, gradual manner, but in short 'packets' or bursts. These bursts appear to coincide with the convective plumes seen in the vertical velocity and vertical angle traces.

Another feature of interest is the mean bivane deflection during periods when the covariance of the wind components is negative. If one examines the idealized turbulent eddy in Figure 59, there are two cases where the covariance is negative. The first, labeled case a, occurs on the 'back side' of a turbulent eddy. In this case, low momentum air rises through buoyancy forces. This is often seen at the surface as a lull in the horizontal wind speed. This lull is reflected in a negative instantaneous value of u'. Simultaneously, due to the increased rising motion, $w' > 0$. The second case, labeled b, occurs on the 'front side' of the eddy, where higher momentum air is brought down towards the surface. This is reflected in an increase in gustiness (i.e., higher horizontal wind speed) near the surface. In this case, $u' > 0$, and $w' < 0$.

Examining the geometry in Figure 60, assuming the magnitudes of u' and w' are identical in each case, and the vane is properly leveled

Momentum Flux in a turbulent eddy: two cases where $u'w' < 0$.

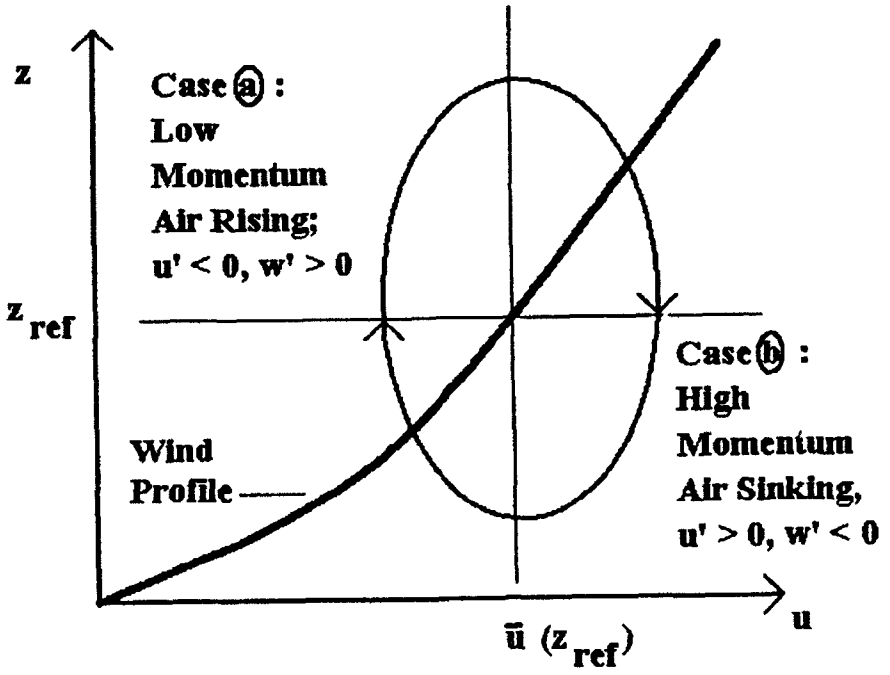

Figure 59. Momentum flux in an idealized turbulent eddy, showing regions of negative wind covariances. In this case, the mean of u is chosen for an eddy centered at a reference height z_{ref}.

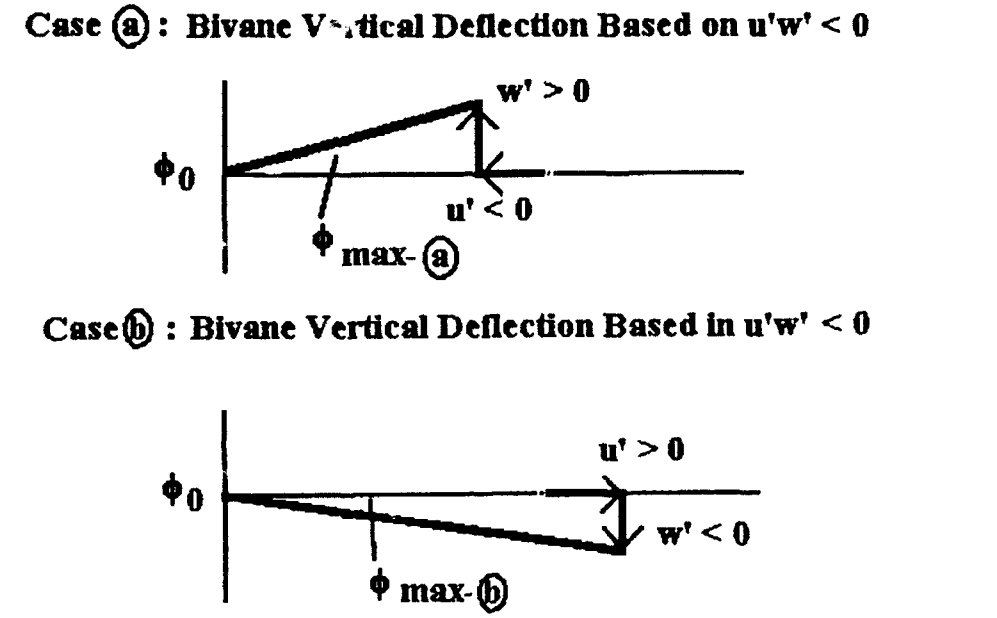

Figure 60. Two cases for maximum magnitude of bivane vertical deflection based on a negative wind covariance. A series of deflections simulating the passage of several idealized eddies is presented below.

to a reference angle such that $\phi_0 = 0$, it is apparent a larger maximum vertical deflection results from case a, which is an upwards displacement. This implies for each idealized turbulent eddy interacting with the bivane, the magnitude of the upwards displacement will be greater than the magnitude of the downward displacement. Thus, over a significant period of time (at least 15 minutes) and assuming the bivane is properly leveled, a net downward-directed momentum flux results in a mean positive (or upward) vertical deflection of the bivane. The results from the last two experiments verify this conclusion (Table 14). In each run, the mean covariances from each instrument system (sonic anemometer and bivane/cup) were negative, and the mean bivane angles (corrected for leveling error) were positive. Note the reverse relationships between calculations from the bivane/cup systems and the sonic anemometer for the two runs. This is further evidence of the cruciform bivane's lesser ability to detect high-frequency perturbations, leading to a greater mean angular displacement and covariance as compared with the sonic anemometer.

An interesting consequence noted in the field was the tendency of the bivane appear to move more quickly when moving downwards past the reference angle. Examining Figure 60, one can see that a greater angular displacement occurs in case a. Thus, an upwards-displaced vane tail would have a greater distance to traverse to reach its maximum displacement (at ϕ_{max-a}). This causes the vane to appear to move slower when displaced upwards from the reference angle than when the displacement is downwards.

Table 14. Comparison of Mean Wind Covariances and Corrected Mean Bivane Vertical Angles for Runs Two and Three.

	Run Two	Run Three
Mean Covariance from Sonic Anemometer	$-0.132\ m^2\ s^{-2}$	$-0.162\ m^2\ s^{-2}$
Mean Covariance from Bivane/Cup Anemometer	$-0.095\ m^2\ s^{-2}$	$-0.225\ m^2\ s^{-2}$
Corrected Mean Vertical Angle from Sonic Anemometer	1.343°	1.739°
Corrected Mean Vertical Angle from Dual-Annulus Bivane (Run Two) and Cruciform Bivane (Run Three)	0.727°	2.145°

The results from the three field experiments support Chimonas' position that mean values for horizontal wind speed and vertical angle measured with a cup anemometer and bivane (with less than ideal response) can yield representative values for momentum flux. That the modified version of his approximation (i.e., the MCAM) yields flux estimations different from the 'true' values is a consequence of: (1) the less than ideal response of the bivane and cup anemometer, and (2) the fact that it is physically impossible for each instrument to sample the same turbulent eddy simultaneously. The experiments confirmed Chimonas' mathematical and physical reasoning by showing flux values obtained from the eddy-correlation method and the MCAM yielded nearly identical flux values when applied to a specific instrument system (sonic anemometer or cup/bivane).

Additionally, the experiments showed that a system comprised of a less-than-ideally responding cup anemometer and bivane (well-matched by

distance constant and natural wavelength, respectively), yields representative momentum flux values using the eddy-correlation method provided the bivane has sufficient high-frequency response. The cup anemometer's ability to detect high-frequency turbulent fluctuations does not appear to be as crucial as for the bivane. This indicates that an accurate measurement of the vertical component is the key ingredient in any measurement of momentum flux. The dual-annulus bivane employed for the first two field tests displayed sufficient high-frequency response to yield accurate flux values. A cruciform-tailed bivane used on the final experiment did not display the same high-frequency sensitivity of the other bivane, but also yielded representative flux estimates.

Unfortunately, instrument failures and time constraints allowed only three field experiments to be conducted. The study was originally envisioned to undertake several times that amount, with varying collection periods, sampling rates, and stability conditions. Because such a small amount of data was examined, the conclusions reached regarding the validity of the tested methods can only be regarded as tentative. Nonetheless, the results presented justify further study of this problem using the varying conditions discussed above.

7.2. Closing Summary

This study was intended to determine whether a bivane and cup anemometer could be used to estimate momentum flux values representative of the actual flux, as determined with a sonic anemometer. Two estimation methods were examined: (1) a modified

version of an approximation suggested by Chimonas (1980), which used mean values of horizontal wind speed and vertical deflection, and (2) an eddy-correlation (i.e., covariance) method, using instantaneous departures from the mean horizontal and vertical components measured and derived from the bivane and cup anemometer.

The cup anemometer and dual-annulus bivane used were chosen for their fast responses and similar distance constants (determined during prior testing). Prior to field testing, each instrument used was thoroughly tested to ensure its operational characteristics and exact transfer functions were known.

Three field experiments were conducted from 30 April 1992 to 13 August 1992. Equipment problems prevented further tests from being conducted. The first test was held under near-neutral near-surface stability, while the latter two took place in moderately unstable conditions. For each experiment, data were collected over a 15 minute period at a sampling rate of 5 Hz. After collection, the data were converted from voltages to standard components using previously determined transfer functions.

A mechanical failure in the dual-annulus bivane necessitated its replacement for the final field experiment. In its place, a larger, slower responding cruciform-tailed bivane was used. Mechanical failure to the sonic anemometer also required its replacement after the first test; however, it was replaced with a unit of comparable response capabilities.

The numerical results for each experiment indicate that both estimation methods produced representative values for momentum flux, as compared with the measured, 'true' value. The numerical near-

equality of the two methods using similar equipment validated Chimonas' physical and mathematical reasoning presented in the development of the mean-values approximation. The flux estimation values derived using the cruciform vane were somewhat higher than those derived with the dual-annulus bivane (in relation to the 'true' value), but were also representative of the true flux.

A lack of data requires that the favorable conclusion tendered above be considered tentative at this point; it is highly desirable that more field testing be undertaken under varying conditions of stability in order to draw a more complete conclusion.

NOTES

NOTES

1. The sonic anemometer used was the Applied Technologies model SWS-211/3 Three-Axis Sonic Wind System.

2. The wind tunnel used for instrument testing is located in the basement of the Civil Engineering building at Purdue University (main campus, West Lafayette, Indiana).

3. The flow distortion corrections for their respective axes are:

If the magnitude of the wind is given by:

$$\text{speed} = (u^2 + v^2 + w^2,)^{1/2}$$

where u, v, and w are the standard wind components, then

The u-axis correction for flow distortion is:

$$\alpha = \cos^{-1}(u/\text{speed})$$

if $\alpha <= 70.0^{\circ}$

$$u=(u/(0.84+(0.16\times(\alpha/70.0))))$$

The v-axis correction for flow distortion is:

$$\beta = \cos^{-1}(v/\text{speed})$$

if $\beta <= 70.0^{\circ}$

$$v=(v/(0.84+(0.16\times(\beta/70.0))))$$

The w-axis correction for flow distortion is:

$$\gamma = \cos^{-1}(w/\text{speed})$$

if $\gamma <= 70.0^{\circ}$

$$w=(w/(0.84+(0.16\times(\gamma/70.0))))$$

4. The cup anemometer used in the experiment was the model 2030 Micro Response Anemometer manufactured by Weathertronics, a division of Qualimetrics, Inc.

5. The wind translator used was a Weathertronics model 2028 duel range wind translator.

6. The acquisition software used was Labtech Acquire© software.

7. The spreadsheet used was Lotus 1-2-3©.

8. The bivane used in the experiment was the Climatronics model P/N 101456 Dual Annulus bivane.

9. The cruciform-tailed bivane used in the third experiment was an R.M. Young model 17003 bivane.

10. The analysis software used was MathCAD©.

11. The A/D computer board used was a CIO-AD08 25 pin board manufactured by Computer Boards, Inc.

12. The computer used was a CompuAdd© 212.

13. The data acquisition software used in the experiments (field tests) was Labtech Notebook©.

14. The smallest detectable eddy lasted 0.8 seconds (peak-to-peak). With an average wind speed of 1.69 m s^{-1}, the smallest eddy would be 1.36 meters in length.

The smallest eddy all instruments would see would be five times the instrument separation (2.0 meters). With a average wind speed of 1.69 m s^{-1}, an eddy would have to persist for no less than 5.92 seconds to be seen by all instruments simultaneously. Note: this is not the most conservative figure; many sources list 10 times the instrument separation as the smallest eddy that all instruments can see.

Using the dual-annulus bivane's natural wavelength or the cup anemometer's distance constant (both approximately 2.5 meters), an average windspeed of 1.69 m s^{-1} implies the smallest eddy they could respond to would have to persist at lease 1.478 seconds.

LIST OF REFERENCES

LIST OF REFERENCES

Applied Technologies Inc., 1980: Three-Axis Sonic Wind System, Applied Technologies Inc., Boulder, CO, 25 pp.

Busch, N.E., and L. Kristensen, 1976: Cup anemometer overspeeding. J. Appl. Meteor., 15, 1328-1332.

Chimonas, G., 1980: Reynolds stress deflections of the bivane anemometer. J. Appl. Meteor., 19, 329-333.

Climatronics Corp., 1980: Dual-Annulus Bivane, Climatronics Corp., Bohemia, N.Y., 9 pp.

Coats, W.G., 1991: A comparative study of the dynamic performance of three bivanes. Masters Thesis, Purdue University, 165 pp.

Finnigan, J.J., F. Einaudi, and D. Fua, 1984: The interaction between an internal gravity wave and turbulence. J. Atmos. Sci., 41, 2409-2436.

Kaganov, E.I, and A.M. Yaglom, 1975: Errors in wind speed measurements by rotation anemometers. Bound. Layer Meteor., 10, 15-34.

Kaimal, J.C., and L. Kristensen, 1990: Time series tapering for short data samples. Bound. Layer Meteor., 57, 187-194.

Qualimetrics Inc., 1985: Micro Response Anemometer Model 2030, Qualimetrics Inc., Sacramento, CA., 12 pp.

R.M. Young, Company, 1977: Gill Bivane, R.M. Young Company, Traverse City, MI, 28 pp.

Simidchiev, D.A., 1986: Compendium of Lecture Notes on Meteorological Instruments, Vol I, World Meteorological Organization, Geneva, Switzerland, 361 pp.

Snow, J.T., D.E. Lund, M.D. Conner, S.B. Harley, and C.B. Pedigo, 1989: The dynamic response of a wind measuring system. J. Atmos. Oceanic Tech, 6(1), 140-146.

Stull, R.B., 1988: An Introduction to Boundary Layer Meteorology, Kluwer Academic Publishers, Boston MA, 665 pp.

Wang, J.Y., and C.M.M. Felton, 1983: Instruments for Physical Environmental Measurements Vol I, Kendall/Hunt Publishers, Dubuque, IA, 378 pp.

APPENDIX

FIRST- AND SECOND-ORDER SYSTEMS

APPENDIX

FIRST- AND SECOND-ORDER SYSTEMS

Although many meteorological instruments represent the state of the atmosphere with a relatively high degree of accuracy, no instrument has a truly ideal response (i.e., having the capability to measure and record atmospheric phenomena instantaneously with total accuracy). Both the cup anemometer and bivane used in this experiment have less than ideal responses. Thus, when either sensor measures the parameter(s) for which it is designed, the resultant output(s) are not equivalent to the 'true' values occurring in nature.

To good approximation, responses for simple meteorological instruments can be modeled using solutions to first- and second-order ordinary differential equations (O.D.E.'s). First-order system responses are similar to those found in cup anemometers and various types of thermometers. Conversely, instruments such as barometers and bivanes display response characteristics similar to responses for second-order systems. These non-ideal systems and their solutions require examination if responses for these instruments are to be properly interpreted and understood.

As modern meteorological measuring systems sample quantities at discrete times, a series of measurements taken over a period of time can be thought of as a piece-wise series of straight lines (or ramps) between measurements and values. Thus, a ramp input is most

appropriate for use as an input forcing function for the appropriate O.D.E.'s. Other inputs (step and sine) are utilized to display several non-ideal response features.

A.1. First-Order System and Solution

A cup anemometer response can be modeled using the first-order system:

$$\frac{dU}{dt} + \frac{U}{\tau} = \frac{f(t)}{\tau} \qquad \text{(A1)}$$

with the initial condition $u = u_0$ at $t(0) = t_0$, and where $f(t)$ is the input (forcing) function, U is the total horizontal wind component, and τ is the time constant of the system.

First-order systems are characterized by a time constant, τ. The time constant τ is defined as the time required for the system response to reach 63% of a step forcing function input (Simidchiev, 1986). Thus, a smaller τ corresponds to a quicker responding sensor.

Solving for the response (based on a ramp input) at time t yields:

$$u(t) = (h - u_0)\left[1-e^{\left[\frac{-\Delta t}{\tau}\right]}\right] + u_0 e^{\left[\frac{-\Delta t}{\tau}\right]} + mh\Delta t\left[2u_0 - 2u_0 e^{\left[\frac{-\Delta t}{\tau}\right]}\right]$$

$$-\tau + t + te^{\left[\frac{-\Delta t}{\tau}\right]}\Bigg] + u_0\left[1-e^{\left[\frac{-\Delta t}{\tau}\right]}\right], \qquad \text{(A2)}$$

where h is the value of the input function at time $t = t_0$, m is the slope of the input function, x_0 is value of the input function at $t = t_0$ (often set equal to zero for simplicity, but included here for generality), and Δt is $t - t_0$.

For modelling purposes, this solution can be used in a piece-wise fashion. The solution becomes:

$$ur_i = U_{i-1} + m_i\,(\delta t - \tau) + \left[\left[\,ur_{i-1} - U_{i-1}\,\right] + m_{i-1}\tau\right]e^{\left[\frac{-\delta t}{\tau}\right]}, \qquad \text{(A3)}$$

where ur_i is the step-wise solution of the estimation (i.e., the instrument's response) of the actual value of the input (forcing function) U_i, δt is the time increment from time t_i to time t_{i+1}, u_0, and m_i is the slope of each step-wise section, given by

$$m_i = \frac{U_i - U_0}{\delta t}$$

A.1.2. Response Characteristics of First-Order Systems

Most of the distortion in the system response is a consequence of the instrument mass. This implies a resistance to dynamic inertial change, and thus physical inability to respond instantaneously to

changes of the measured quantity. Several common response features include amplitude and phase distortion, phase lag, transient waveforms, and dynamic error. Phase lag, phase and amplitude distortion, and transient waveforms can be seen in Figure A1. This figure shows a sinusoidal forcing function (for which an exact solution is known) and two responses with different time constants. The transient portion of the waveform is evident in both responses between 0 and 20 time periods (note that time and displacement are relative, non-dimensional values).

Transient error is a result of the "settling" of the response after abrupt changes in the forcing function (Simidchiev, 1986). The transient occurs after a change in the pattern of the forcing function, and usually persists between 5τ and 10τ. Accordingly, Figure A1 indicates a more pronounced and longer lasting transient waveform for the response with the higher time constant.

Phase lag and phase and amplitude distortion are consequences of the instruments inability to instantaneously detect and record changes in the forcing function. Responses with larger time constants are more drastically distorted. Figure A1 shows the response with τ=0.75 attains only 40% of the amplitude of the response with τ=0.15. The latter is also approximately 45° out of phase with the input signal, while the former is nearly 90° out of phase. Another important consideration is the frequency of change of the parameter being measured. A rapidly changing parameter (i.e., wind speed or direction) will display a more pronounced response distortion than a slowly changing parameter (i.e., ambient temperature).

The combination of these errors results in dynamic error--the

Figure A1. Generalized response for first-order system with sine wave input forcing function, with different time constants, τ. Initial conditions: x_0=2.0, t_0=0, $\int x_n$=6.283.

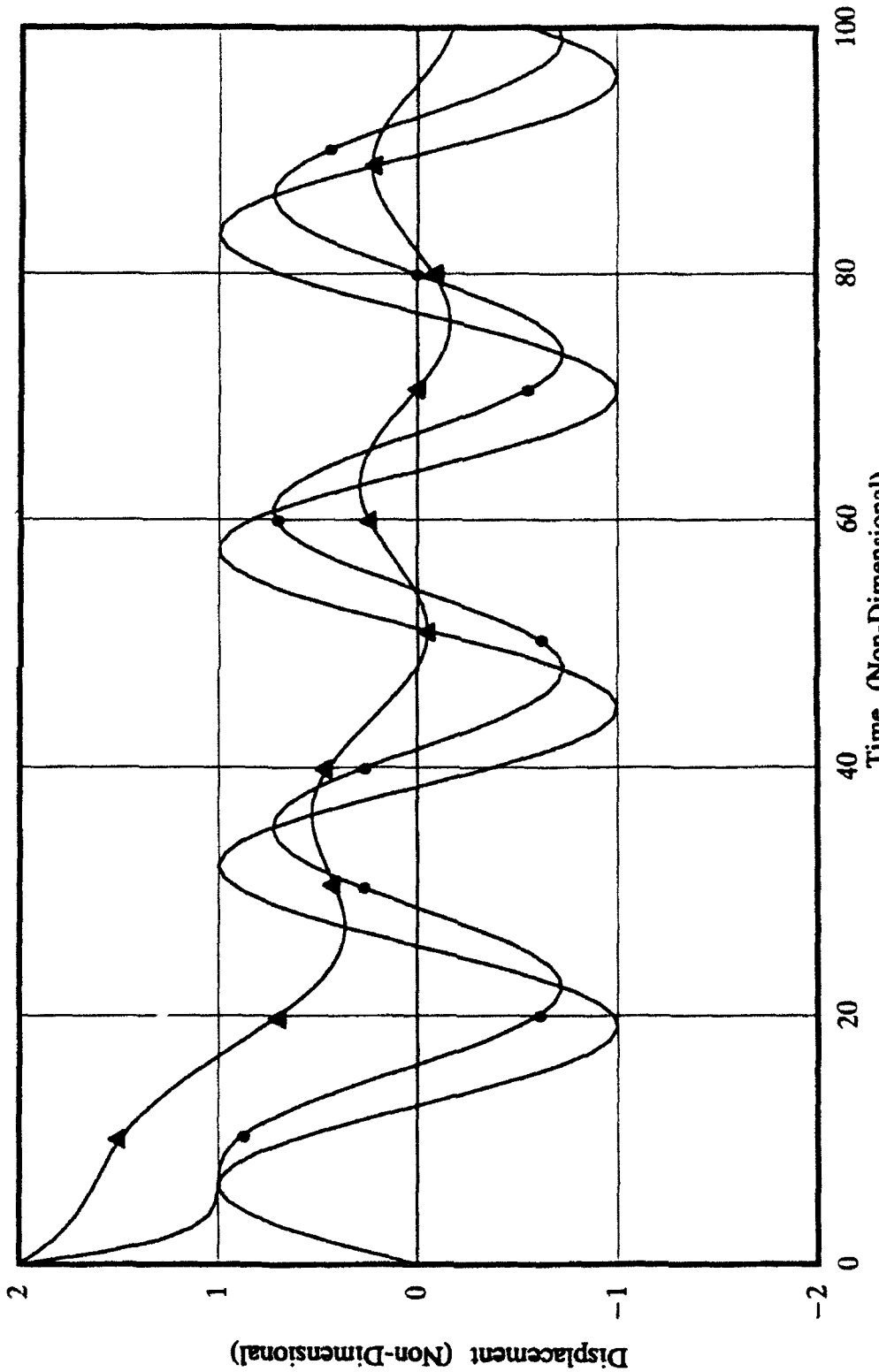
Displacement (Non-Dimensional)
2
1
0
−1
−2
0
20
40
60
80
100
Time (Non-Dimensional)
Sine Input
Response with τ = 0.15
Response with τ = 0.75

Figure A1

instantaneous difference between the actual value of the parameter being measured compared with the value indicated by the response. Averaged over a time-series, first-order responses with larger time constants have larger dynamic errors. Figure A2 shows two responses to a ramp input with differing time constants. Although phase lag and amplitude distortion are difficult to identify, the response with the higher time constant clearly has the longer transient and greater dynamic error. This pattern is again noted in Figure A3, where the input is a step function.

A.2. Second-Order System and Solution

Second order systems are characterized by two quantities: a damping ratio, ς, and a natural frequency, ω_n, which relate to the damping characteristics of the amplitude and frequency of the oscillatory response (Simidchiev, 1986). The damping ratio determines the vane's oscillatory damping characteristics. The natural frequency characterizes the frequency of directional change of the vane (Wang and Felton, 1983).

An underdamped bivane ($0 < \varsigma < 1$) responds similarly to a solution for a second-order system. This response can be modeled using the solution to the system:

$$\frac{d^2\phi}{dt^2} + 2\omega\varsigma \frac{d\phi}{dt} + \omega^2\phi = \omega^2(f(t')), \qquad \text{(A4)}$$

Figure A2. As in Fig. 48, for ramp input forcing function. Initial conditions: h=5.0, x_0=0, m=0.5, t_0=0.

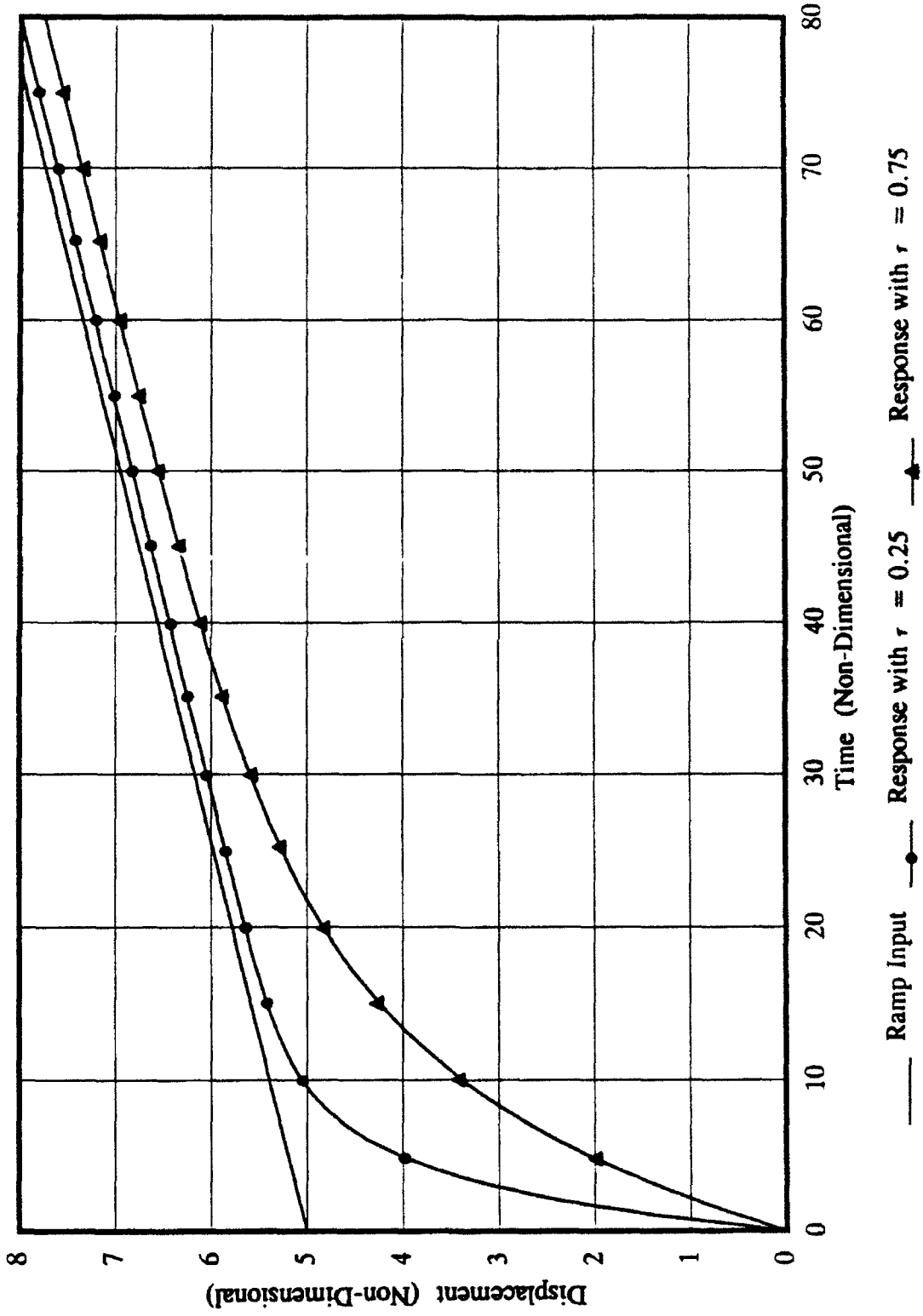
Displacement (Non-Dimensional)
0
1
2
3
4
5
6
7
8
0
10
20
30
40
50
60
70
80
Time (Non-Dimensional)
Ramp Input
Response with r = 0.25
Response with r = 0.75

Figure A2

Figure A3. As in Fig. 48, for step input forcing function. Initial conditions: $x_0=t_0=0$, h=2.0.

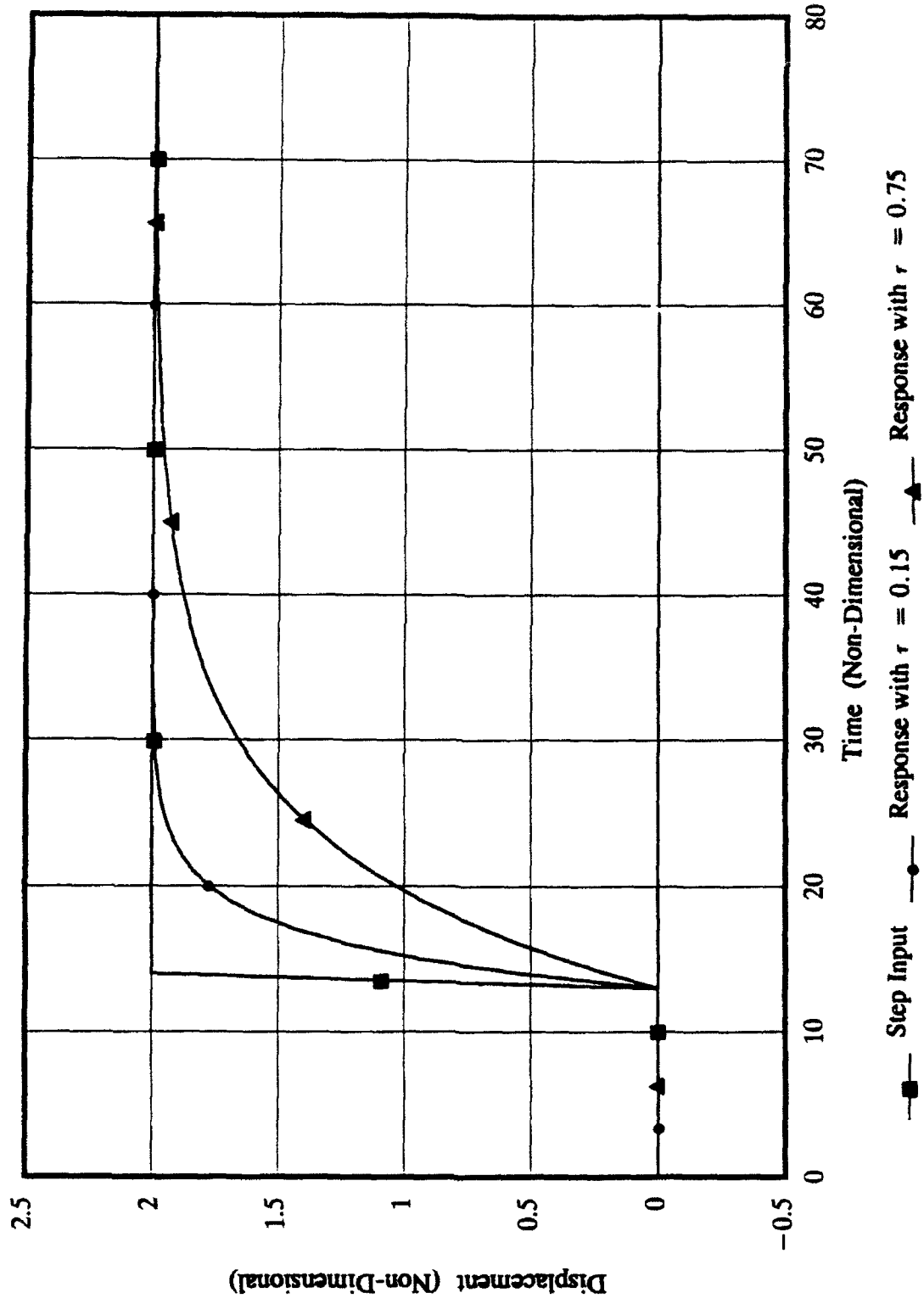
Displacement (Non-Dimensional)
2.5
2
1.5
1
0.5
0
−0.5
0
10
20
30
40
50
60
70
80
Time (Non-Dimensional)
Step Input
Response with r = 0.15
Response with r = 0.75

Figure A3

where h is the value the forcing function's initial value $t' = t_i - t_0$, and with initial conditions

$t'(0) = t'_0$, and,

$$\phi'_0 = \left.\frac{d\phi}{dt}\right|_{(t'_0)}$$

Second-order systems have more possible solutions than their first-order counterparts. A solution for the system given in (A4) with a ramp forcing function is a good approximation of the response of a bivane. Such a solution is:

$$\phi(t) = \left[e^{-\varsigma\delta t\omega} \cos\left(\omega\delta t(1-\varsigma^2)^{1/2}\right)\right]\left[\frac{2m\omega}{\omega} - \left[h - \phi_0\right]\right] +$$

$$\left[e^{-\varsigma\delta t\omega} \sin\left(\omega\delta t(1-\varsigma^2)^{1/2}\right)\right]\left[\frac{m(2\varsigma^2-1)}{\omega(1-\varsigma^2)^{1/2}} + \frac{\phi'_0}{\omega(1-\varsigma^2)^{1/2}} - \frac{\varsigma(h-\phi_0)}{(1-\varsigma^2)^{1/2}}\right] +$$

$$m\delta t + \left[\frac{2m\varsigma}{\omega}\right] - \left[h-\phi_0\right], \qquad \text{(A5)}$$

where m is the slope of the ramp, $\phi = \phi_0$ at $t(0) = t_0$, and $\delta t = t_i - t_0$.

As before, a piece-wise analogy to this solution above can be modeled. Unlike the piece-wise solution for the first-order system,

the first derivative of the solution is also needed to determine the slope of the previously computed portion of the response.

The related piece-wise solution to (A5) is:

$$\phi_{i+1} = \left[e^{-\omega\delta t\varsigma}\cos(\omega\delta t(1-\varsigma^2)^{1/2})\right]\left[\frac{2\varsigma m_i}{\omega} - (\Phi_i-\phi_i)\right] +$$

$$\left[e^{-\omega\delta t\varsigma}\sin(\omega\delta t(1-\varsigma^2)^{1/2})\right]\left[\frac{m_i(2\varsigma^2-1)}{\omega(1-\varsigma^2)^{1/2}} + \frac{d\phi_i}{\omega(1-\varsigma^2)^{1/2}} - \frac{\varsigma(\Phi_i-\phi_i)}{(1-\varsigma^2)^{1/2}}\right]$$

$$+ \Phi_{i+1} - \left[\frac{2m_i\varsigma}{\omega}\right], \qquad \text{(A6)}$$

where Φ_i is the value of the forcing function at time t_i, m_i is the slope of the solution between times t_i and t_{i+1}, given by:

$$m_i = \frac{\Phi_{i+1} - \Phi_i}{\delta t},$$

and

$$d\phi_i = \left.\frac{d\phi}{dt}\right|_i$$

A.2.2. Response Characteristics of Second-Order Systems

Second-order system responses feature all of the previously discussed characteristics of first-order responses. Additionally, since second-order responses are a indicative of both oscillatory and

translational motions, overshoot error also exists.

Overshoot occurs during oscillatory motion when an abrupt change in the forcing function occurs. As the wind direction changes, the resultant change in aerodynamic forces causes an force imbalance on either side of the vane tail. As a result, the tail pivots towards a point of relative force equilibrium. As the tail moves, however, its increasing kinetic energy is added to the initial force imbalance, causing the tail to move past the equilibrium point. Once past this point, the tail speed decreases as it again encounters an increasing force imbalance opposite to the one initially encountered. This pattern repeats itself until all oscillatory motion is damped out, or until another abrupt change in the forcing is noted.

Overshoot increases with lower damping ratios and natural frequencies. Either of these, or both in combination, affect the magnitude of the overshoot. Figure A4 shows an input ramp function along with two responses. Each response has the same natural frequency, but the one response has a much lower damping ratio than the other. The response with the lower damping ratio has significant overshoot, while the other response has no none at all. This is to be expected; a lower damping ratio corresponds to greater degree of system underdamping. Note that dynamic error is not always instantaneously greater for responses with lower damping ratios; however, cumulative error over a time series will normally be greater for such responses, as it takes longer for the response to reach equilibrium.

Figure A5 shows the same input ramp function, but with responses with equivalent damping ratios and different natural frequencies. In

Figure A4. Generalized response for second-order system with ramp input forcing function, similar natural frequencies (ω_n) and different damping ratios (ζ). Initial conditions: $h=x_0=t_0=0$, $m=1.0$.

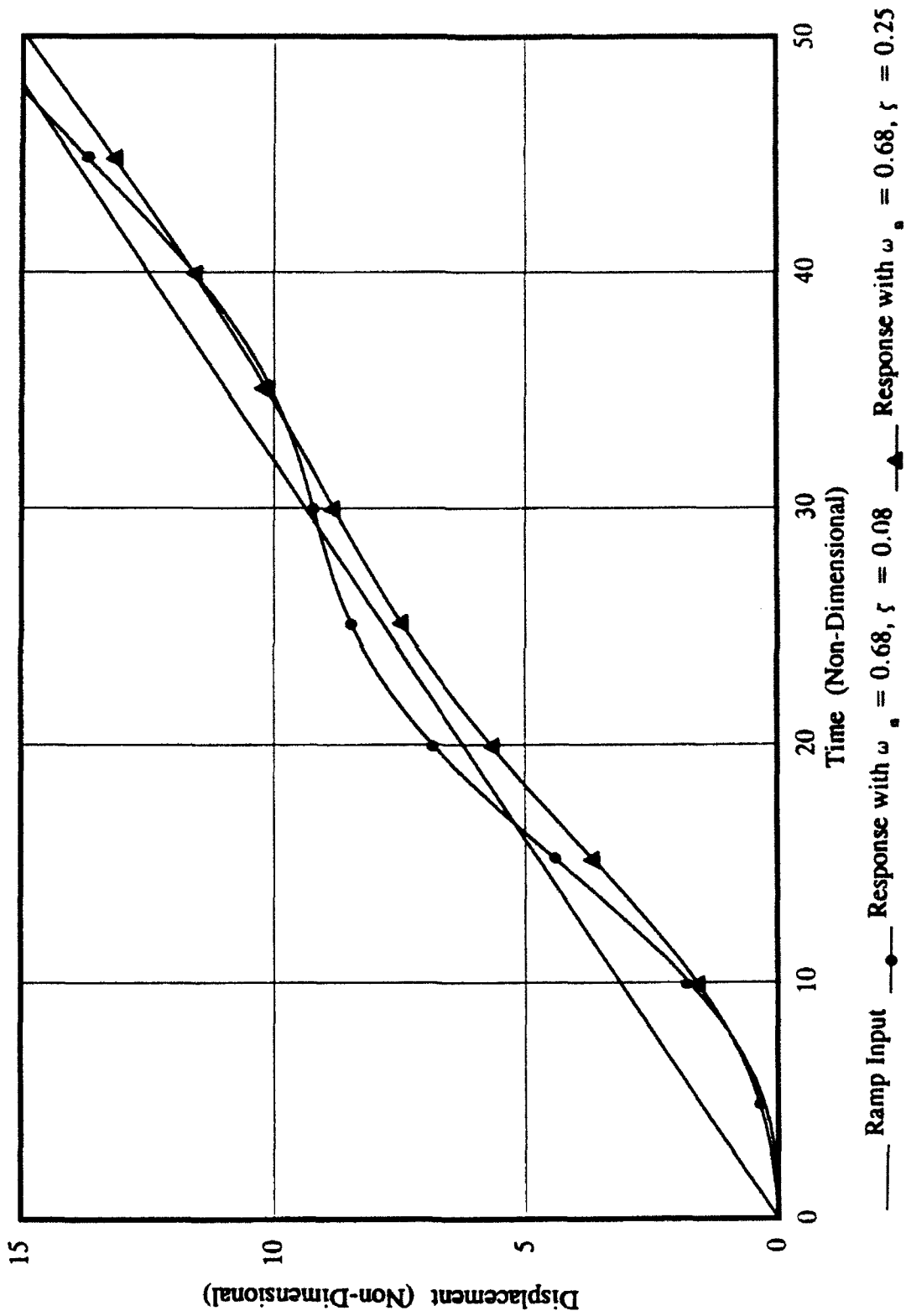
Displacement (Non-Dimensional)
0
5
10
15
0
10
20
30
40
50
Time (Non-Dimensional)
Ramp Input
Response with ω_n = 0.68, ζ = 0.08
Response with ω_n = 0.68, ζ = 0.25

Figure A4

this case, the response with the lower ω_n demonstrates greater overshoot. Note however, with few exceptions, it has a greater instantaneous dynamic error than its counterpart. It also takes considerably longer to reach equilibrium than the response with the larger ω_n. This is easily seen if one considers the natural wavelength, λ_n. λ_n is the characteristic length the vane tail would traverse if it followed a sine wave in an undamped response (Wang and Felton, 1983), and is the inverse of the natural frequency. Thus, a smaller ω_n implies a larger λ_n, and a subsequently larger overshoot.

Note that this result is not necessarily analogous to a one derived from a smaller damping ratio. While decreases in damping ratio and natural frequency both tend to increase overshoot, they rarely affect overall system responses in an identical fashion.

Figure A5. As in Fig. 51, with similar damping ratios (ζ) and different natural frequencies (ω_n). Initial conditions: $h=x_0=t_0=0$, $m=1.0$.

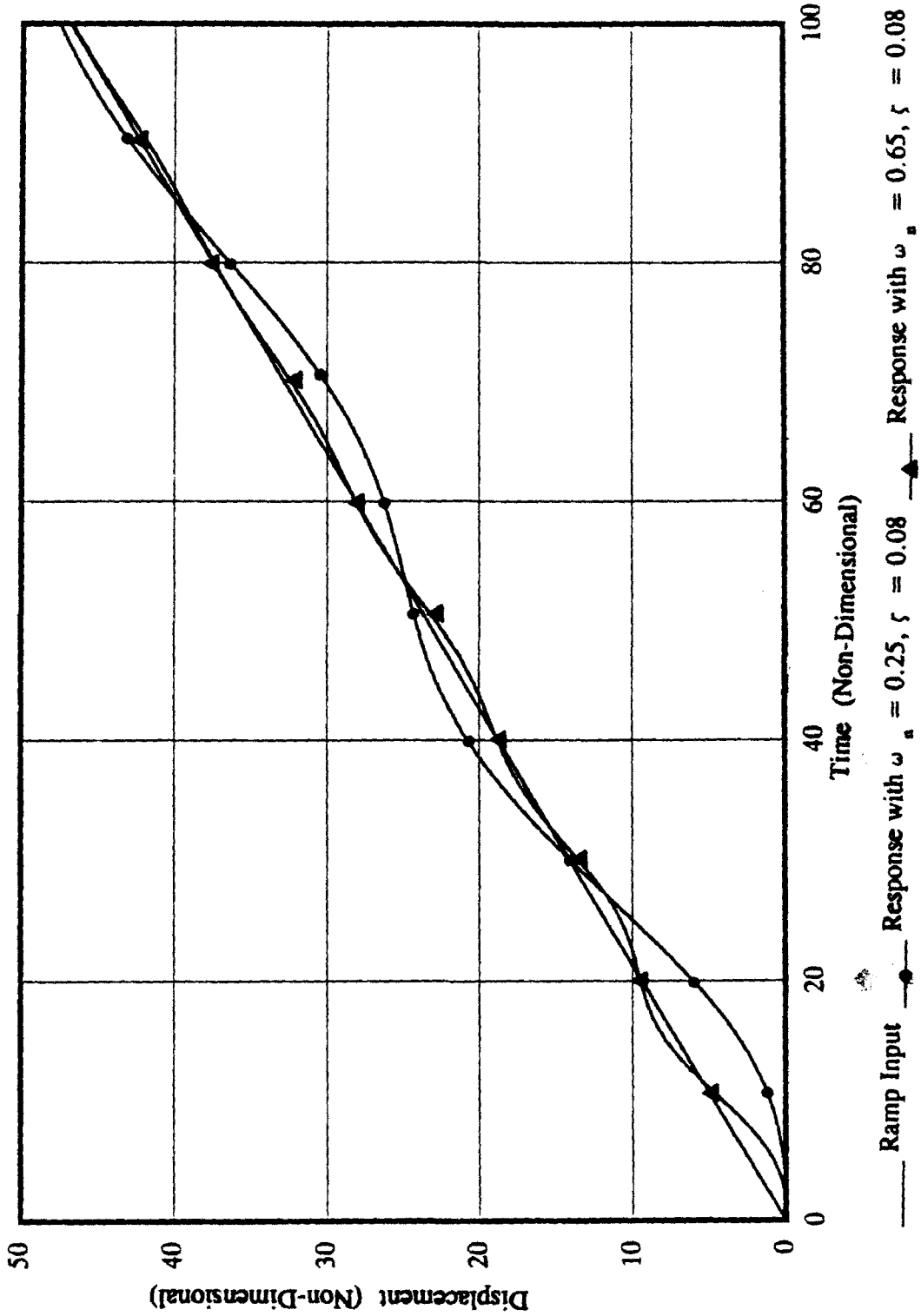
Displacement (Non-Dimensional)
0
10
20
30
40
50
0
20
40
60
80
100
Time (Non-Dimensional)
Ramp Input
Response with ω_n = 0.25, ζ = 0.08
Response with ω_n = 0.65, ζ = 0.08

Figure A5